NASA TM X-1165

EFFECT OF CONFIGURATION VARIABLES ON THE SUBSONIC LONGITUDINAL STABILITY CHARACTERISTICS OF A HIGH-TAIL TRANSPORT CONFIGURATION

By Edward J. Ray and Robert T. Taylor

Langley Research Center
Langley Station, Hampton, Va.

NATIONAL AERONAUTICS AND SPACE ADMINISTRATION

For sale by the Clearinghouse for Federal Scientific and Technical Information
Springfield, Virginia 22151 – Price $4.00

BLANK PAGE

EFFECT OF CONFIGURATION VARIABLES ON THE SUBSONIC LONGITUDINAL STABILITY CHARACTERISTICS OF A HIGH-TAIL TRANSPORT CONFIGURATION

By Edward J. Ray and Robert T. Taylor
Langley Research Center

SUMMARY

An investigation has been made to determine the effects at high angles of attack of configuration variables on the static aerodynamic characteristics of a typical high-tail transport configuration. Tests were made in the Langley high-speed 7- by 10-foot tunnel at a Mach number of 0.21 and a Reynolds number of 0.78×10^6, based on the wing mean aerodynamic chord. Data are also included from tests made in the Langley transonic dynamics tunnel to determine the effect of Mach number. The test angle-of-attack range extended from about -5° to 50°.

The configuration variables which were investigated included body size and shape, nacelle size and location, wing section, and horizontal-tail vertical position, size, and taper ratio. The effects of wing leading-edge devices and wing double-slotted flaps on the longitudinal aerodynamic characteristics were determined for the basic high-tail configuration. In addition, the control effectiveness of the horizontal stabilizers and the effectiveness of the spoiler, aileron, and rudder controls were determined for selected test configurations to angles of attack of about 50°. Preliminary sideslip effects were also determined for the basic configuration.

The investigation showed that nonlinearity of the post-stall pitching-moment curve was traceable, to a large extent, to the nacelle wake which at high angles of attack blankets the horizontal tail. The fuselage-forebody lift, at high angles of attack, was also shown to influence the pitch curve past the stall of the wing. Factors such as increased fuselage cross-section size and increased forebody length aggravated the post-stall pitch nonlinearity, but fuselage wake effects did not change the available tail power to any appreciable extent.

Increased horizontal-tail size was shown to have a favorable effect on the post-stall pitch curve. Auxiliary horizontal-tail surfaces located low on the after part of the fuselage provided a similar but more pronounced linearizing effect. Significant improvements in the post-stall pitching-moment characteristics were obtained by relocating the aft-mounted nacelles to positions where the nacelles were shielded by the wake of the wing or fuselage.

INTRODUCTION

In the past several years many aircraft have been built which have employed horizontal stabilizers mounted high on the vertical fin. Research conducted from 1947 to 1958 has shown that such configurations properly designed exhibit linear pitching-moment characteristics up to the angle of attack at which the wing stalls. Beyond the primary wing stall, however, very little is documented concerning configuration variables which tend to produce satisfactory pitching-moment characteristics. Therefore, the National Aeronautics and Space Administration has initiated an experimental wind-tunnel program in order to study the configuration variables which might be expected to affect the linearity of the pitching-moment curve beyond the primary wing stall.

The purpose of this paper is to present selected results obtained from the experimental wind-tunnel program to provide an indication of the effects of: body size and shape, nacelle size and location, wing leading-edge devices, wing double-slotted flap, wing section, and horizontal-tail vertical position, size, and taper ratio on the longitudinal aerodynamic characteristics of a typical high-tail transport configuration. In addition, experimental results are included herein which show the control effectiveness of the horizontal stabilizer and the effectiveness of the spoiler, aileron, and rudder controls of the test configurations. Preliminary sideslip effects are also included for the basic configuration.

Tests were conducted in the Langley high-speed 7- by 10-foot tunnel at a Mach number of 0.21 and a Reynolds number of 0.78×10^6, based on the wing mean aerodynamic chord. Data are also included from tests made in the Langley transonic dynamics tunnel to determine the effect of Mach number. The test angle-of-attack range extended from about -5° to 50°.

In order to expedite publication, these data are presented without detailed analysis.

SYMBOLS

The data which are presented herein are referred to the body-axis system with the exception of lift and drag which are referred to the stability-axis system. All the data contained herein are referred to a moment center located at the 0.40 point of the mean aerodynamic chord of the basic wing. (See figs. 1(a) to (d).) The coefficients were nondimensionalized by using the geometry of the basic wing with the exception of the coefficients for the configurations having reduced wing aspect ratios. (See table I.)

The units used for the physical quantities defined in this paper are given both in U.S. Customary Units and in the International System of Units (SI). Factors relating the two systems are given in reference 1.

A	aspect ratio, b^2/S
b	reference wing span, 46.40 inches (117.86 centimeters)
c	local chord of airfoil, inches (centimeters)
$\bar{c}$	mean aerodynamic chord of basic wing, 6.69 inches (16.99 centimeters)
C_D	drag coefficient, $\frac{\text{Drag}}{qS}$
C_L	lift coefficient, $\frac{\text{Lift}}{qS}$
C_l	rolling-moment coefficient, $\frac{\text{Rolling moment}}{qSb}$
C_{l_β}	effective dihedral parameter, $\partial C_l/\partial\beta$
C_m	pitching-moment coefficient, $\frac{\text{Pitching moment}}{qS\bar{c}}$
C_n	yawing-moment coefficient, $\frac{\text{Yawing moment}}{qSb}$
C_{n_β}	directional stability parameter, $\partial C_n/\partial\beta$
C_Y	side-force coefficient, $\frac{\text{Side force}}{qS}$
L/D	lift-drag ratio
$(L/D)_{max}$	maximum lift-drag ratio
M	free-stream Mach number
q	free-stream dynamic pressure, pounds per square foot (newton per square meter)
S	area of basic wing, including body intercept, 1.92 square feet (0.1784 square meter)
S_a	area of auxiliary horizontal tail, square feet (square meters)
S_t	area of horizontal tail, square feet (square meters)
R	Reynolds number based on $\bar{c}$
x	longitudinal distance from the leading edge of airfoil section, measured in reference plane

z_u vertical distance from airfoil section reference plane to upper surface of airfoil (positive direction up)

z_l vertical distance from airfoil section reference plane to lower surface of airfoil (positive direction up)

z_t vertical distance from wing reference plane to horizontal tail reference plane (positive direction up)

i_t incidence of horizontal tail (negative trailing edge up), degrees

α angle of attack, degrees

δ_a deflection of aileron (negative trailing edge up), degrees

δ_r deflection of rudder (negative trailing edge right), degrees

β sideslip angle, degrees

Model components:

B_1 "pear-shaped" body having larger radius on top

B_2 "pear-shaped" body having larger radius on bottom

B_3 circular body

B_4 small body

B_5 combination of B_1 and B_2. B_2 shape forward and B_1 shape rearward

B_6 shortened B_1

W_1 basic wing, having NACA 64A409 airfoil section

W_2 basic wing equipped with double-slotted flaps

W_3 wing having NACA 23012 airfoil section

H_1 small horizontal tail having taper ratio 0.29 and $\frac{S_t}{S} = 0.17$

H_2 medium horizontal tail having taper ratio 0.29 and $\frac{S_t}{S} = 0.22$

H_3 large horizontal tail having taper ratio 0.29 and $\frac{S_t}{S} = 0.30$

H_4 large horizontal tail having taper ratio 1.00 and $\frac{S_t}{S} = 0.28$

N_1 small nacelle

N_2 medium (basic) nacelle

N_3 large nacelle

V_1 vertical tail having horizontal-tail pivot 10.80 inches (27.43 centimeters) above wing reference plane

V_2 vertical tail having horizontal-tail pivot 12.80 inches (32.51 centimeters) above wing reference plane

V_3 vertical tail having horizontal-tail pivot 8.80 inches (22.35 centimeters) above wing reference plane

V_4 vertical tail having horizontal-tail pivot 6.90 inches (17.53 centimeters) above wing reference plane

V_5 vertical tail having horizontal-tail pivot in wing reference plane

V_6 vertical tail having horizontal-tail pivot 1.0 inch (2.54 centimeters) below wing reference plane

H_{A1} small auxiliary horizontal tail having $\frac{S_a}{S} = 0.04$

H_{A2} medium auxiliary horizontal tail having $\frac{S_a}{S} = 0.08$

H_{A3} large auxiliary horizontal tail having $\frac{S_a}{S} = 0.13$

S full-span spoiler on upper surface of right wing panel

S_1 inboard spoiler on upper surface of right wing panel

DESCRIPTION OF MODELS

Drawings of four of the test configurations, various model components, and nacelle arrangements are presented in figures 1(a) to (m). Photographs of the basic configuration installed in the two test facilities are shown in figure 2. The geometric characteristics of the model components and ordinates of the high-lift devices are presented in tables I and II, respectively.

Bodies

The typical cross section of the basic body B_1 had slightly flattened sides, a circular bottom portion, and a larger circular top portion. Except

for small areas near the nose and the aft part of body 1, the differences in the radii of the circular portions resulted in a "pear-shaped" fuselage. (See fig. 1(a).) Body 2 B_2 as shown in figure 1(b) was an inverted version of body 1. Figure 1(c) shows the details of the center body B_3. The volumes of bodies 1, 2, and 3 were very nearly the same; however, the volume of body 4 was somewhat smaller. The characteristic cross section of the smaller body B_4 (fig. 1(d)) was similar in shape to the typical cross section of body 1. Body 5 (no drawing included) was similar to bodies 1 and 2 in that the cross section of the forward portion was that of body 2 and of the rearward portion was that of body 1. The irregularities occurring at the juncture of two different body shapes were faired at fuselage station 31.70 (80.52). Body 6 (no drawing included) was the basic body B_1 with 6 inches of the fuselage removed from the body just ahead of the wing apex.

Wings

The three wings which were tested in the present investigation are referred to as W_1, W_2, and W_3. The basic wing W_1 was composed of NACA 64A409 airfoil sections oriented streamwise. A limited control-effectiveness study was made with a spoiler and aileron system on the right panel of W_1. Details of the spoiler and aileron arrangement are shown in figure 1(e). The high-lift wing W_2 was identical to W_1 with the exception of the full-span leading-edge slat and double-slotted flaps on W_2. Details of the slat and flap system are shown in figure 1(f) and ordinates of the slat, vane, and flap are presented in table II. The wing W_3 having an aspect ratio of 7.8 was identical in planform to W_1 but differed in airfoil section. The W_3 airfoil was composed of NACA 23012 sections oriented streamwise. The W_3 configuration was also tested with lower wing aspect ratios reduced by clipping the tips of the wing. The root chords of all the test wings were located on the bodies at the same fuselage station.

Horizontal Tails, Auxiliary Horizontal Tails, and Vertical Tails

The horizontal tails, auxiliary horizontal tails, and vertical tails were composed of NACA 0009 airfoil sections oriented streamwise. The 0.25 point of the mean aerodynamic chord of each horizontal tail was at fuselage station 51.20 (130.05) for all the tests in order to maintain a constant horizontal-tail moment arm. Figure 1(g) shows the details of the horizontal tails.

The positions of the 0.25 point of the mean aerodynamic chord of the three auxiliary horizontal tails were identical with respect to the moment reference center and the wing reference plane. Details of the auxiliary horizontal tails are shown in figure 1(h).

The vertical tail was equipped with a rudder which could be deflected 20°. A drawing showing the dimensions of the vertical tail with rudder is presented as figure 1(i).

Nacelles

Details of the three test nacelles in the original locations are shown in figure 1(j). The basic nacelles N_2 were tested in several positions other than the position indicated in figure 1(j). Figure 1(k) shows the basic nacelles N_2 in the wing-mounted position and figure 1(l) indicates the location of the basic nacelles in the aft position. In addition to the aforementioned nacelle positions, changes were made in the basic nacelle location which consisted of only a longitudinal relocation. These nacelle positions are shown in figure 1(m).

TESTS AND CORRECTIONS

The basic investigation was made in the Langley high-speed 7- by 10-foot tunnel with the slots in the test section closed. Additional tests were conducted at Mach numbers ranging from 0.20 to 0.91 in the Langley transonic dynamics tunnel, a variable-pressure continuous-flow facility. The average test conditions in the 7- by 10-foot tunnel during the investigation were a free-stream Mach number of 0.21, a free-stream dynamic pressure of 65 lb/sq ft (3112 N/m^2), and a Reynolds number based on $\bar{c}$ of 0.78×10^6. The average test conditions which existed in the transonic dynamics tunnel during the investigation are shown in the following table:

M	Stagnation pressure		Stagnation temperature		R
	lb/sq ft	N/m^2	°F	°K	
0.20	2 000	95 760	80	299.82	0.71×10^6
.40	1 150	55 062	105	313.71	.71
.60	850	40 698	130	327.59	.71
.80	440	21 067	120	322.04	.43
.86	430	20 588	120	322.04	.43
.91	400	19 152	130	327.59	.43

The investigation included tests of six bodies combined with various model components. All test models were sting mounted and forces and moments were measured by means of a six-component, strain-gage balance mounted within the model bodies. The angle-of-attack range extended from, at least, -5° to 47°. Transition strips approximately 1/8 inch (0.3175 centimeter) wide of No. 100 carborundum grains were placed at the 5-percent chord of the airfoils, bodies, and nacelles.

The angles of attack have been corrected for combined deflection of the sting-support system and balance under load. Pressures at the base of the bodies were corrected to correspond to the free-stream static pressure. The axial-force coefficients due to internal skin friction of the nacelles were calculated for each test Mach number and were subtracted for all configurations investigated. Jet-boundary corrections calculated by the method of reference 2 have been applied to the angle-of-attack and drag values obtained from the investigation in the Langley high-speed 7- by 10-foot tunnel. In addition, the data obtained in the 7- by 10-foot tunnel were corrected for blockage as determined by the method of reference 3. The jet-boundary and blockage corrections for the tests in the Langley transonic dynamics tunnel were found to be negligible.

Throughout the investigation, the test configurations were retested for each comparison which was made. For example, the basic configuration was retested when the effect of nacelle size or horizontal-tail size was determined. Discrepancies which are attributed to balance inaccuracies, slight errors in horizontal-tail settings, and model roughness were noted in the repeat tests. The maximum discrepancies of the longitudinal aerodynamic data included herein are shown in the following table:

C_L	±0.0100
C_D	±0.0007
C_m ($\alpha = -10^\circ$ to 20°)	±0.02
C_m ($\alpha = 20^\circ$ to 50°)	±0.01
$(L/D)_{max}$	±0.15

PRESENTATION OF RESULTS

The basic data determined from the investigation are presented in figures 3 to 30. The effects of several configuration variables on the longitudinal stability characteristics of the basic configuration are summarized in figures 31 to 35.

The longitudinal stability characteristics for each of the test configurations have been included in the data figures; however, the lift and drag results for all the test configurations are not presented herein. The drag data which are presented were selected on the basis of acceptable repeatability and agreement with estimated values. In most cases, the drag coefficients which were determined at high angles of attack, that is, angles of attack above approximately 20°, are not shown in the data figures. An outline of the contents of the data figures is as follows:

DISCUSSION

The basic results of the investigation, shown in figures 3 to 30 are presented without detailed analysis in order to expedite the publication of the data. It should be remembered in using these data that all the results contained herein have been referred to a moment center located at the 0.40 point of the mean aerodynamic chord of the basic wing. The summary figures (figs. 31 to 35) have been prepared to emphasize the effects of the configuration variables on the longitudinal stability characteristics of the basic high-tail configuration. The discussion contained herein is restricted to the summary curves and pertains only to the longitudinal stability characteristics of several of the test configurations at a Mach number of 0.21, which corresponds to a Reynolds number of 0.78×10^6.

A comparison of the longitudinal stability characteristics for the basic B_1 configuration and the small B_4 configuration, both with and without the horizontal tail, is shown in figure 31. It will be noted from figure 31 that the smaller body B_4 configuration is less unstable than the basic body B_1 configuration, both with and without the horizontal tail. In addition, a comparison of the pitching-moment curves for configurations B_1 and B_4 indicates that, at an angle of attack of about 34°, the increment in pitching-moment coefficient between the tail-off curve and the tail-on curve at each fuselage size is approximately equal, an indication that the larger fuselage is equally destabilizing with or without the horizontal tail. The difference in the longitudinal stability characteristics of the two configurations, therefore, is attributed primarily to direct forebody lift rather than to changes in the flow environment (wake effect) at the horizontal tail.

The effects of nacelle position on the longitudinal stability characteristics of the basic configuration are summarized in figure 32. An examination of the pitching-moment curves for the basic configuration, shown in the center of the figure, indicates that the nacelle-pylon combination generally provides a larger negative moment between angles of attack of 8° and 25°. At angles of attack above 25°, however, the nacelle arrangement is destabilizing, a result indicating a significant effect of the nacelles on the flow environment at the horizontal tail. The longitudinal stability characteristics of the basic configuration with several other nacelle arrangements are shown in figure 32 to illustrate the improvements in pitching-moment characteristics which can be achieved by relocating the nacelles. For instance, the results for the

configuration with the nacelles in the aft position show that fuselage-mounted nacelles may be added with essentially no effect on pitch.

The effect of horizontal-tail height on the longitudinal stability characteristics of the basic configuration is shown in figure 33. These results at low angle of attack are in general agreement with past research on the T-tail problem, at an angle of attack of about 40°, however, these data show a steady tendency of the pitch curves ($i_t = 0°$) to approach the tail-off curve as tail height increases.

The effect of adding horizontal-tail area to the basic high-tail configuration while maintaining the same horizontal-tail arm and height is shown in figure 34. A comparison of the pitching-moment curves for the basic configuration and for the basic configuration having a larger horizontal tail indicates that the additional horizontal-tail area resulted in a sizable increase in the stability level of the basic configuration throughout the angle-of-attack range and eliminated the nose-up pitching moment at high angles of attack. The losses in longitudinal stability, however, resulting from the impingement of the wake system on the horizontal tails were very nearly the same for the two configurations. Figure 35 shows the effect of additional low-horizontal-tail area, in the form of auxiliary horizontal tails, on the longitudinal stability characteristics of the basic configuration. The auxiliary horizontal tails were placed on the after fuselage, slightly above the wing-chord plane extended, with the 0.25 point of the mean aerodynamic chord of each auxiliary tail at the same fuselage station. (See fig. 1(h).) As shown in figure 35, the additional low-horizontal-tail area was effective in alleviating the "pitch-up" tendency of the basic configuration at angles of attack above the wing stall. An assessment of the effect of the additional low-horizontal-tail area, as compared with the effect of the additional high-horizontal-tail area, can be made from the results shown in figures 34 and 35. Values given in table I show that the difference between the horizontal-tail area of the basic configuration with the medium high tail H_2 and the configuration with the large high tail H_3 (fig. 34) was approximately equal to the difference in horizontal-tail area between the basic configuration and the basic configuration with the auxiliary horizontal tail H_{A2} (fig. 35). A comparison of the pitching-moment results for those configurations ($B_1V_1W_1N_2H_3$ and $B_1V_1W_1N_2H_2H_{A2}$) indicates that the additional low-horizontal-tail area, at a somewhat shorter moment arm, was more effective past the wing stall than the additional high-horizontal-tail area. This effect was expected since the auxiliary horizontal tails are not immersed in the wake system of the configuration at the higher angles of attack.

CONCLUDING REMARKS

The results of the study have indicated that the pitching-moment nonlinearity past the stall of the wing resulted primarily from the nacelle wake which envelops the horizontal tail at high angles of attack. The fuselage-forebody lift also influenced the pitch curve at high angles of attack past the

stall of the wing. Increases in fuselage cross-section size and forebody length aggravated the post-stall pitch nonlinearity.

Increased horizontal-tail size favorably affected the post-stall pitch curve. Auxiliary horizontal-tail surfaces located low on the after part of the fuselage provided a similar but more pronounced linearizing effect. Significant improvements in the post-stall pitching-moment characteristics were obtained by relocating the aft-mounted nacelles to positions where the nacelles were shielded by the wake of the wing or fuselage.

Langley Research Center,
National Aeronautics and Space Administration,
Langley Station, Hampton, Va., July 22, 1965.

REFERENCES

1. Mechtly, E. A.: The International System of Units - Physical Constants and Conversion Factors. NASA SP-7012, 1964.

2. Gillis, Clarence L.; Polhamus, Edward C.; and Gray, Joseph L., Jr.: Charts for Determining Jet-Boundary Corrections for Complete Models in 7- by 10-Foot Closed Rectangular Wind Tunnels. NACA WR L-123, 1945. (Formerly NACA ARR L5G31.)

3. Herriot, John G.: Blockage Corrections for Three-Dimensional-Flow Closed-Throat Wind Tunnels, With Consideration of the Effect of Compressibility. NACA Rept. 995, 1950. (Supersedes NACA RM A7B28.)

TABLE I.- GEOMETRIC CHARACTERISTICS OF MODEL COMPONENTS

Body 1 (basic), body 2, and body 5:	
Length	49.50 in. (125.73 cm)
Maximum width	5.80 in. (14.73 cm)
Maximum height	6.50 in. (16.51 cm)
Body 3:	
Length	49.50 in. (125.73 cm)
Maximum width	6.00 in. (15.24 cm)
Maximum height	6.00 in. (15.24 cm)
Fineness ratio	8.26
Body 4:	
Length	49.50 in. (125.73 cm)
Maximum width	4.24 in. (10.77 cm)
Maximum height	5.62 in. (14.28 cm)
Body 6:	
Length	43.50 in. (110.49 cm)
Maximum width	5.80 in. (14.73 cm)
Maximum height	6.50 in. (16.51 cm)
Wing 1 (basic):	
Leading-edge sweep	28°
Span	46.40 in. (117.86 cm)
Root chord	9.50 in. (24.13 cm)
Tip chord	2.40 in. (6.10 cm)
Mean aerodynamic chord	6.69 in. (16.99 cm)
Area	1.92 sq ft (0.1784 m^2)
Aspect ratio	7.8
Airfoil section	NACA 64A409
Wing 3 (aspect ratio 7.8):	
Leading-edge sweep	28°
Span	46.40 in. (117.86 cm)
Root chord	9.50 in. (24.13 cm)
Tip chord	2.40 in. (6.10 cm)
Mean aerodynamic chord	6.69 in. (16.99 cm)
Area	1.92 sq ft (0.1784 m^2)
Airfoil section	NACA 23012

TABLE I.- GEOMETRIC CHARACTERISTICS OF MODEL COMPONENTS - Continued

Wing 3 (aspect ratio 6.5):		
Leading-edge sweep		28°
Span	41.40 in.	(105.16 cm)
Root chord	9.50 in.	(24.13 cm)
Tip chord	3.20 in.	(8.13 cm)
Mean aerodynamic chord	6.87 in.	(17.45 cm)
Area	1.83 sq ft	(0.1700 m^2)
Airfoil section		NACA 23012
Wing 3 (aspect ratio 5.25):		
Leading-edge sweep		28°
Span	35.40 in.	(89.92 cm)
Root chord	9.50 in.	(24.13 cm)
Tip chord	3.90 in.	(9.91 cm)
Mean aerodynamic chord	7.09 in.	(18.01 cm)
Area	1.65 sq ft	(0.1533 m^2)
Airfoil section		NACA 23012
Wing 3 (aspect ratio 4.0):		
Leading-edge sweep		28°
Span	29.00 in.	(73.66 cm)
Root chord	9.50 in.	(24.13 cm)
Tip chord	4.73 in.	(12.01 cm)
Mean aerodynamic chord	7.38 in.	(18.75 cm)
Area	1.43 sq ft	(0.1329 m^2)
Airfoil section		NACA 23012
Horizontal tail 1:		
Leading-edge sweep		38°
Span	14.00 in.	(35.56 cm)
Root chord	5.15 in.	(13.08 cm)
Tip chord	1.52 in.	(3.86 cm)
Mean aerodynamic chord	3.67 in.	(9.32 cm)
Area	0.32 sq ft	(0.0297 m^2)
Aspect ratio		4.3
Taper ratio		0.29
S_t/S		0.17
Airfoil section		NACA 0009
Horizontal tail 2 (basic):		
Leading-edge sweep		38°
Span	16.12 in.	(40.95 cm)
Root chord	5.82 in.	(14.78 cm)

TABLE I.- GEOMETRIC CHARACTERISTICS OF MODEL COMPONENTS - Continued

Tip chord	1.67 in. (4.24 cm)
Mean aerodynamic chord	4.13 in. (10.49 cm)
Area	0.42 sq ft (0.0390 m^2)
Aspect ratio	4.3
Taper ratio	0.29
S_t/S	0.22
Airfoil section	NACA 0009
Horizontal tail 3:	
Leading-edge sweep	38°
Span	18.80 in. (47.75 cm)
Root chord	6.90 in. (17.53 cm)
Tip chord	2.00 in. (5.08 cm)
Mean aerodynamic chord	4.90 in. (12.45 cm)
Area	0.58 sq ft (0.0539 m^2)
Aspect ratio	4.3
Taper ratio	0.29
S_t/S	0.30
Airfoil section	NACA 0009
Horizontal tail 4:	
Leading-edge sweep	15°
Span	18.80 in. (47.75 cm)
Root chord	4.04 in. (10.26 cm)
Tip chord	4.04 in. (10.26 cm)
Mean aerodynamic chord	4.04 in. (10.26 cm)
Area	0.53 sq ft (0.0492 m^2)
Aspect ratio	4.6
Taper ratio	1.00
S_t/S	0.28
Airfoil section	NACA 0009
Auxiliary horizontal tail 1:	
Leading-edge sweep	60°
Span (not including body intercept)	3.66 in. (9.30 cm)
Root chord (at body juncture)	4.35 in. (11.05 cm)
Tip chord	2.00 in. (5.08 cm)
Mean aerodynamic chord	3.32 in. (8.43 cm)
Area (not including body intercept)	0.08 sq ft (0.0074 m^2)
Aspect ratio	1.2
Taper ratio	0.46
S_a/S	0.04
Airfoil section	NACA 0009

TABLE I.- GEOMETRIC CHARACTERISTICS OF MODEL COMPONENTS - Concluded

Auxiliary horizontal tail 2:	
Leading-edge sweep	60°
Span (not including body intercept)	5.90 in. (14.99 cm)
Root chord (at body juncture)	5.72 in. (14.53 cm)
Tip chord	2.00 in. (5.08 cm)
Mean aerodynamic chord	4.16 in. (10.57 cm)
Area (not including body intercept)	0.16 sq ft (0.0149 m^2)
Aspect ratio	1.5
Taper ratio	0.35
S_a/S	0.08
Airfoil section	NACA 0009
Auxiliary horizontal tail 3:	
Leading-edge sweep	60°
Span (not including body intercept)	7.80 in. (19.81 cm)
Root chord (at body juncture)	7.00 in. (17.78 cm)
Tip chord	2.00 in. (5.08 cm)
Mean aerodynamic chord	4.96 in. (12.60 cm)
Area (not including body intercept)	0.24 sq ft (0.0223 m^2)
Aspect ratio	1.8
Taper ratio	0.29
S_a/S	0.13
Airfoil section	NACA 0009
Vertical tail 1 (basic):	
Leading-edge sweep	38°
Area	0.36 sq ft (0.0334 m^2)
Airfoil section	NACA 0009
Nacelle 1:	
Length	8.13 in. (20.65 cm)
Maximum diameter	2.00 in. (5.08 cm)
Inlet diameter	1.25 in. (3.18 cm)
Exit diameter	1.25 in. (3.18 cm)
Nacelle 2:	
Length	9.15 in. (23.24 cm)
Maximum diameter	2.30 in. (5.84 cm)
Inlet diameter	1.50 in. (3.81 cm)
Exit diameter	1.50 in. (3.81 cm)
Nacelle 3:	
Length	11.44 in. (29.06 cm)
Maximum diameter	2.88 in. (7.32 cm)
Inlet diameter	1.75 in. (4.45 cm)
Exit diameter	1.75 in. (4.45 cm)

TABLE II.- ORDINATES OF HIGH-LIFT DEVICES USED ON WING 2

x/c	z_u/c	z_l/c
Slat		
0	0	0
.01000	.03076	-.02823
.02000	.04100	-.04107
.05000	.05923	-.05384
.07500	.07461	-.05884
.10000	.08153	-.05653
.15000	.09000	-.04100
.20000	.09230	-.02561
.30000	.09230	0
.40000	.08730	.02046
.50000	.08461	.02576
.60000	.07192	.02823
.70000	.05615	.02576
.80000	.04615	.01538
.90000	.02823	.01030
1.00000	.01030	0
Vane		
0	0	0
.01250	.03796	-.02685
.02500	.05203	-.03388
.05000	.07407	-.04092
.07500	.09027	-.04472
.10000	.10972	-.04398
.15000	.12685	-.03796
.20000	.14444	-.02962
.30000	.16296	-.01407
.40000	.16666	.00100
.50000	.16018	.01796
.60000	.14444	.03009
.70000	.11712	.03194
.80000	.08333	.03009
.90000	.04500	.01796
.95000	.02601	.01074
1.00000	0	0

TABLE II.- ORDINATES OF HIGH-LIFT DEVICES USED ON WING 2 - Concluded

x/c	z_u/c	z_l/c
Flap		
0	0.04306	0.04305
.01000	.06805	.01833
.02500	.09166	.01078
.05000	.11018	.00666
.07500	.12314	0
.10000	.13101	0
.15000	.14074	0
.20000	.14722	0
.30000	.14722	0
.40000	.13472	0
.50000	.11805	0
.60000	.09444	0
.70000	.07824	0
.80000	.04907	0
.90000	.02615	0
.95000	.01226	0
1.00000	0	0

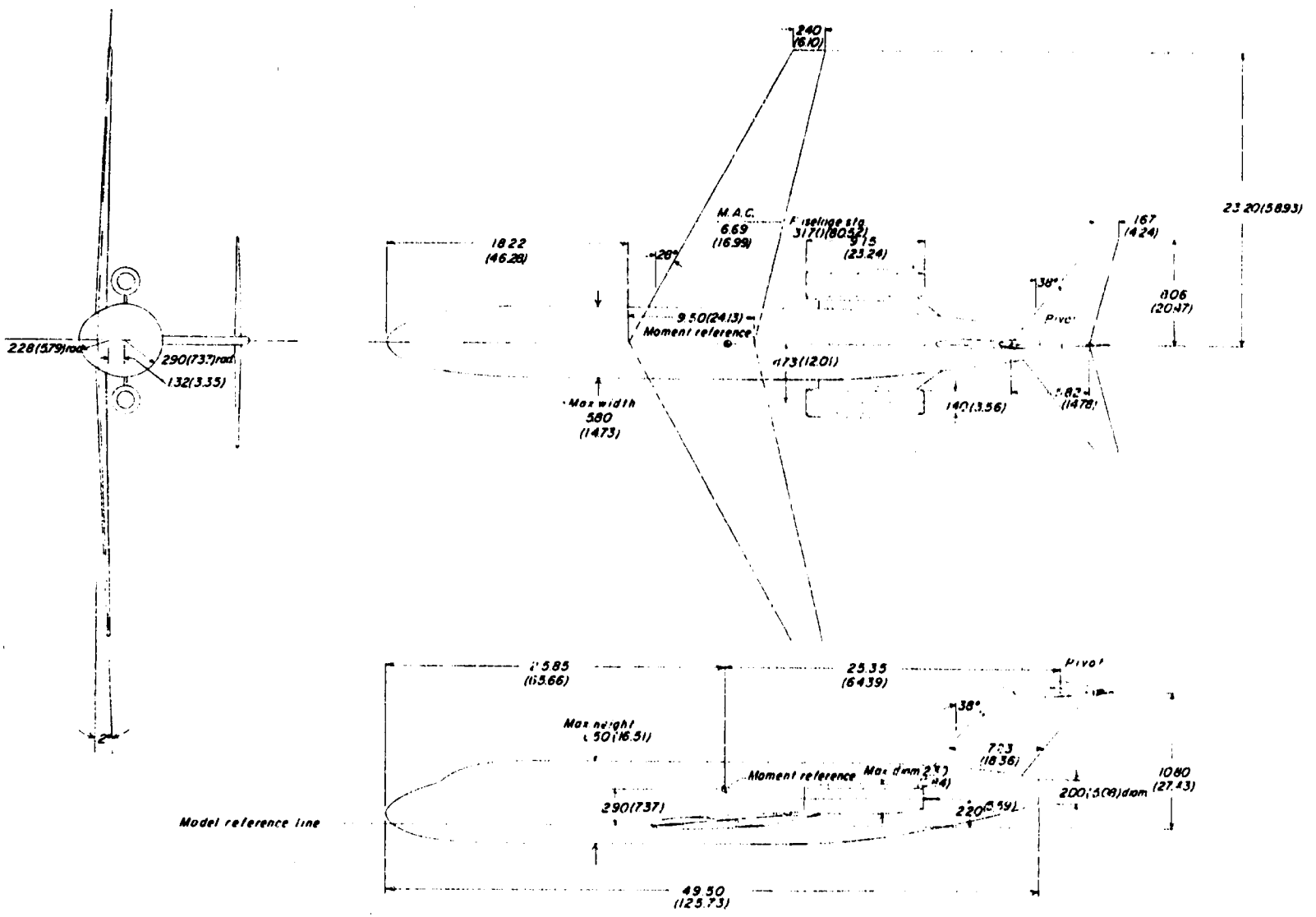

(a) Three-view drawing of basic configuration $B_1V_1W_1N_2H_2$.

Figure 1.- Details of models. All linear dimensions are in inches (centimeters).

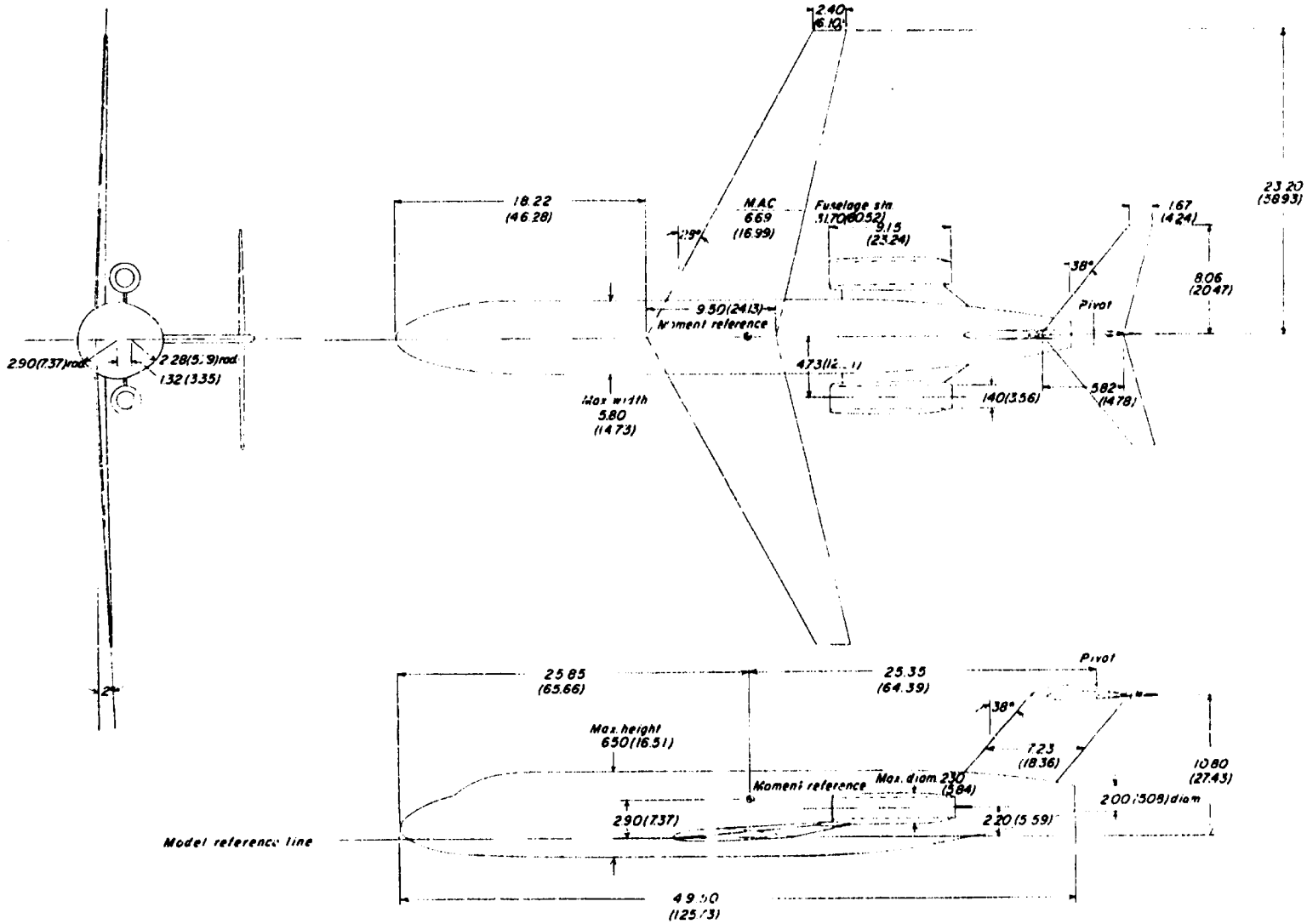

(b) Three-view drawing of configuration $B_2V_1W_1N_2H_2$.

Figure 1.- Continued.

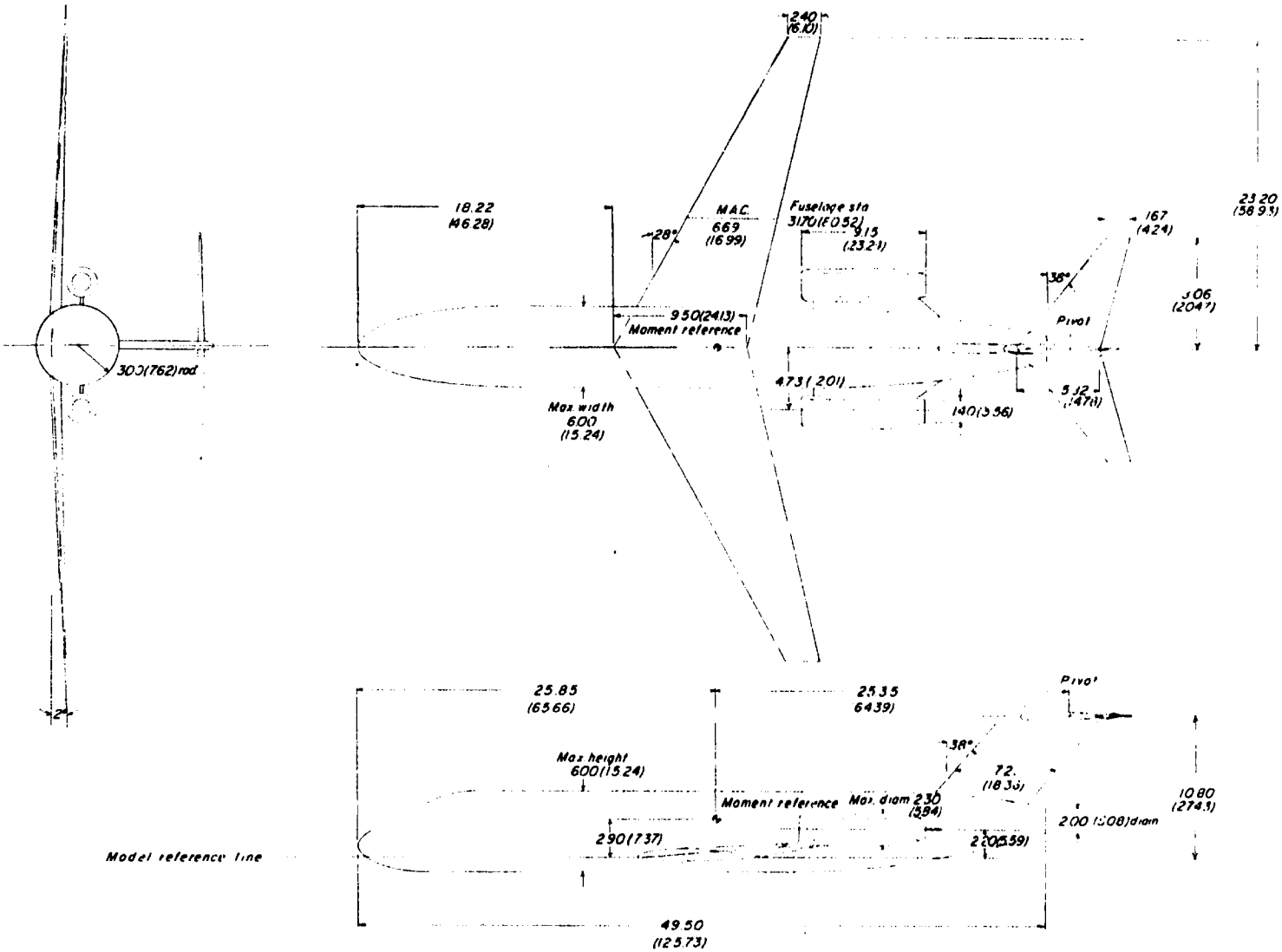

(c) Three-view drawing of configuration $B_3V_1W_1N_2H_2$.

Figure 1.- Continued.

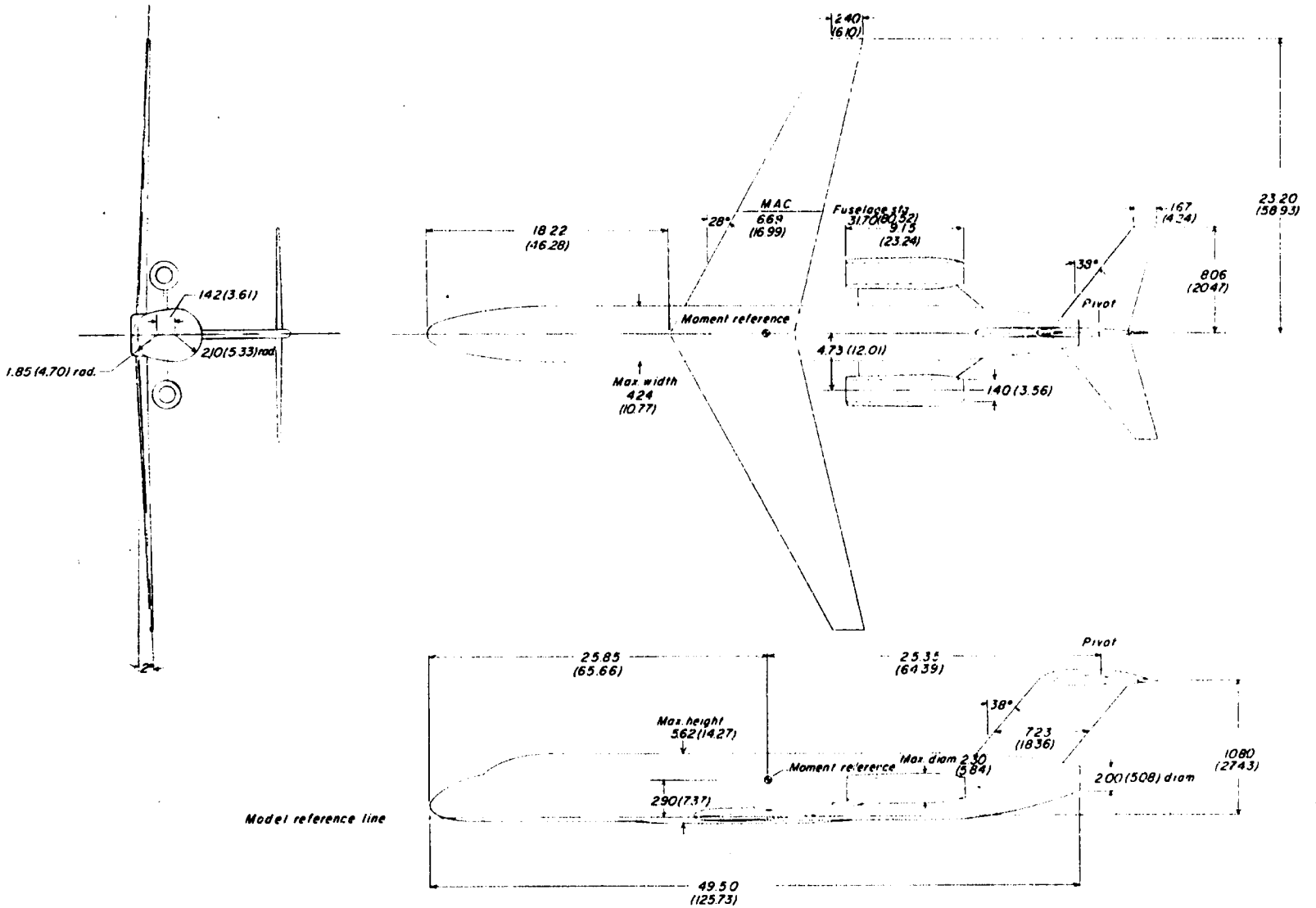

(d) Three-view drawing of configuration $B_4V_1W_1N_2H_2$.

Figure 1.- Continued.

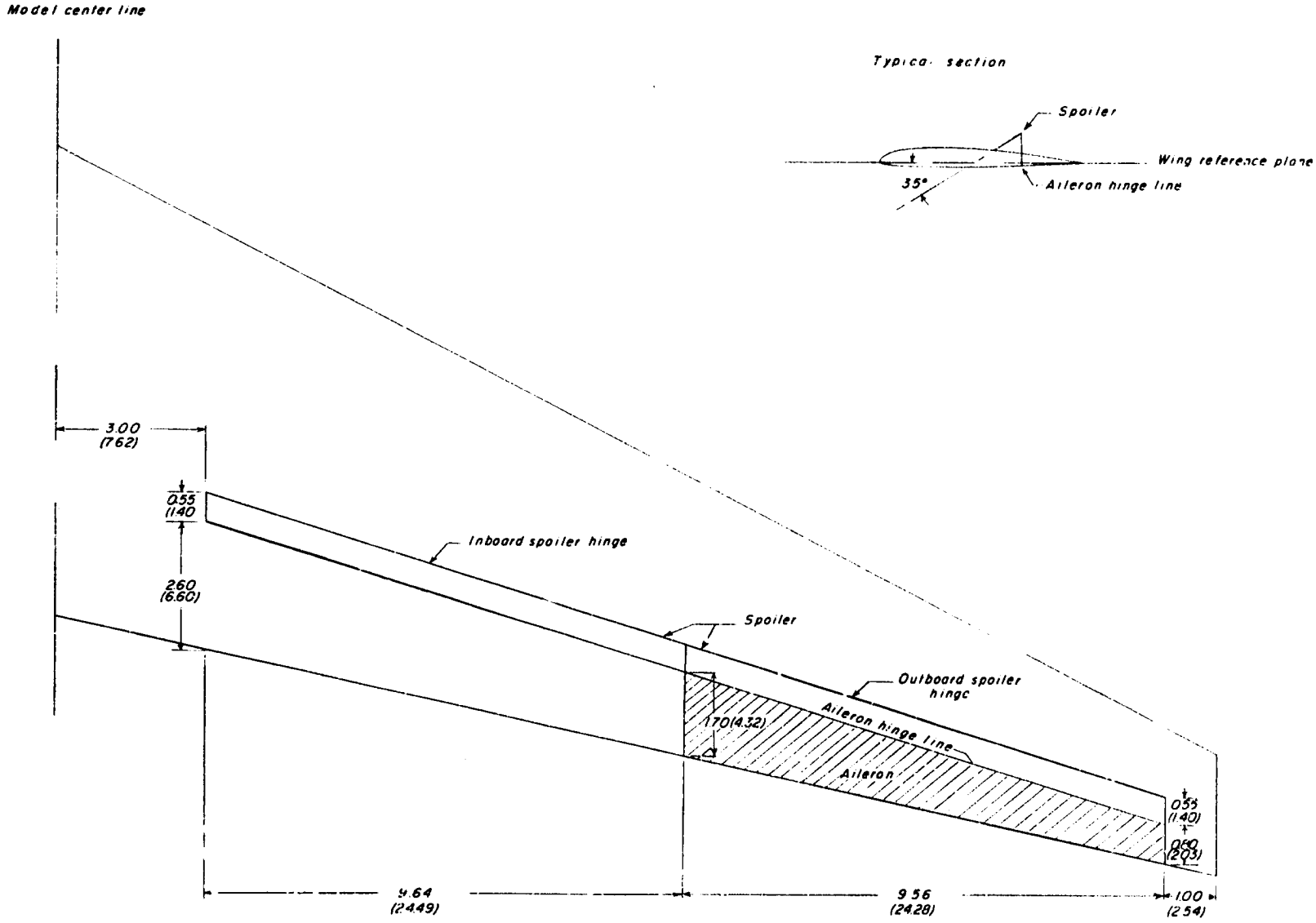

(e) Details of aileron and spoiler on right panel of wing 1.

Figure 1.- Continued.

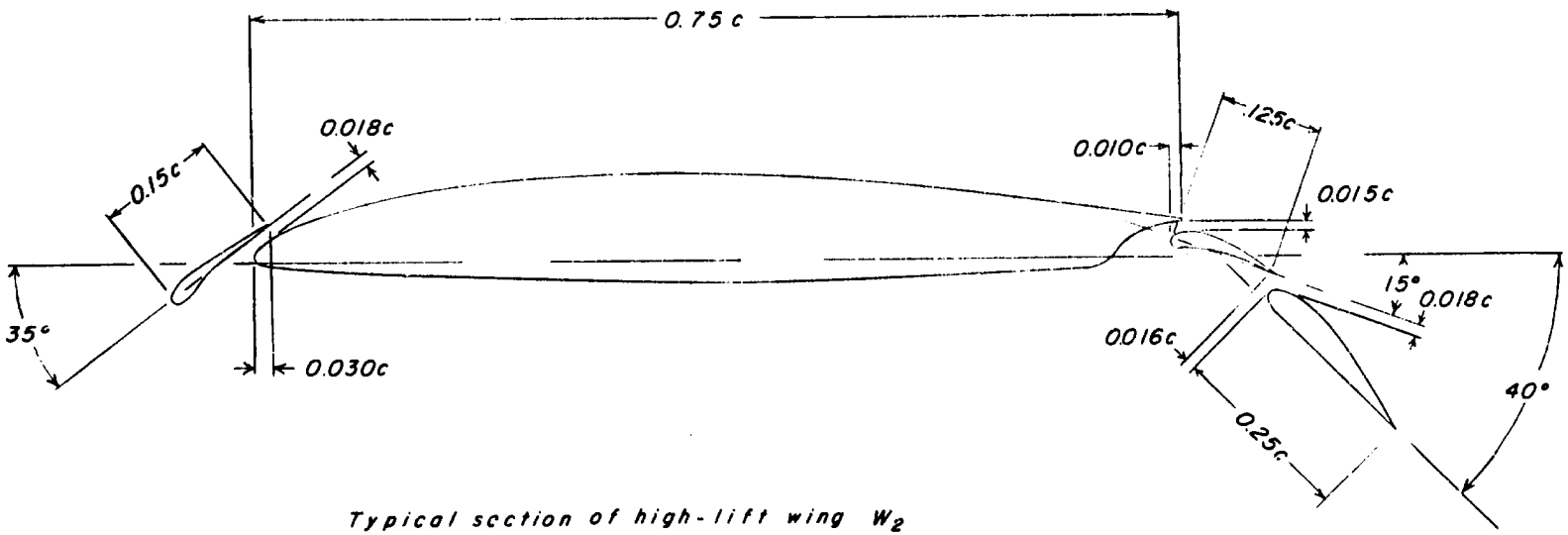

Typical section of high-lift wing W_2

(f) Details of wing high-lift devices.

Figure 1.- Continued.

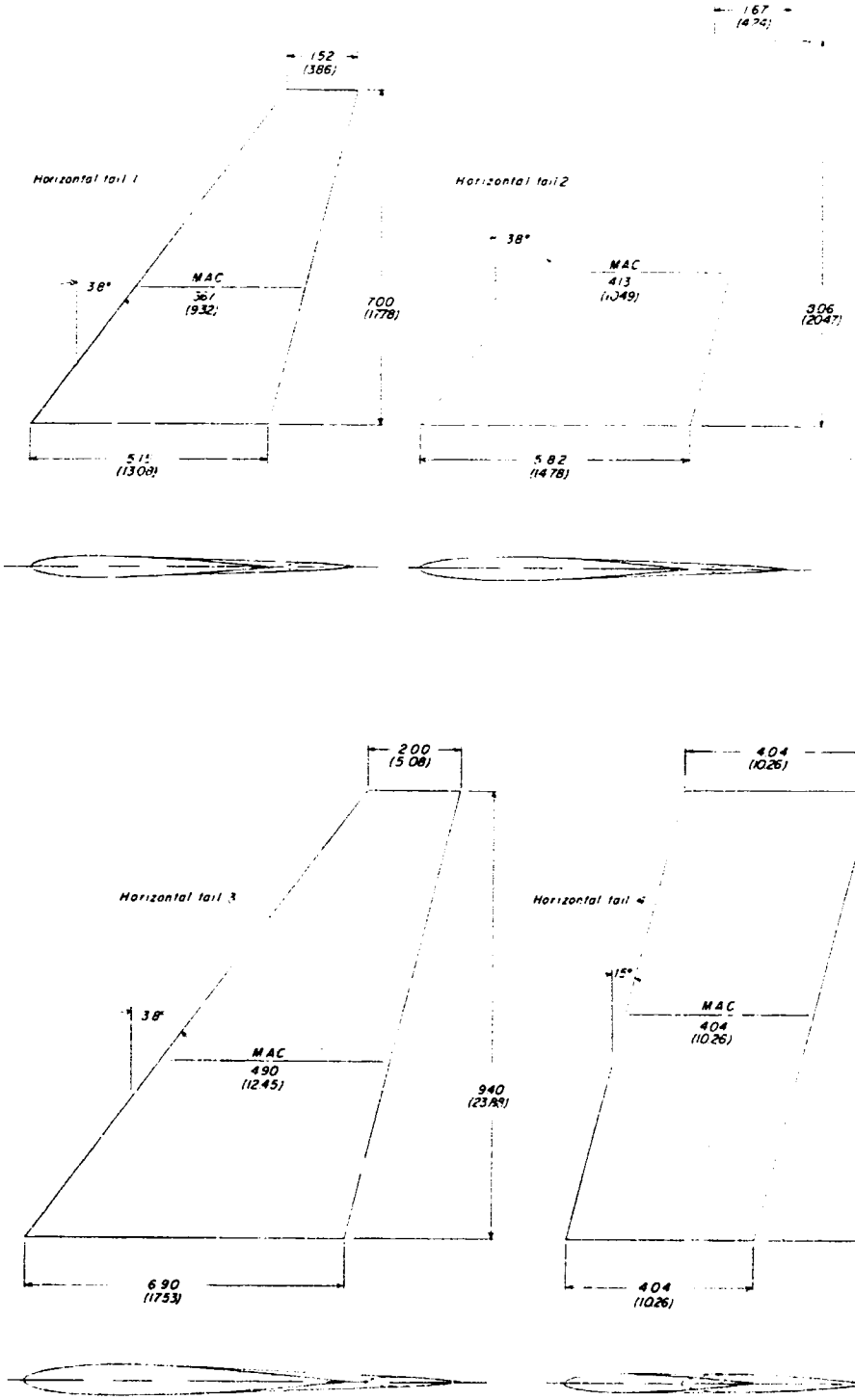

(g) Details of horizontal tails.

Figure 1.- Continued.

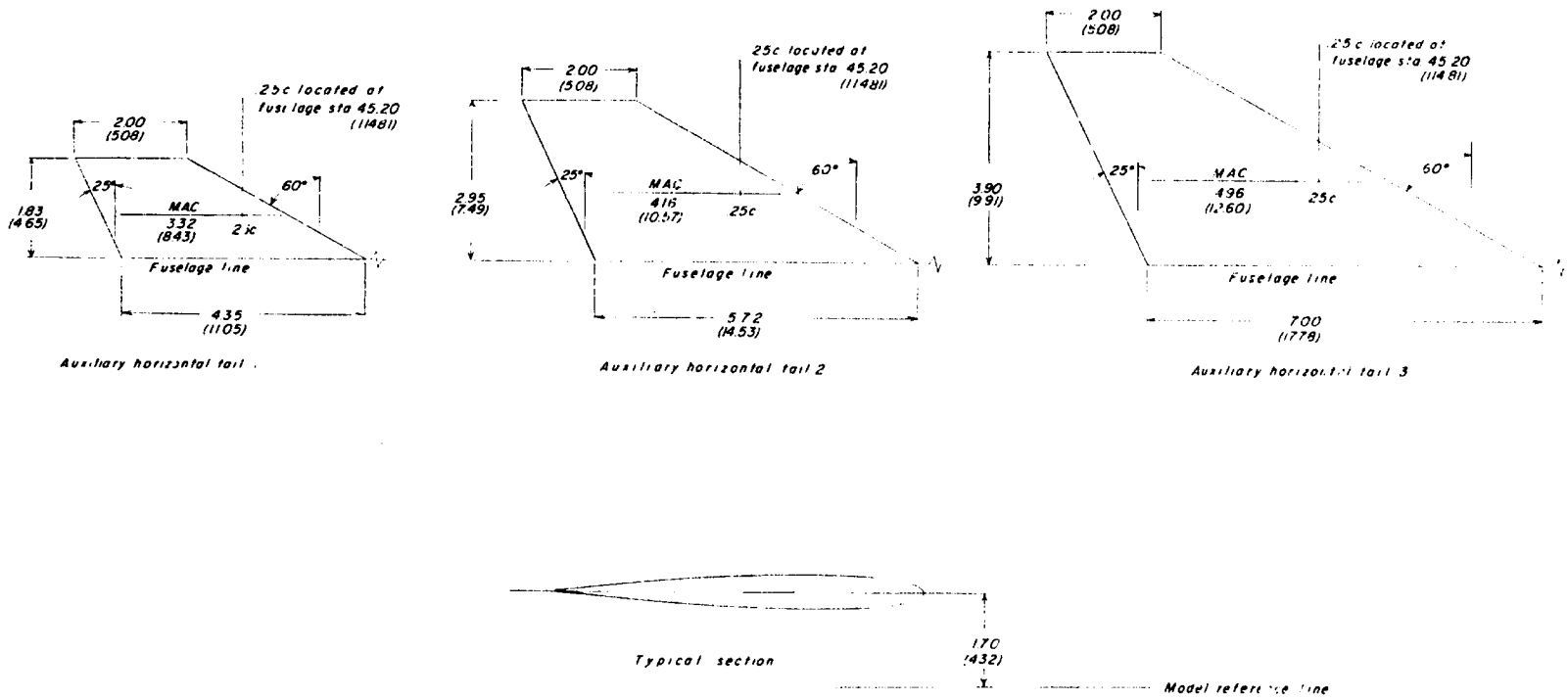

(h) Details of auxiliary horizontal tails.

Figure 1.- Continued.

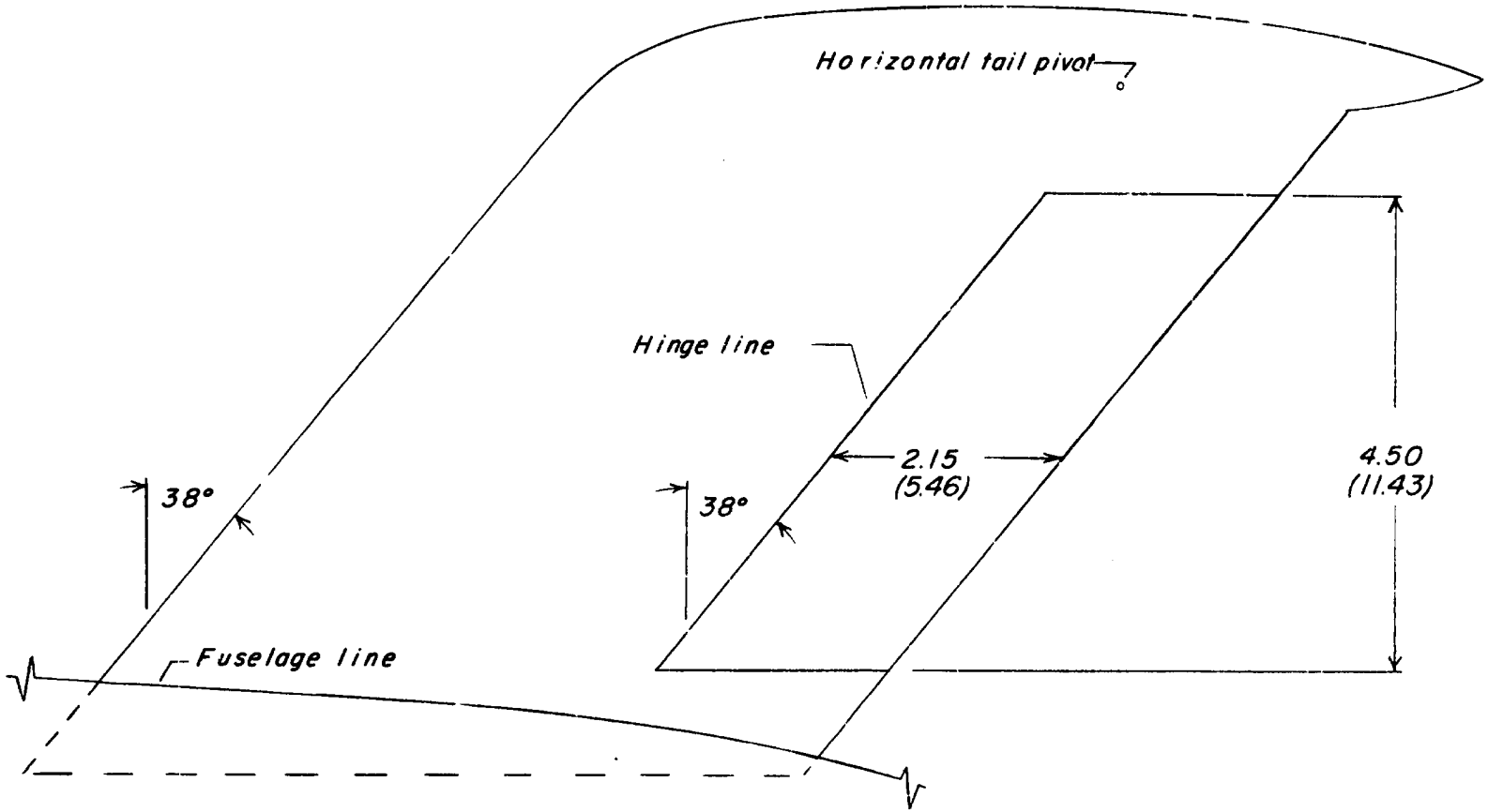

(i) Details of rudder.

Figure 1.- Continued.

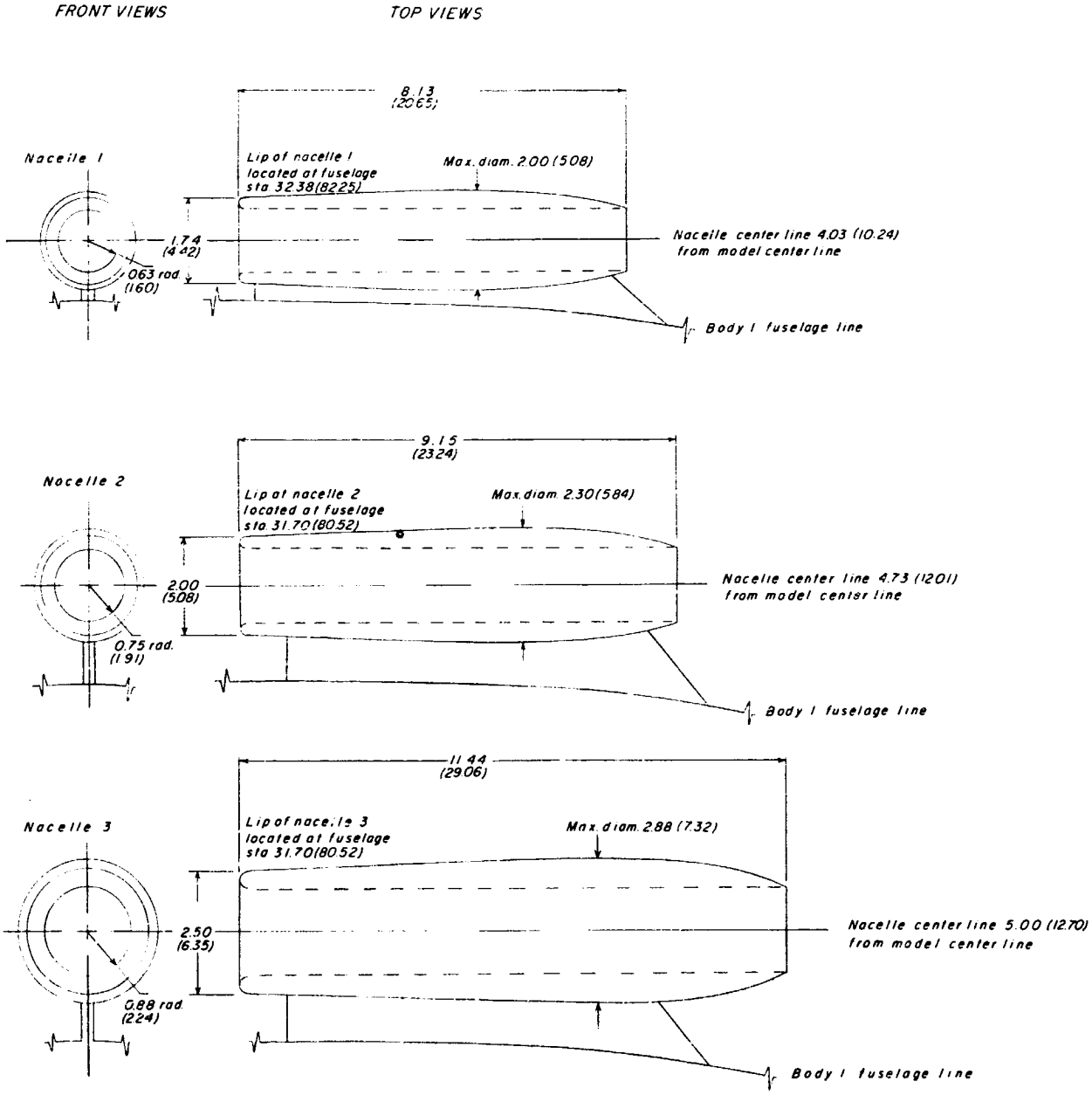

(j) Details of nacelles.

Figure 1.- Continued.

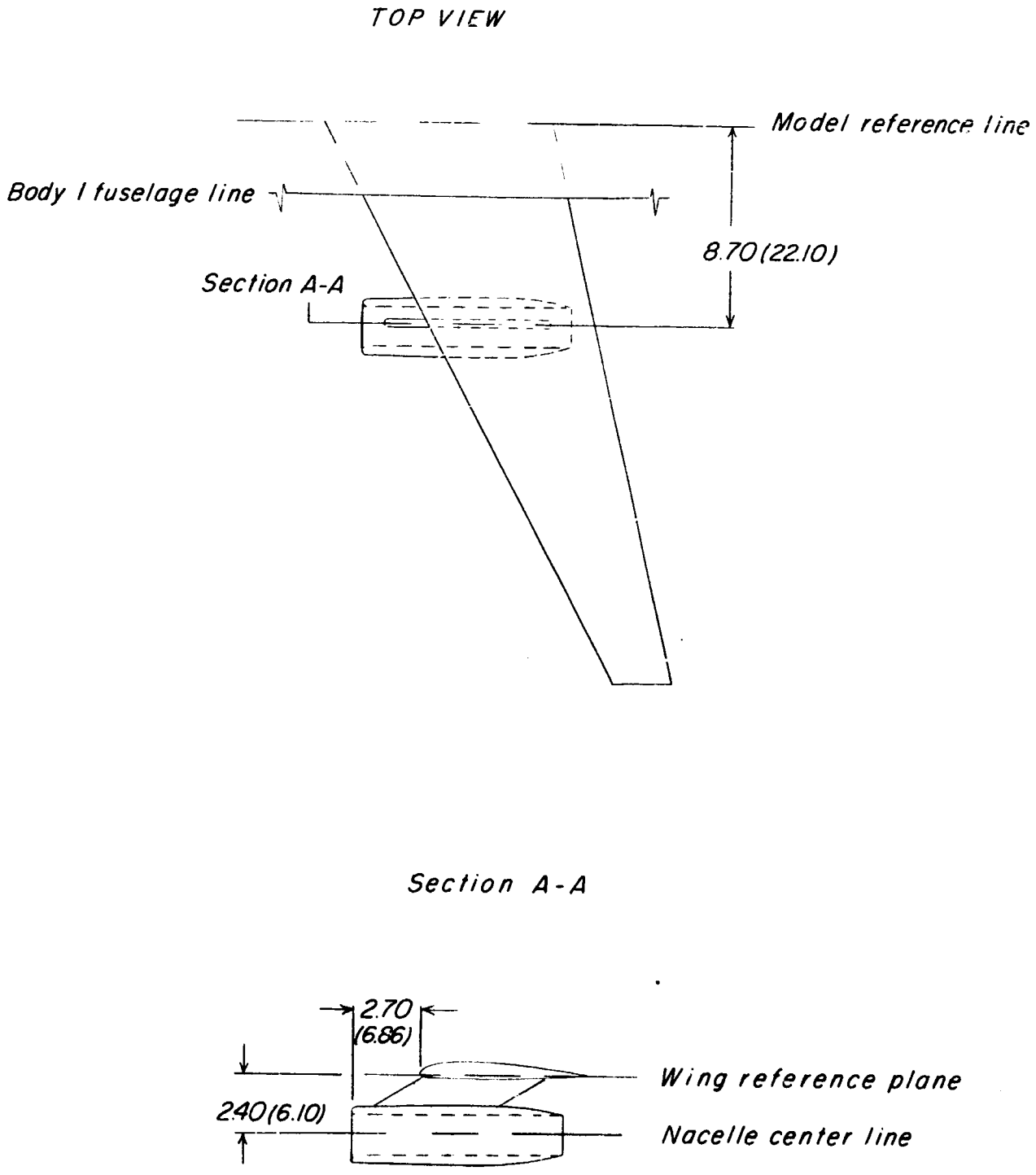

(k) Nacelle 2 in wing-mounted position.

Figure 1.- Continued.

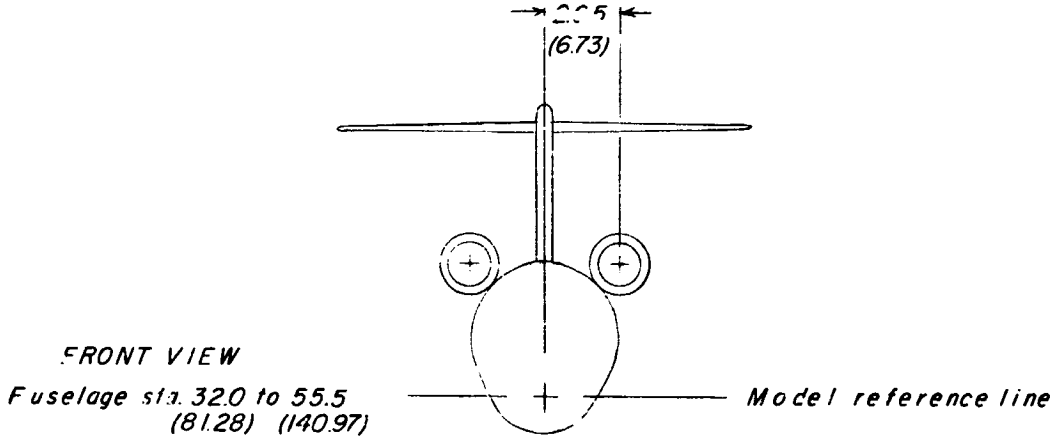

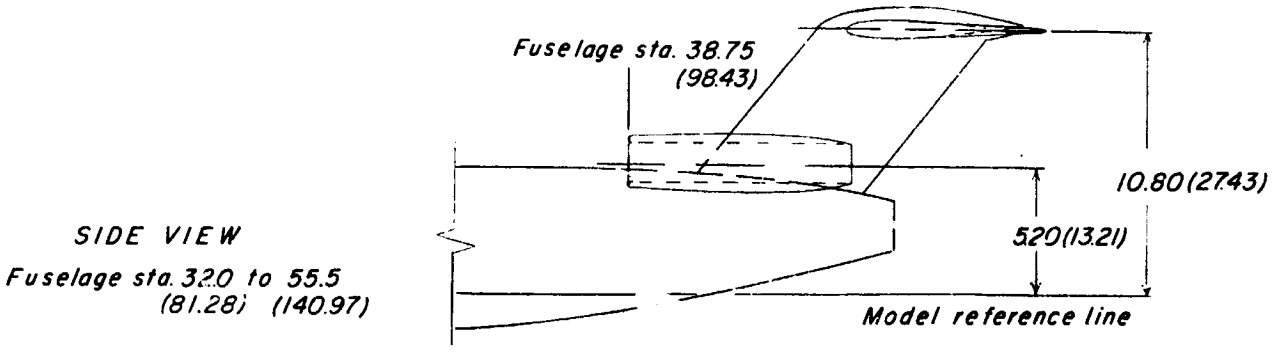

(l) Nacelle 2 in aft position on body 1.

Figure 1.- Continued.

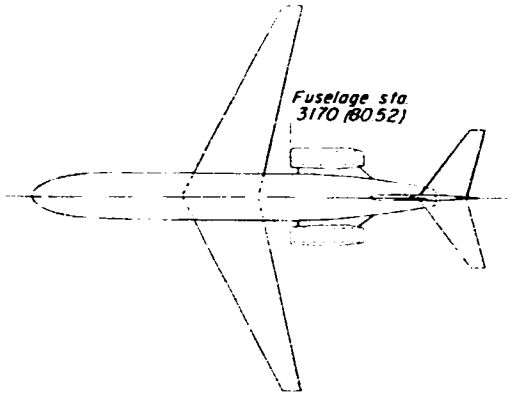

Basic configuration

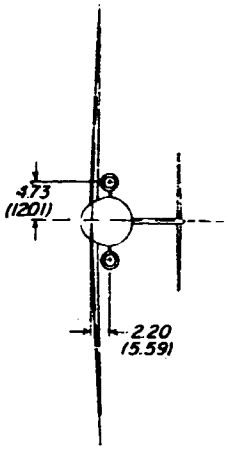

Typical front view

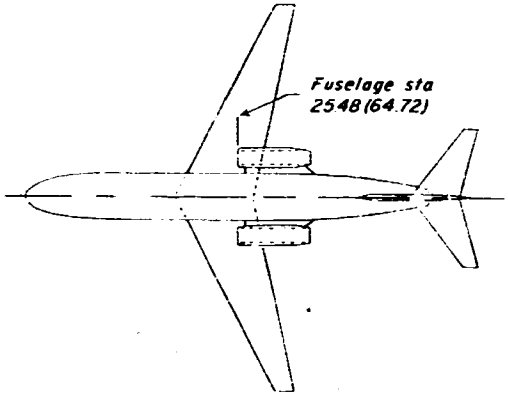

Configuration with nacelles moved forward 0.93$\bar{c}$

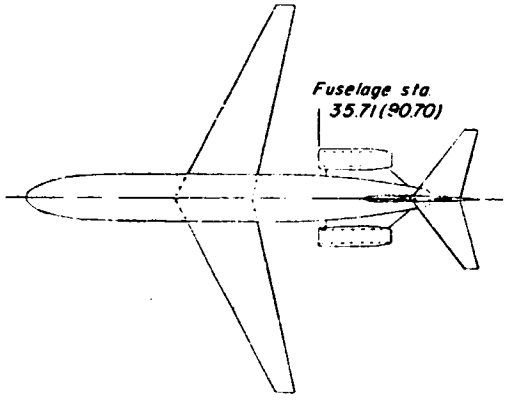

Configuration with nacelles moved aft 0.60$\bar{c}$

(m) Various longitudinal positions of nacelle 2 on body 1.

Figure 1.- Concluded.

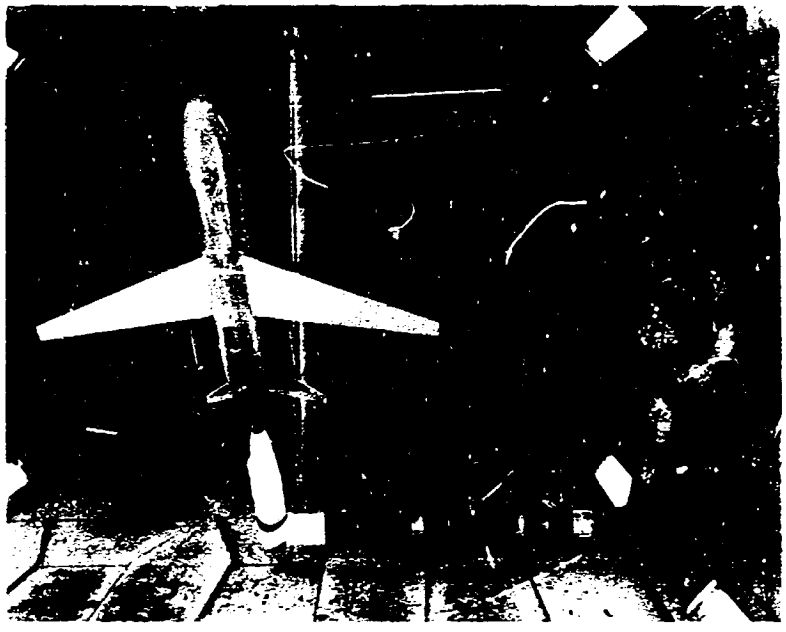

L-64-9083

(a) Basic configuration in Langley high-speed 7- by 10-foot tunnel.

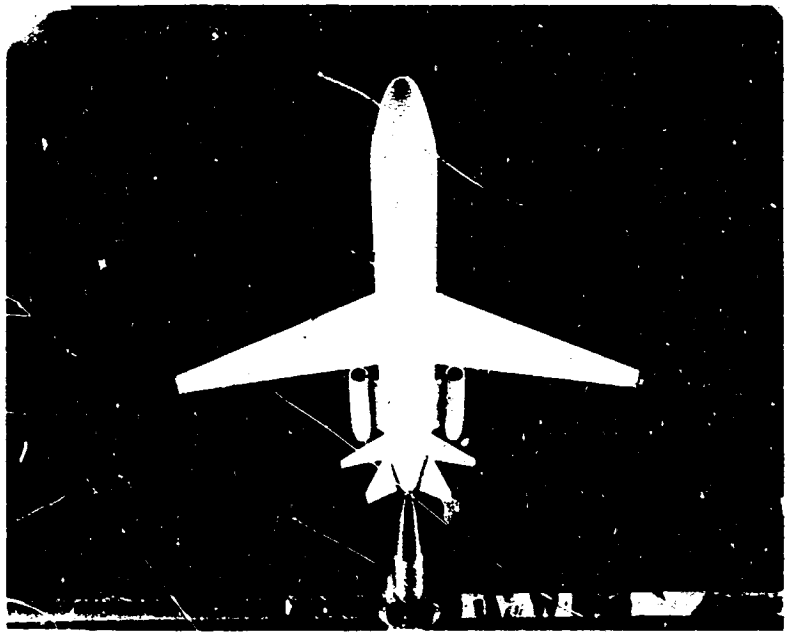

L-64-10,850

(b) Basic configuration with large auxiliary horizontal tail in Langley transonic dynamics tunnel.

Figure 2.- Photographs of basic configuration $B_1V_1W_1H_2N_2$ with and without auxiliary horizontal tails.

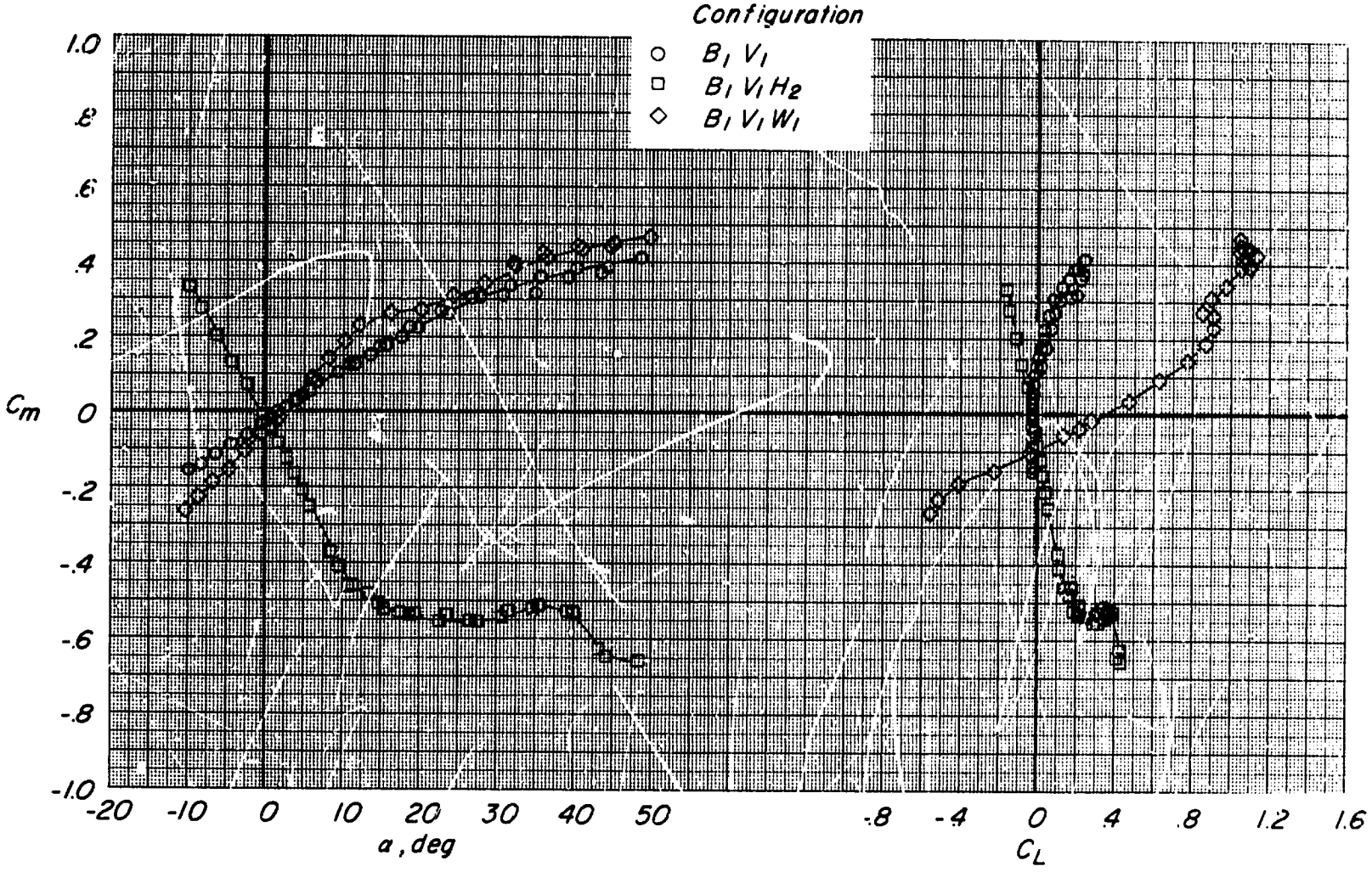

(a) Body 1 with various components.

Figure 3.- Effect of model components on longitudinal aerodynamic characteristics.
M = 0.21; R = 0.78 x 10^6.

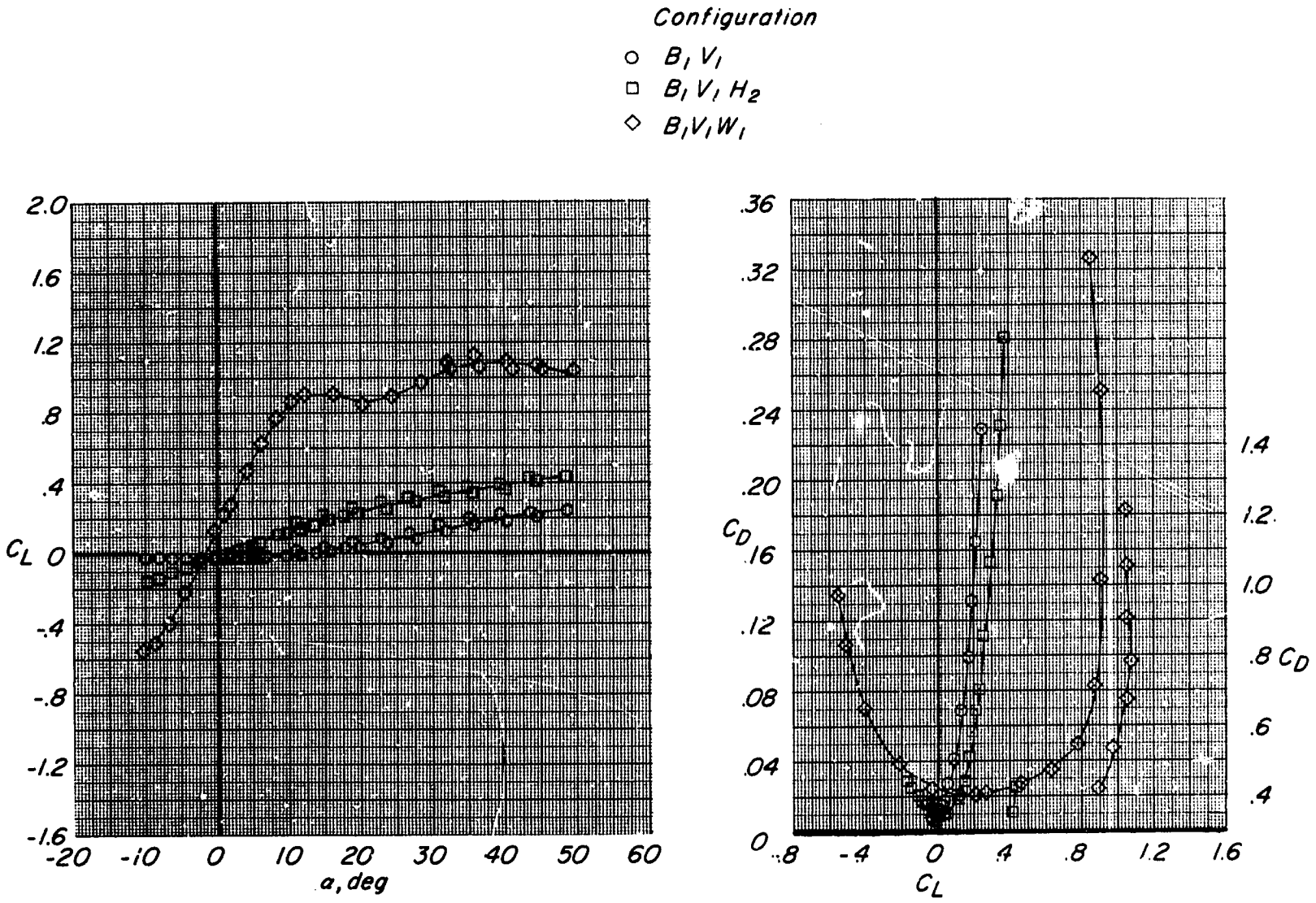

(a) Continued.

Figure 3.- Continued.

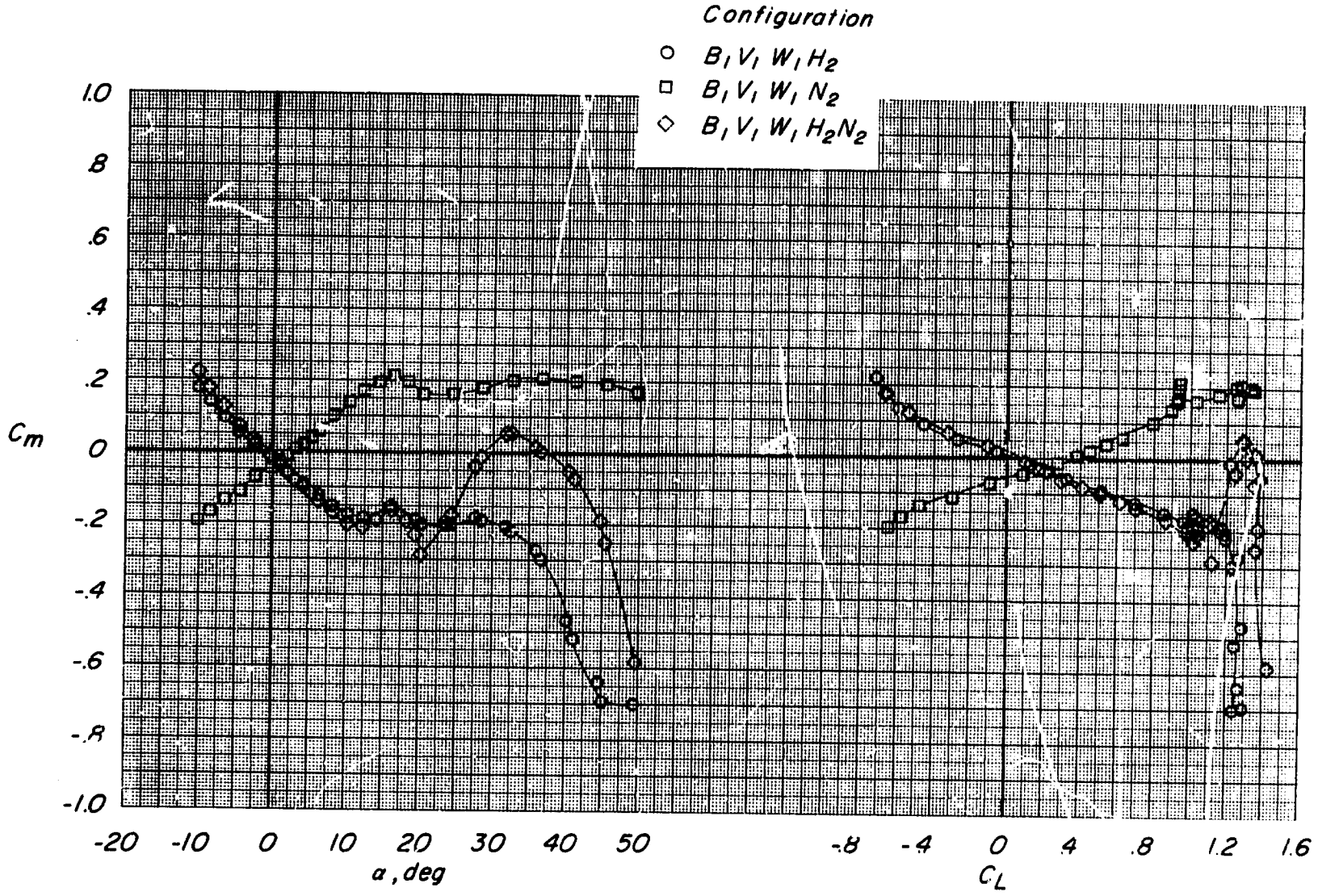

(a) Continued.

Figure 3.- Continued.

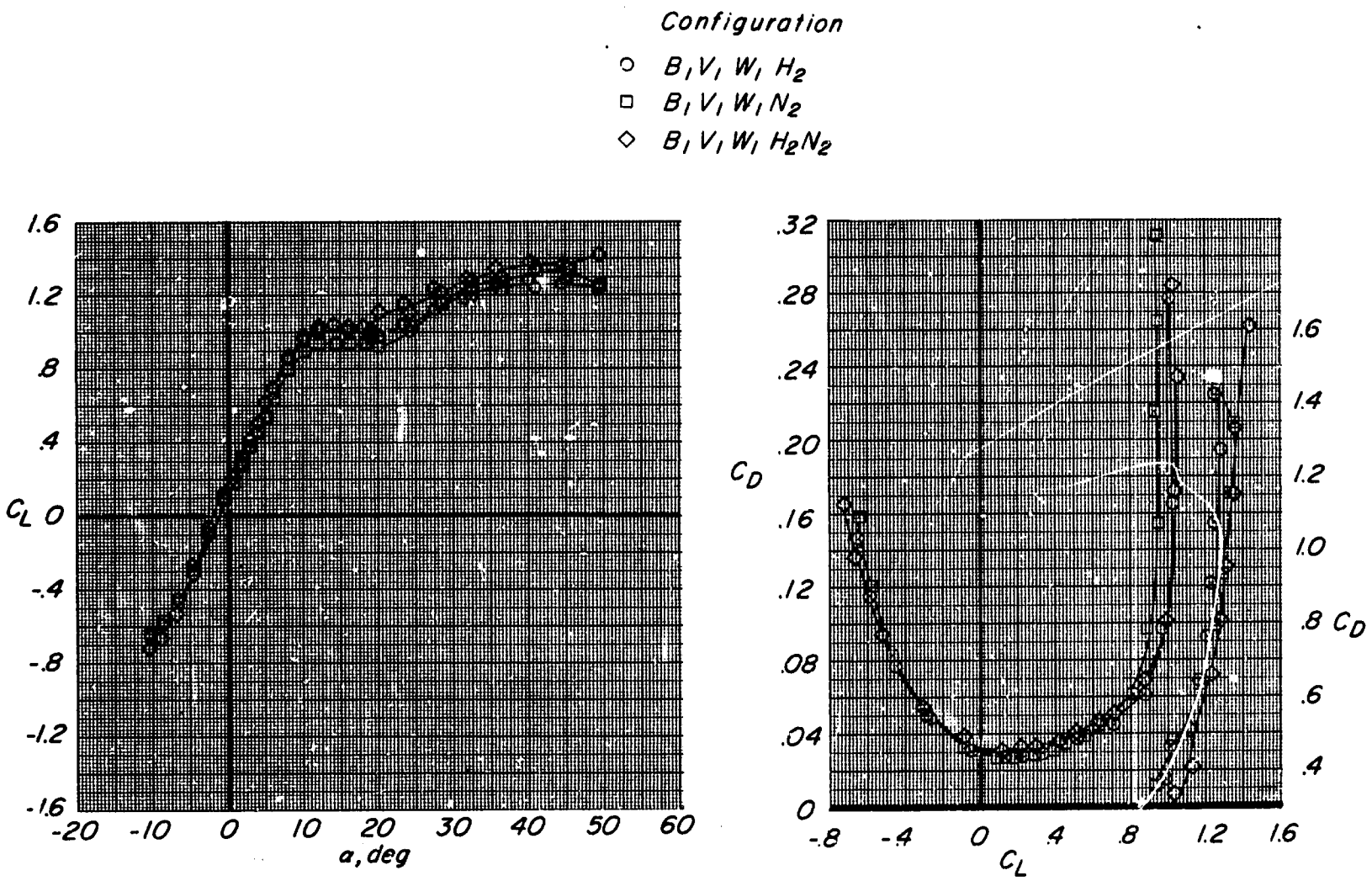

(a) Concluded.

Figure 3.- Continued.

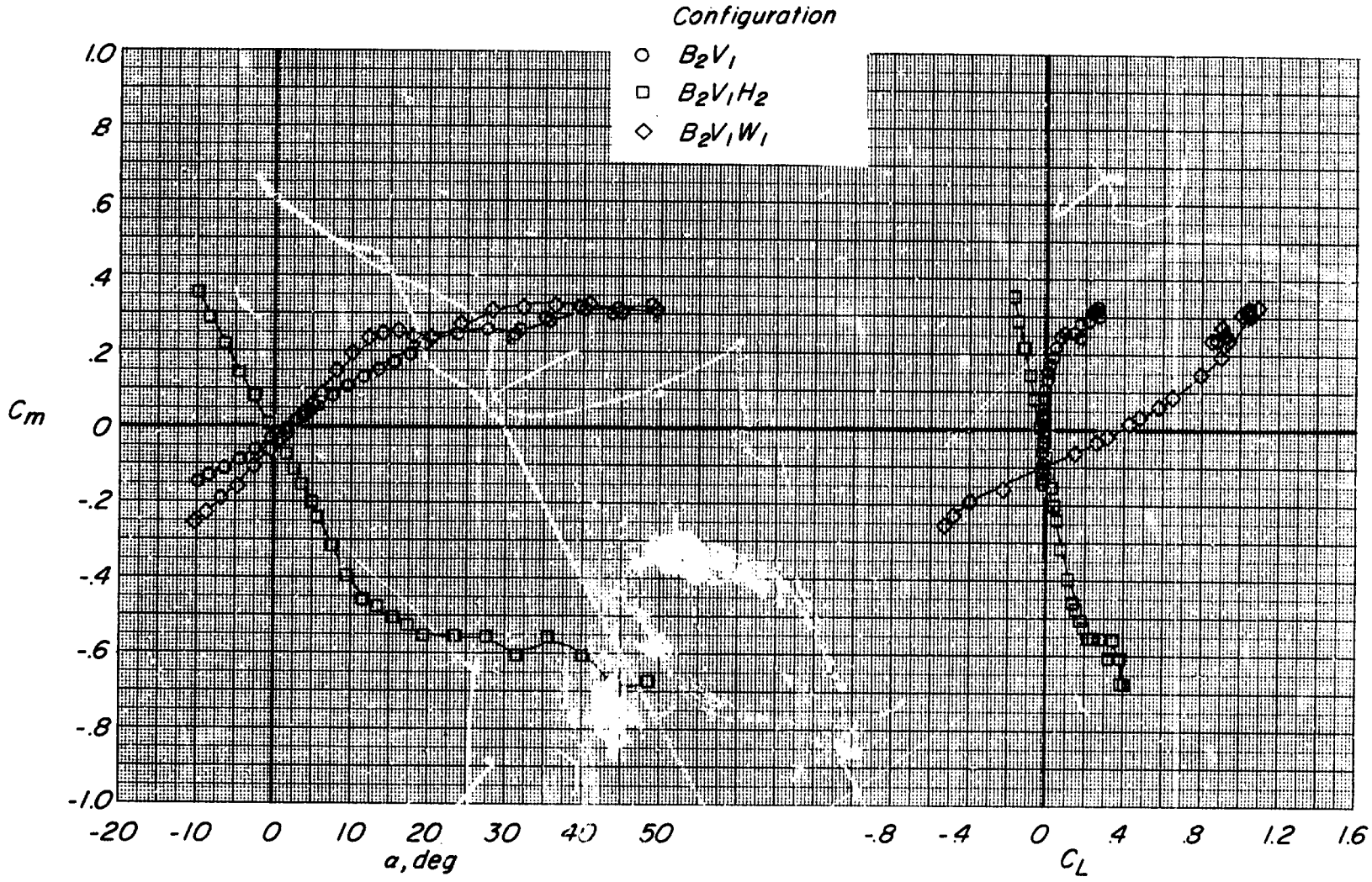

(b) Body 2 with various components.

Figure 3.- Continued.

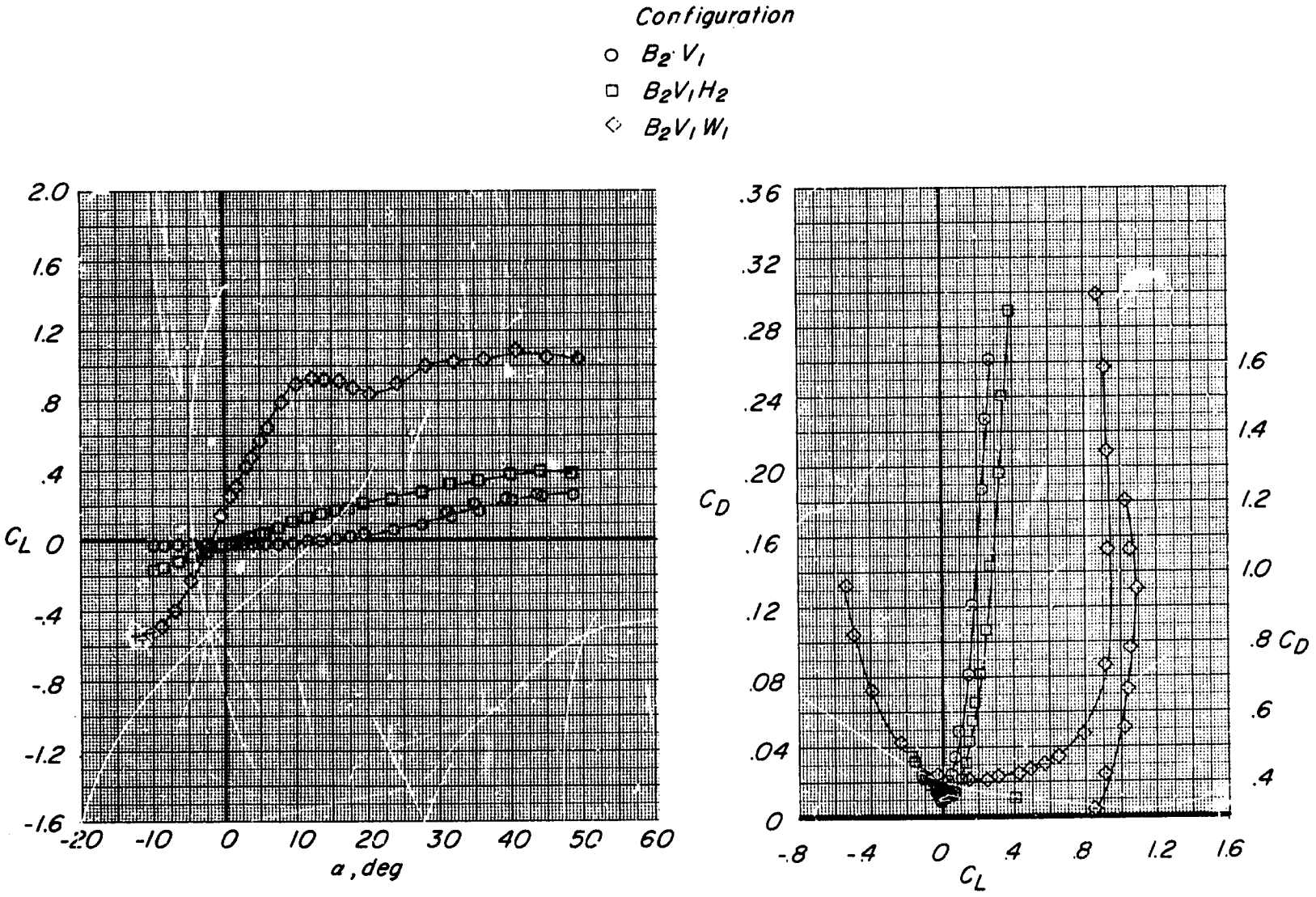

(b) Continued.

. Figure 3.- Continued.

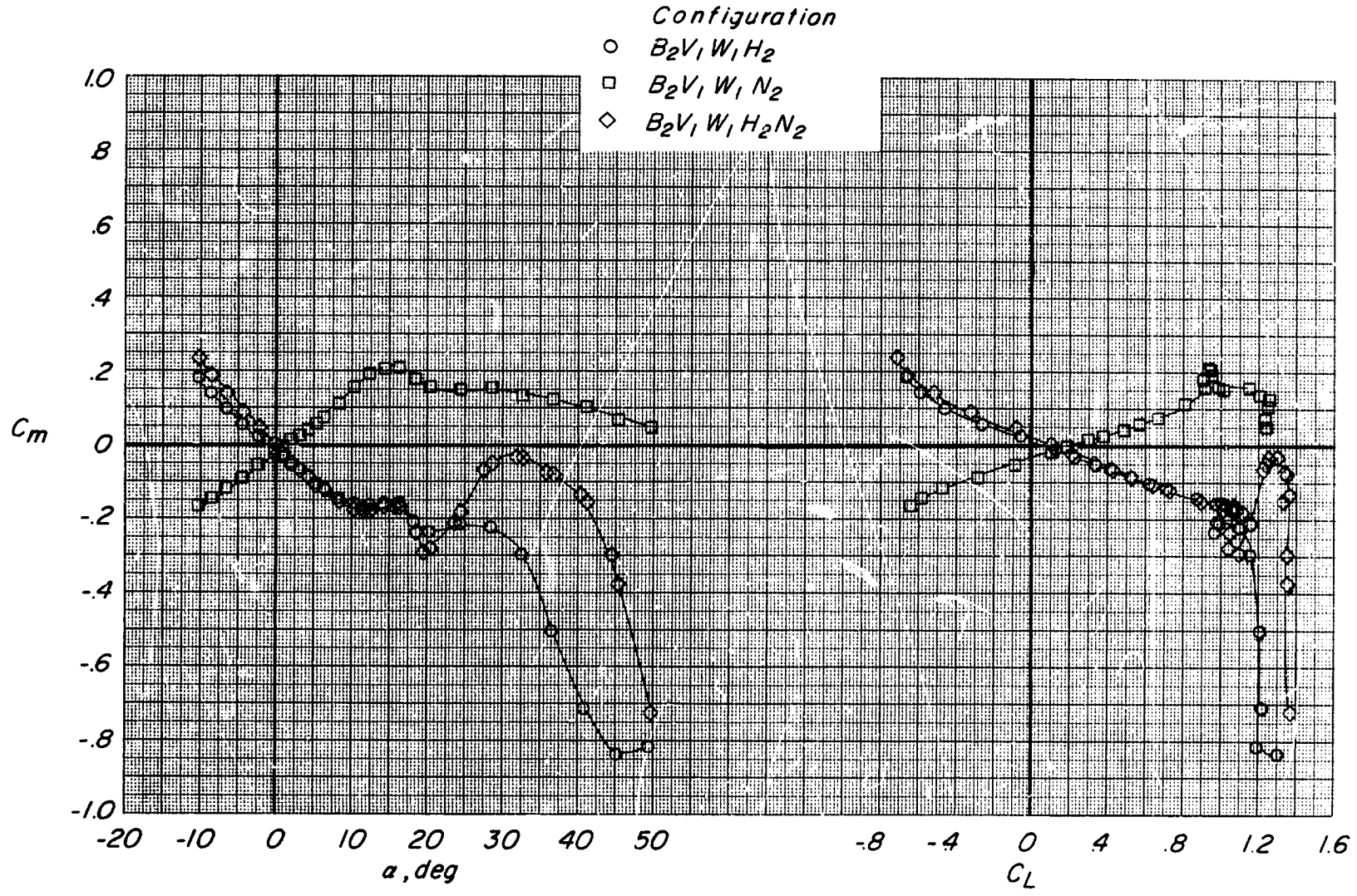

(b) Continued.

Figure 3.- Continued.

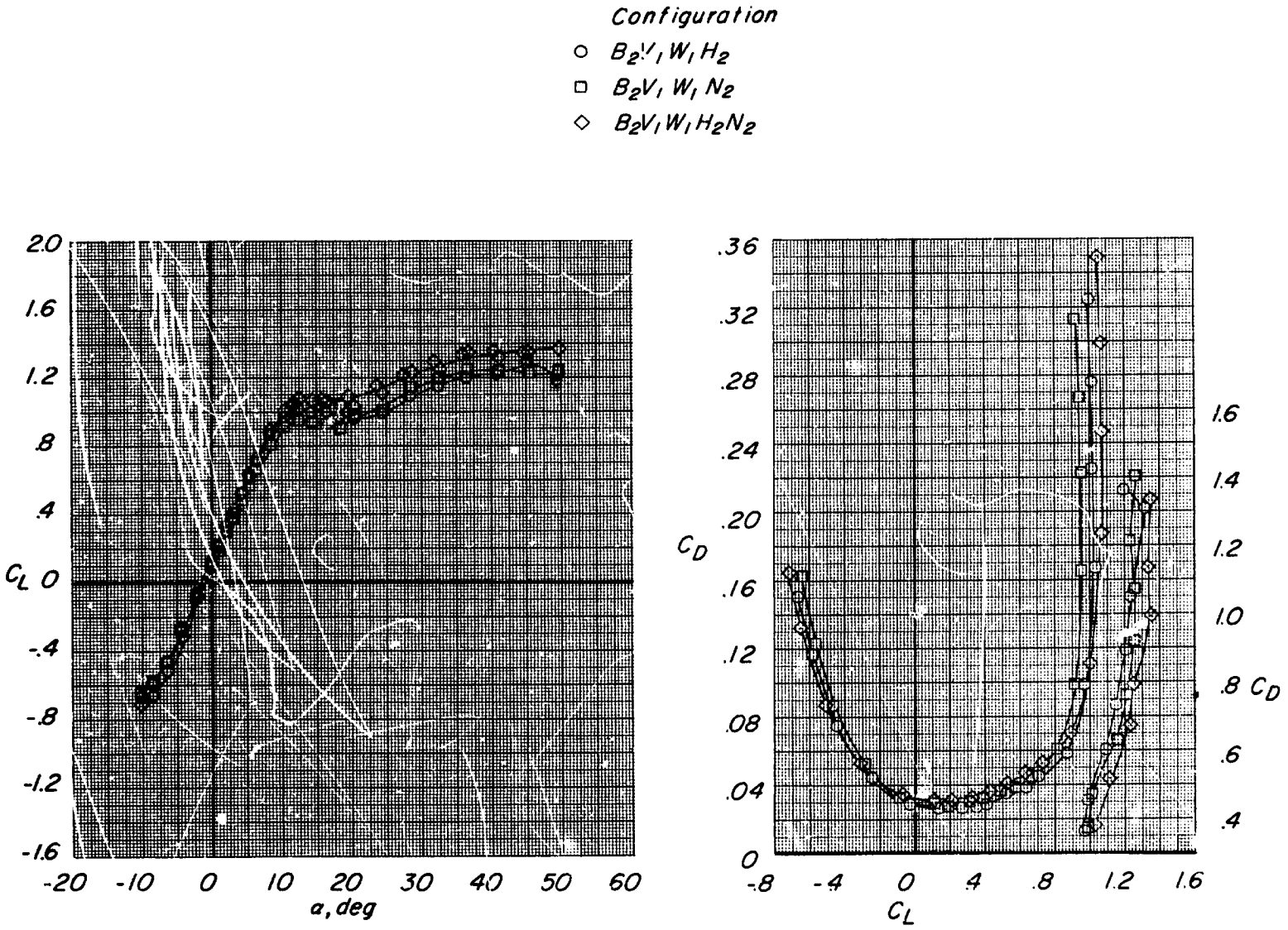

(b) Concluded.

Figure 3.- Continued.

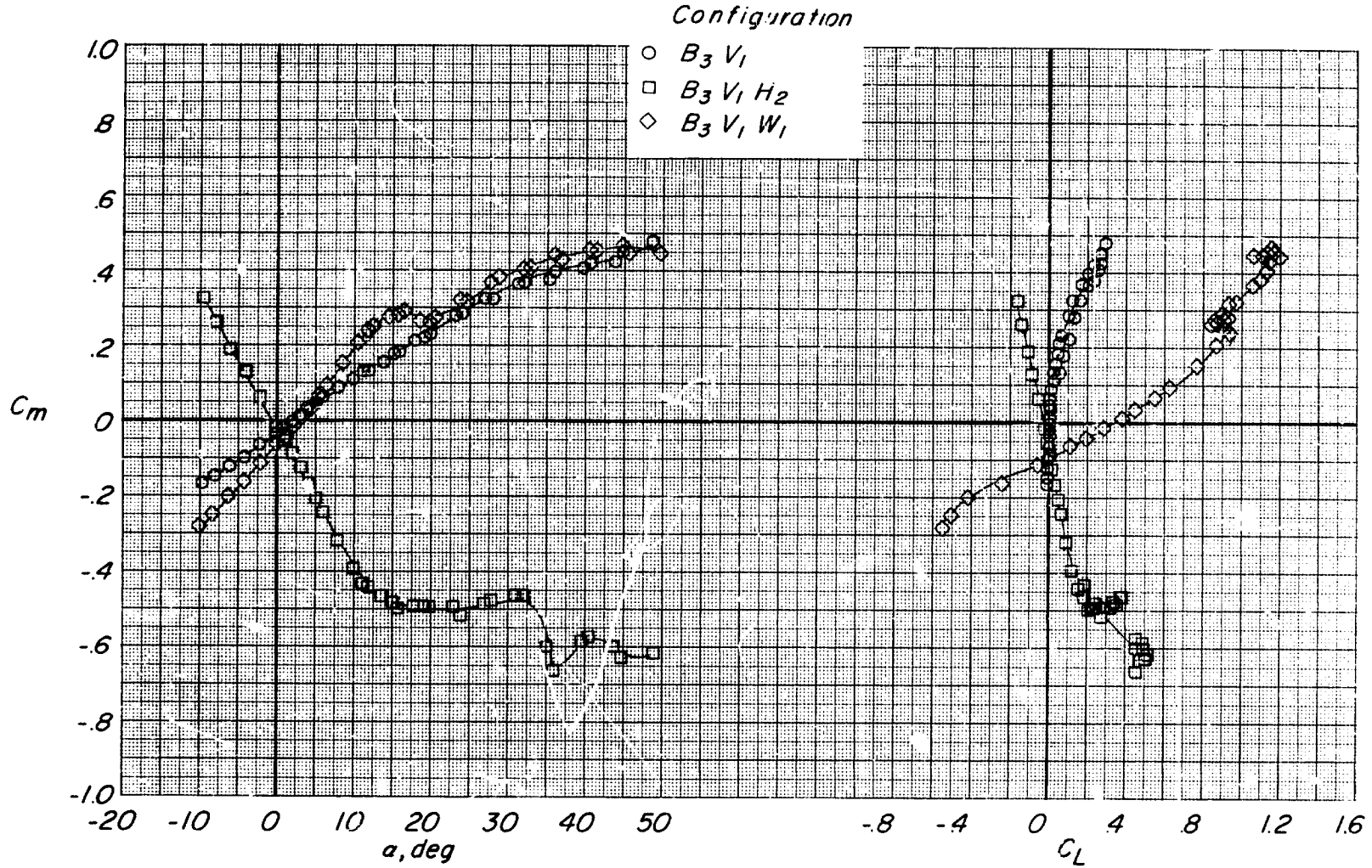

(c) Body 3 with various components.

Figure 3.- Continued.

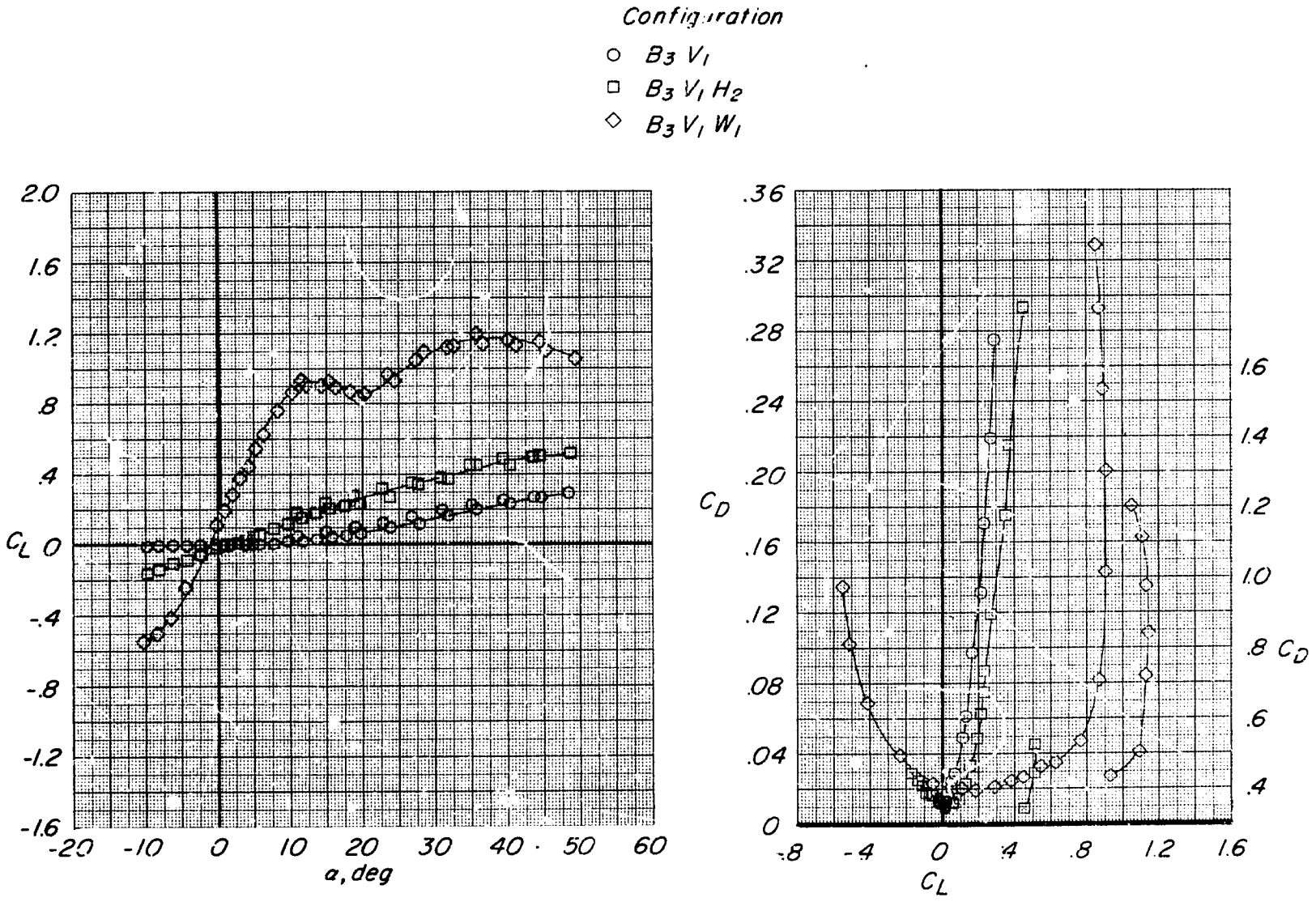

(c) Continued.

Figure 3.- Continued.

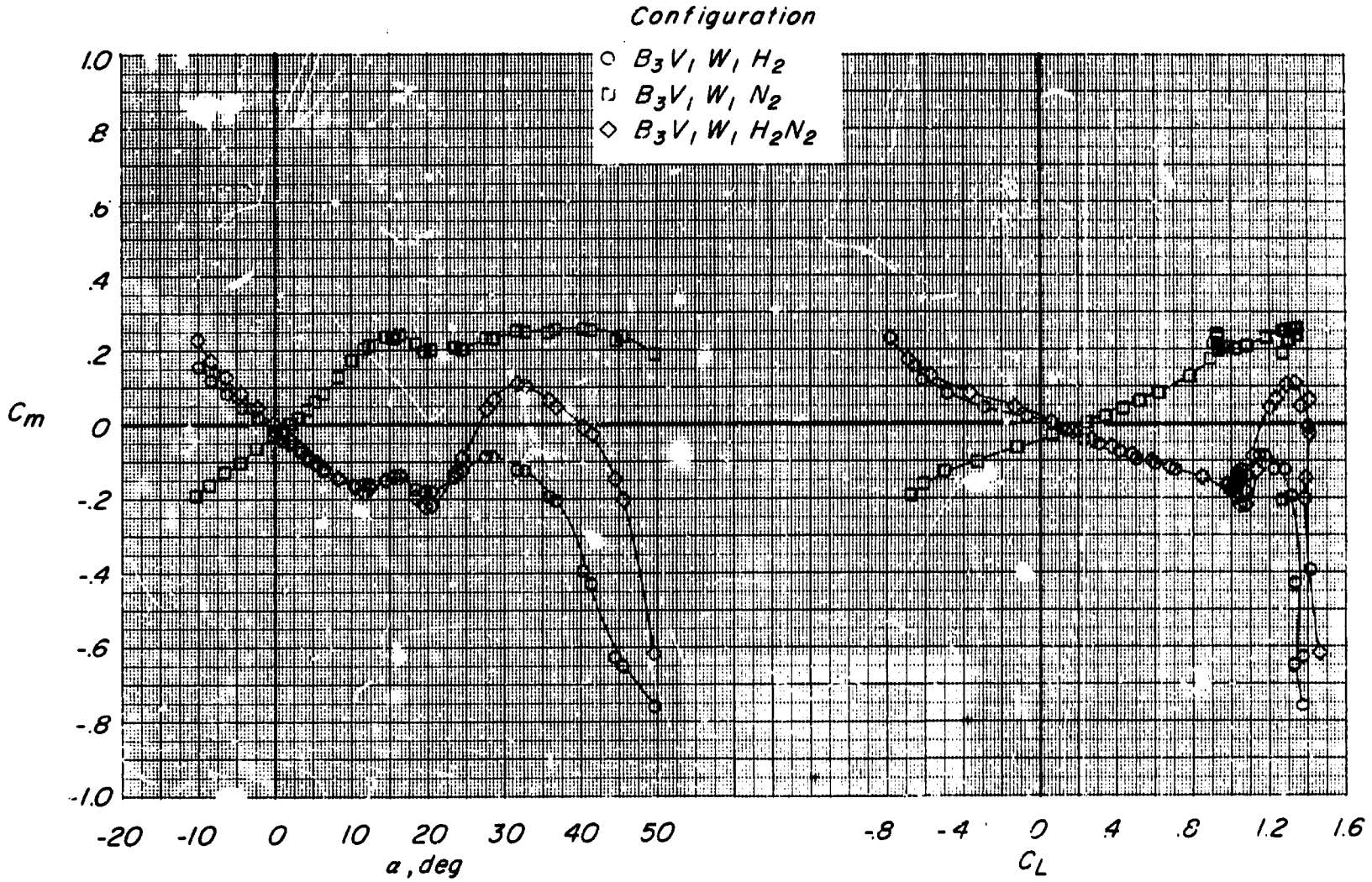

(c) Continued.

Figure 3.- Continued.

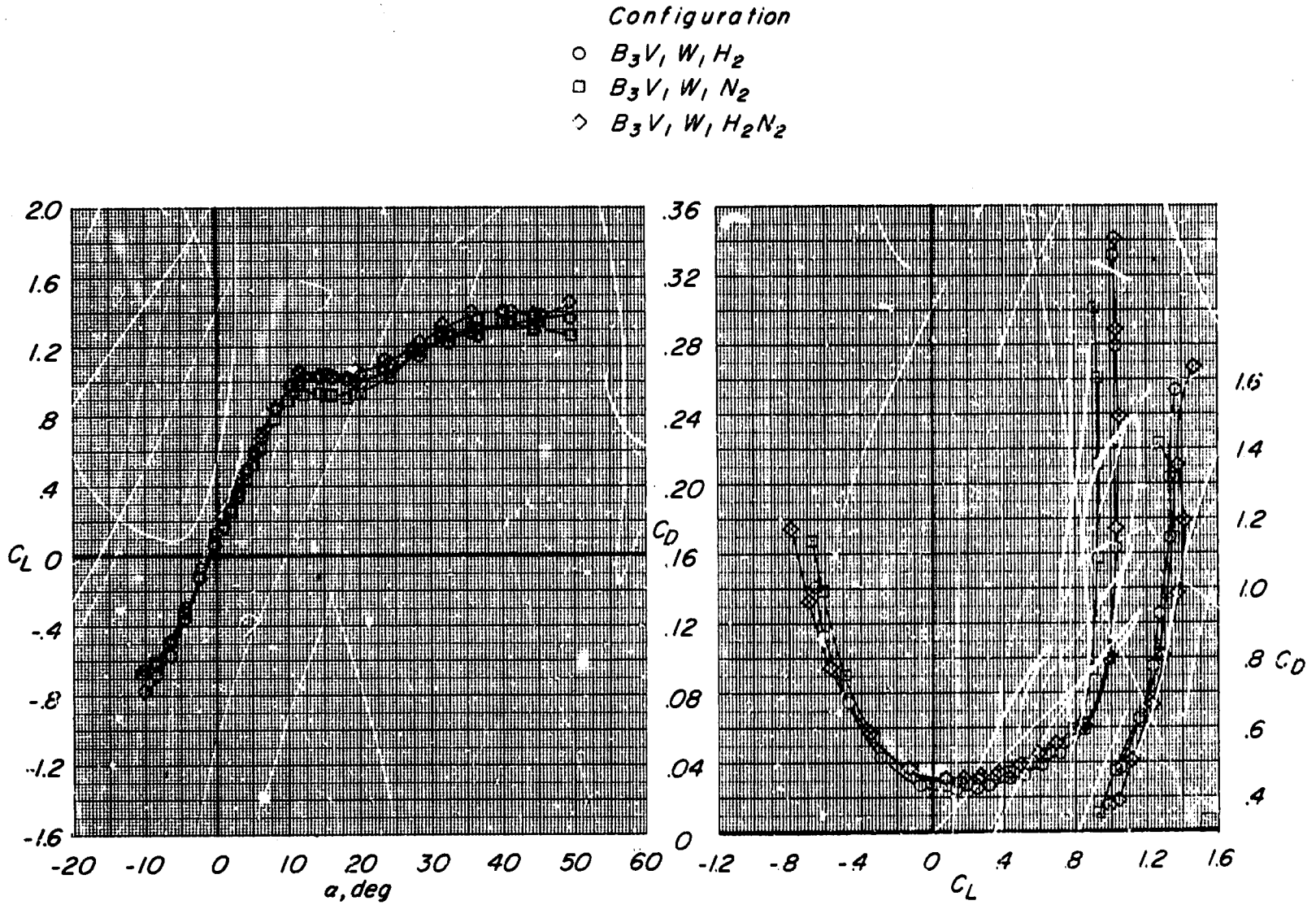

(c) Concluded.

Figure 3.- Continued.

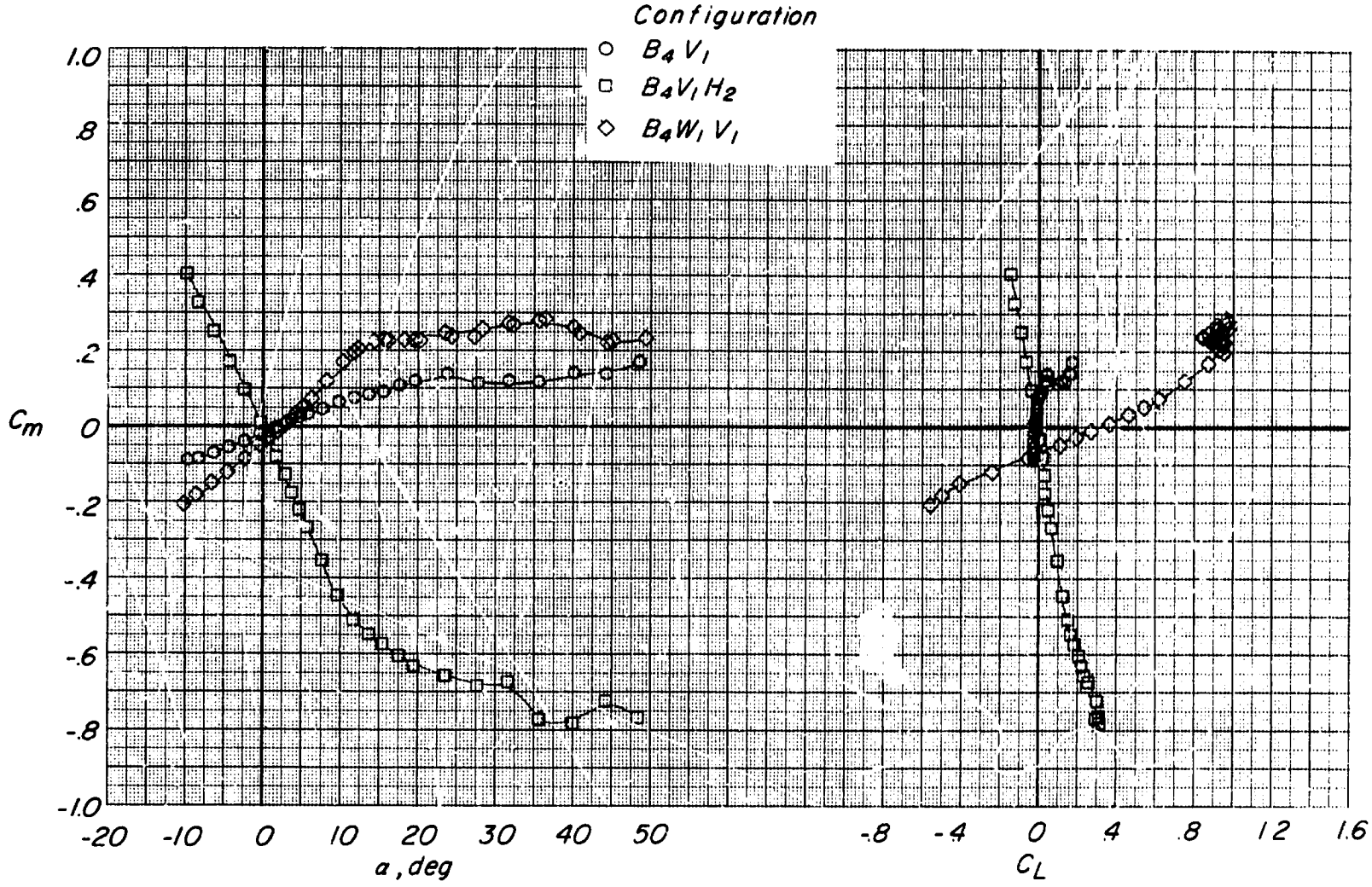

(d) Body 4 with various components.

Figure 3.- Continued.

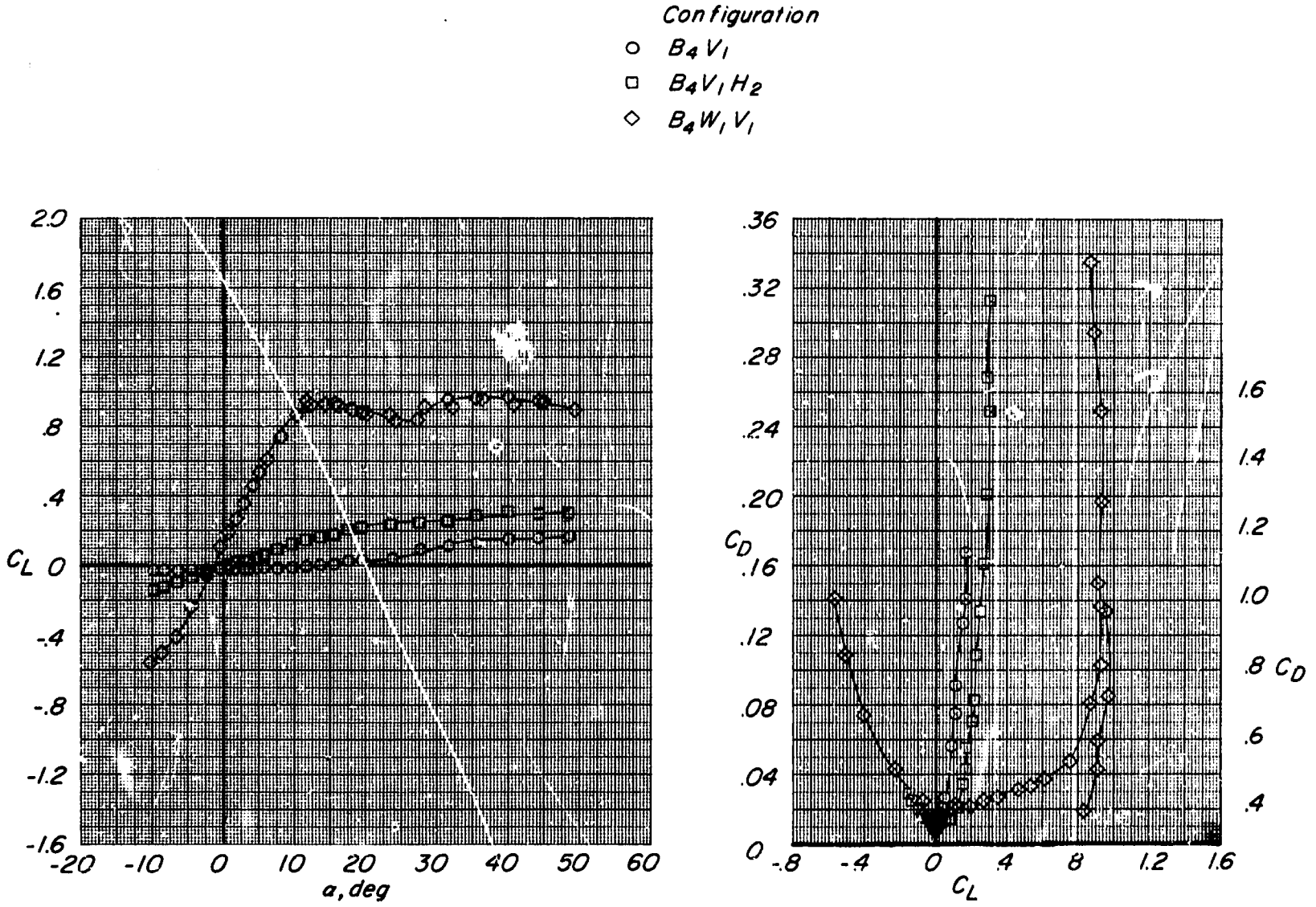

(d) Continued.

Figure 3.- Continued.

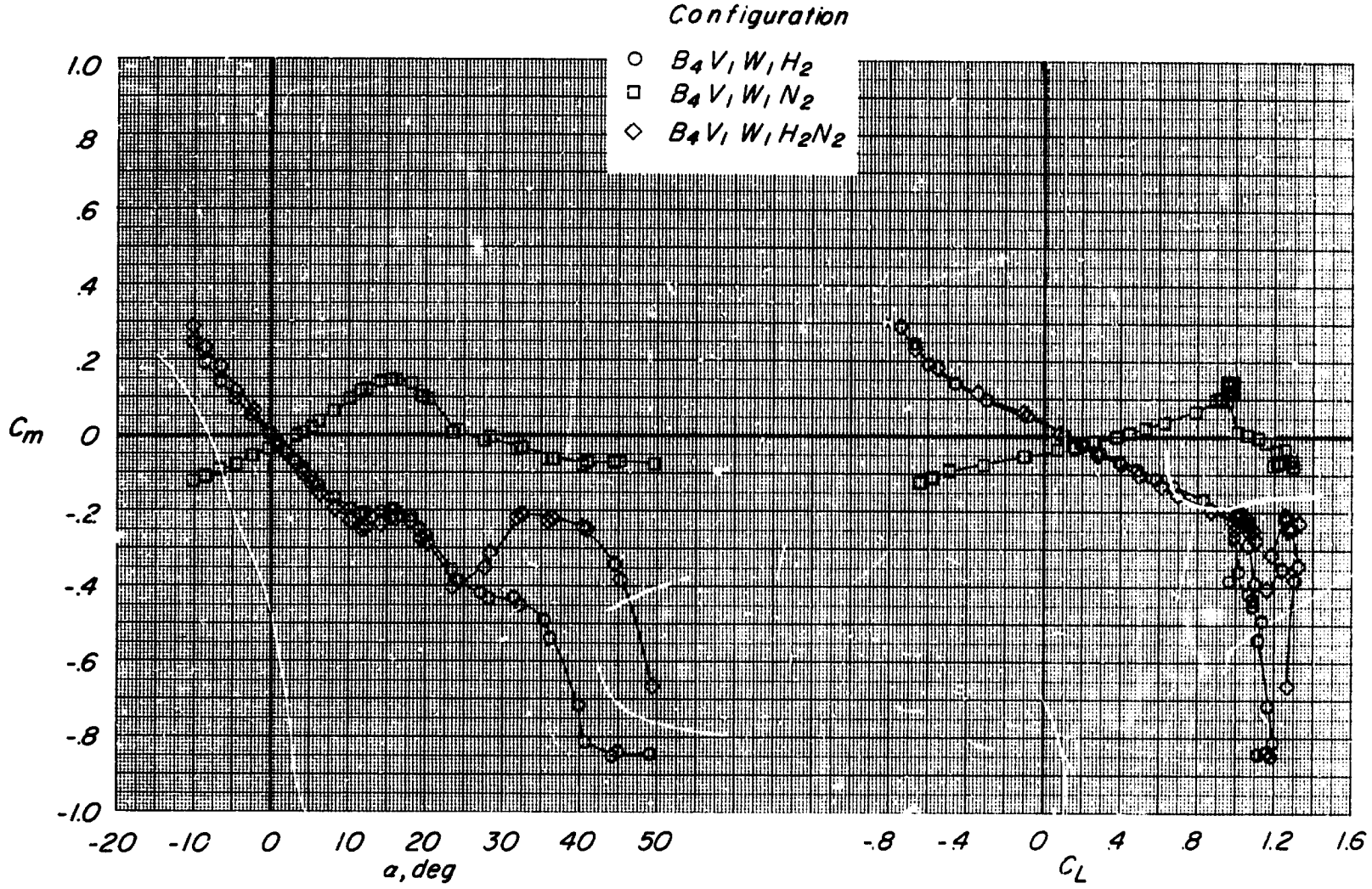

(d) Continued.

Figure 3.- Continued.

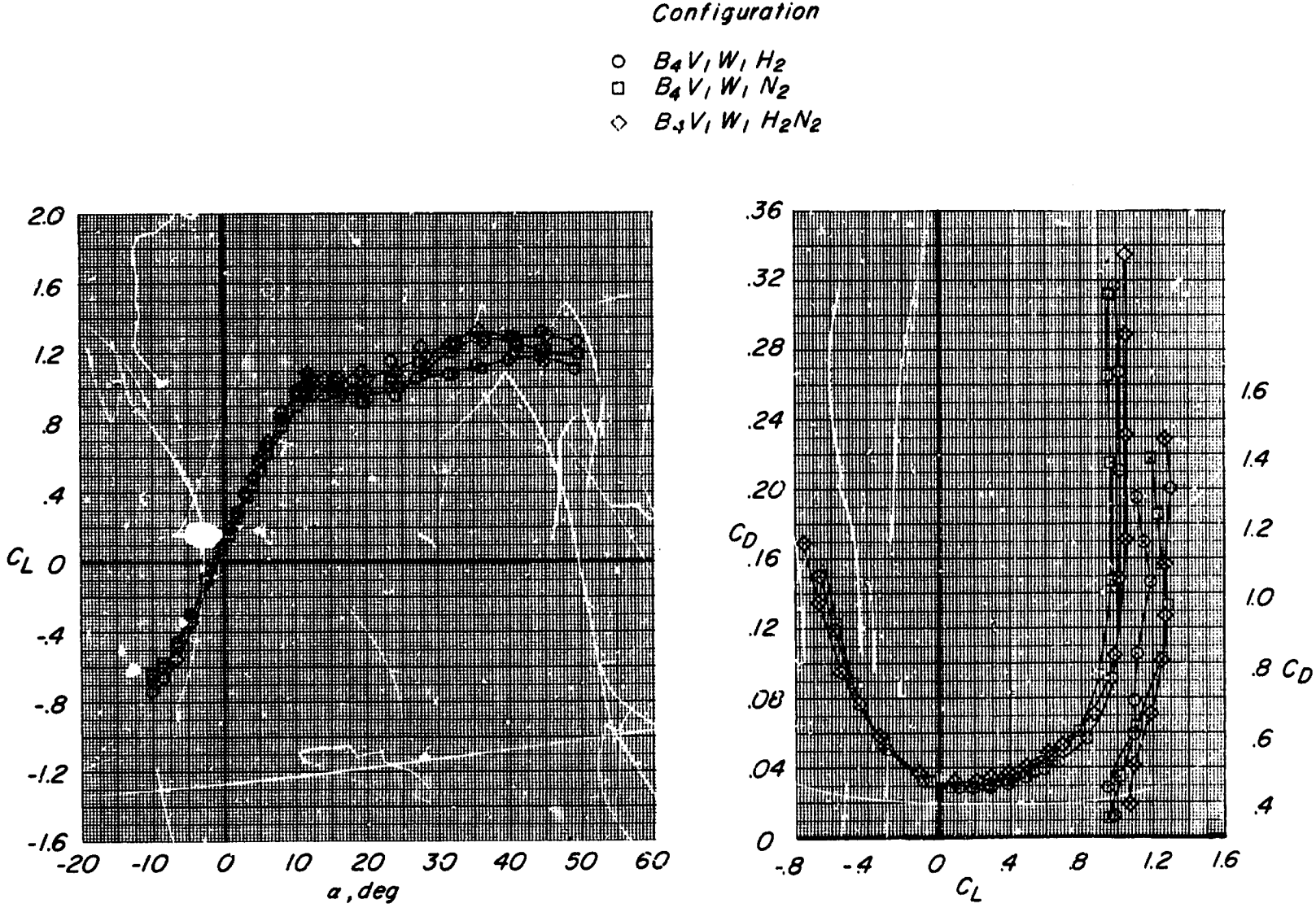

(d) Concluded.

Figure 3.- Concluded.

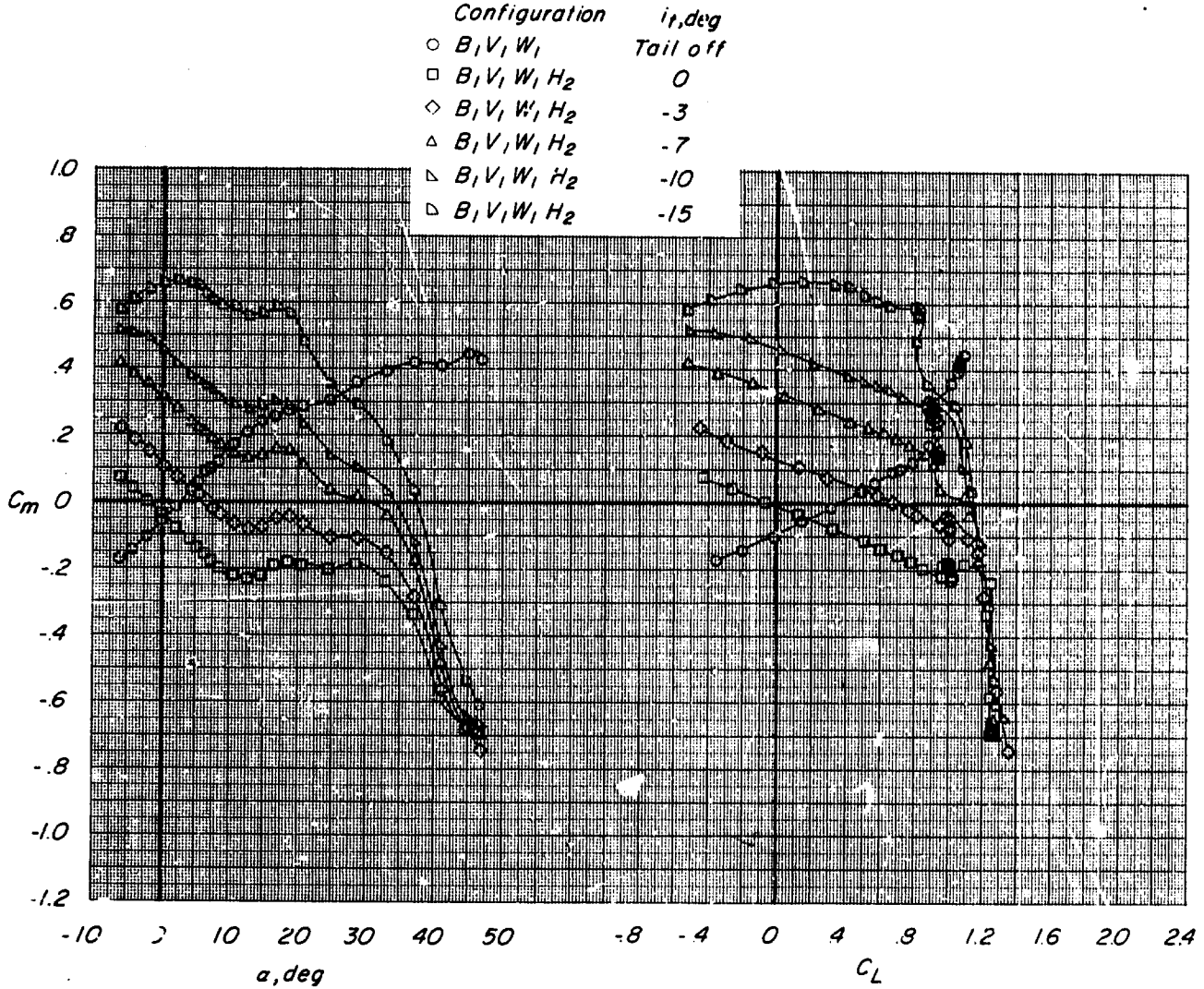

(a) Variation of C_m with α and C_L.

Figure 4.- Longitudinal control effectiveness of body 1 configuration without nacelles ($B_1V_1W_1H_2$). M = 0.21; R = 0.78×10^6.

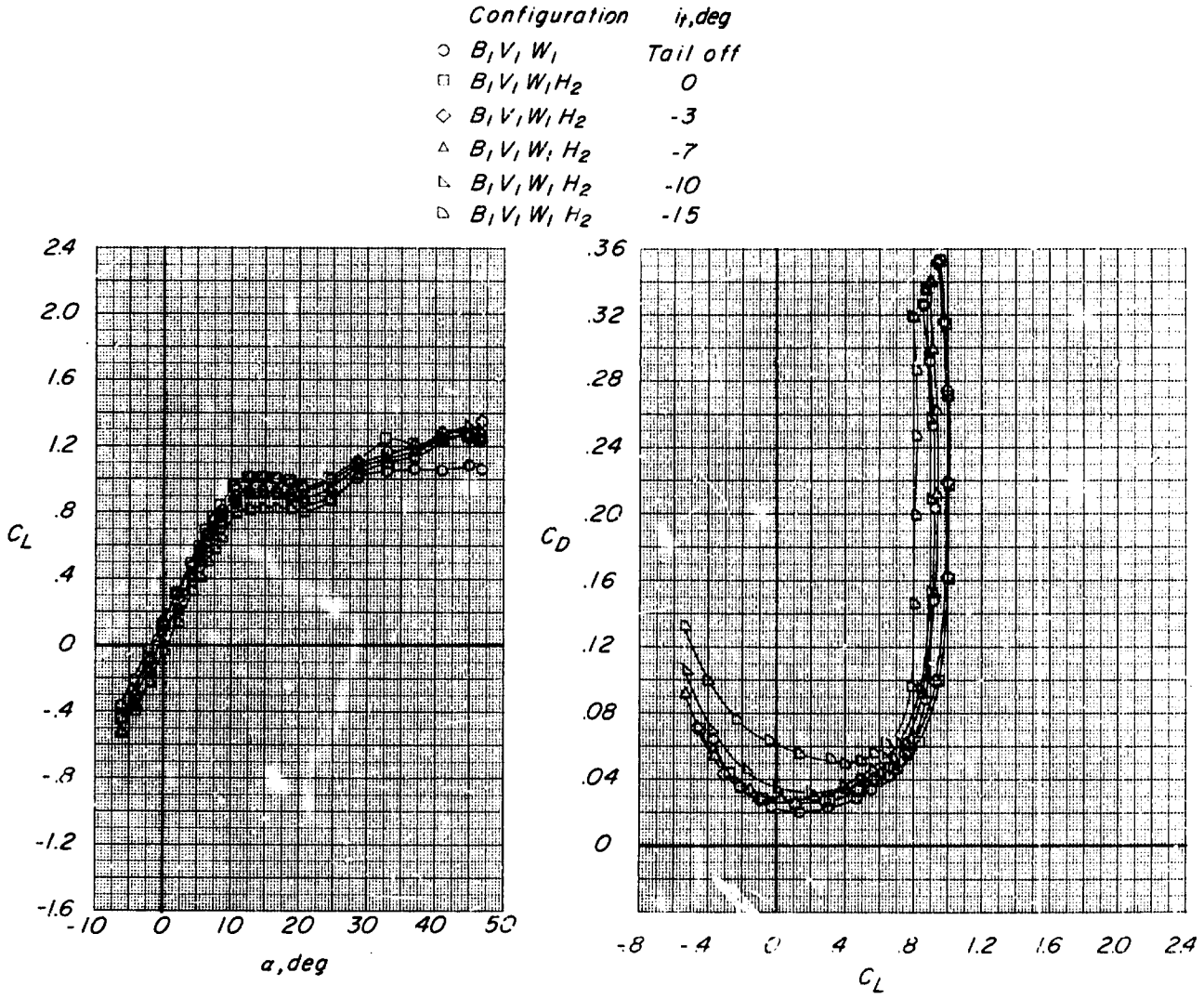

(b) Variation of C_L with α and C_D with C_L.

Figure 4.- Continued.

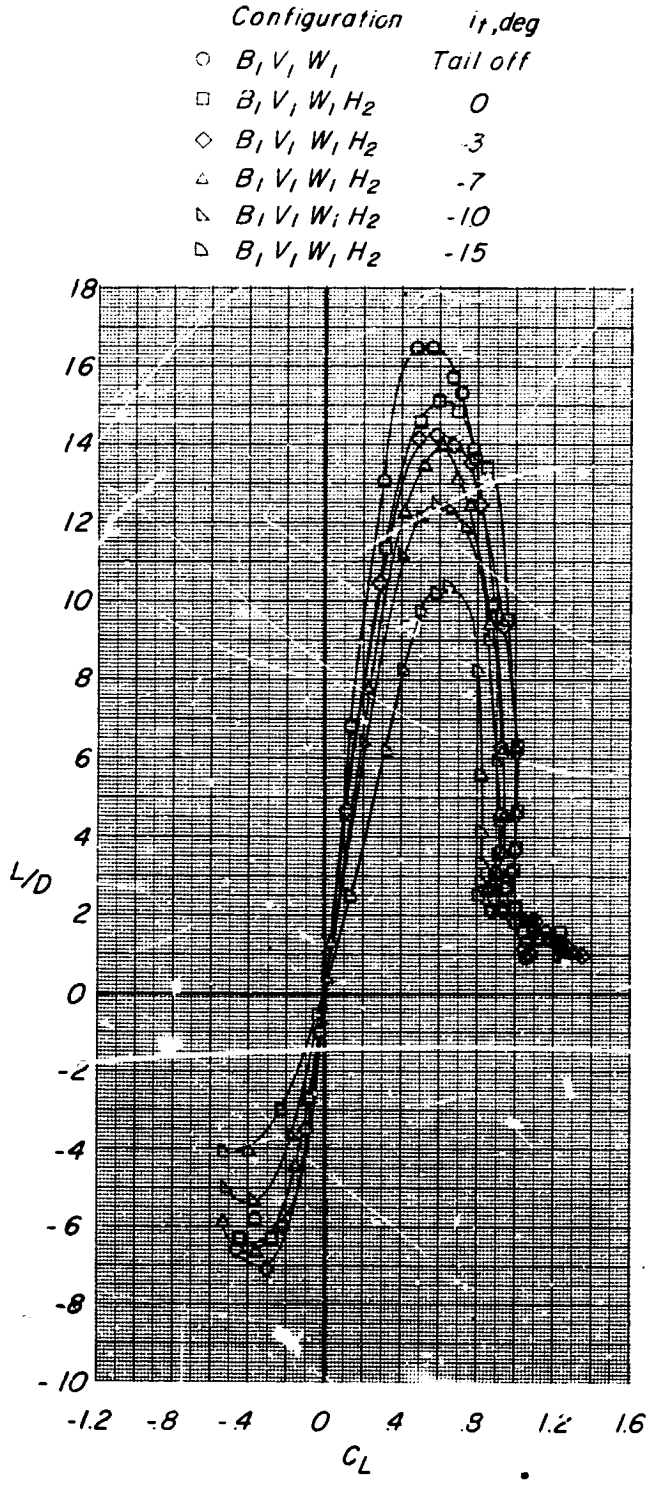

(c) Variation of L/D with C_L.

Figure 4.- Concluded.

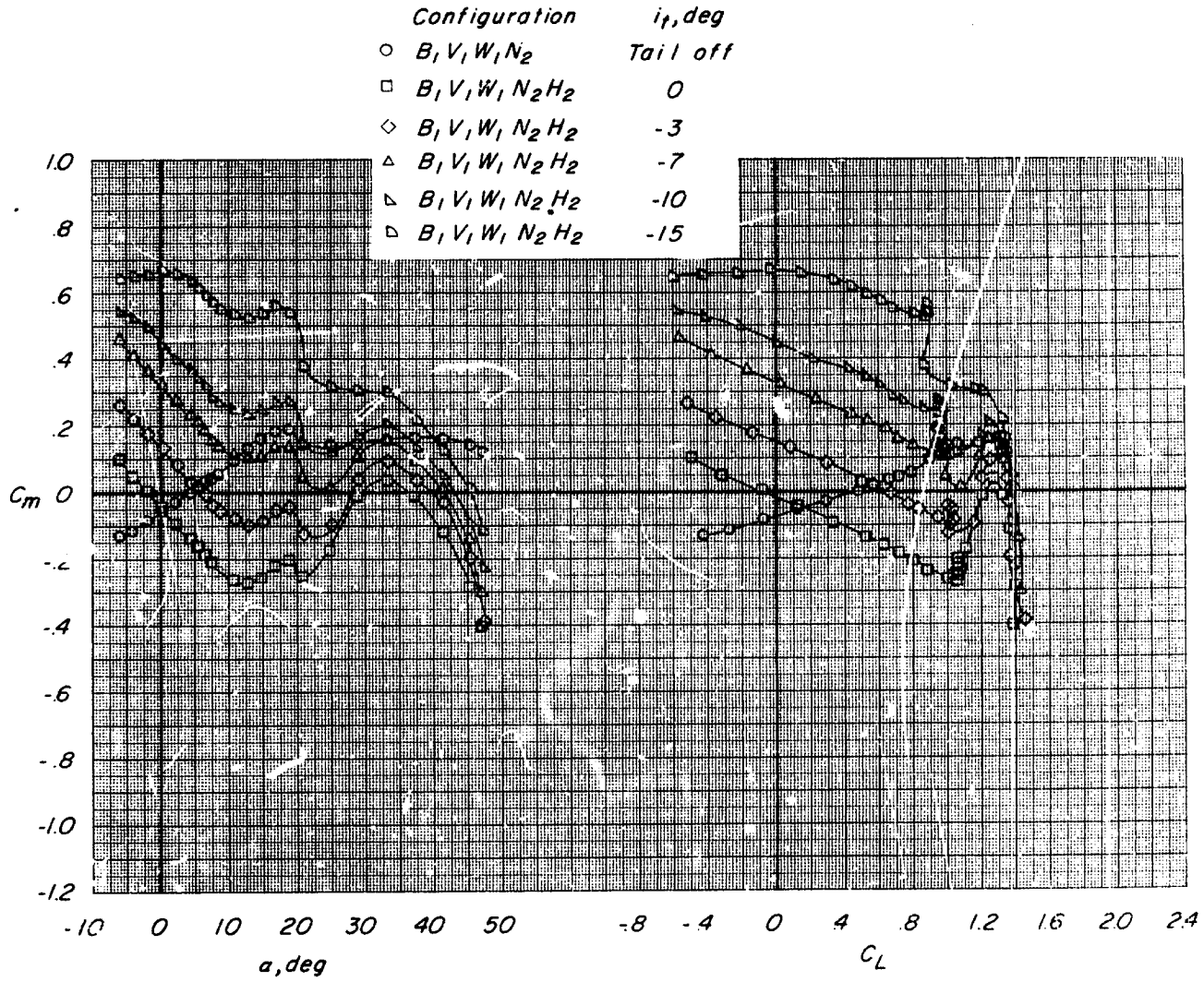

(a) Variation of C_m with α and C_L.

Figure 5.- Longitudinal control effectiveness of body 1 configuration with nacelles ($B_1V_1W_1N_2H_2$). M = 0.21; R = 0.78×10^6.

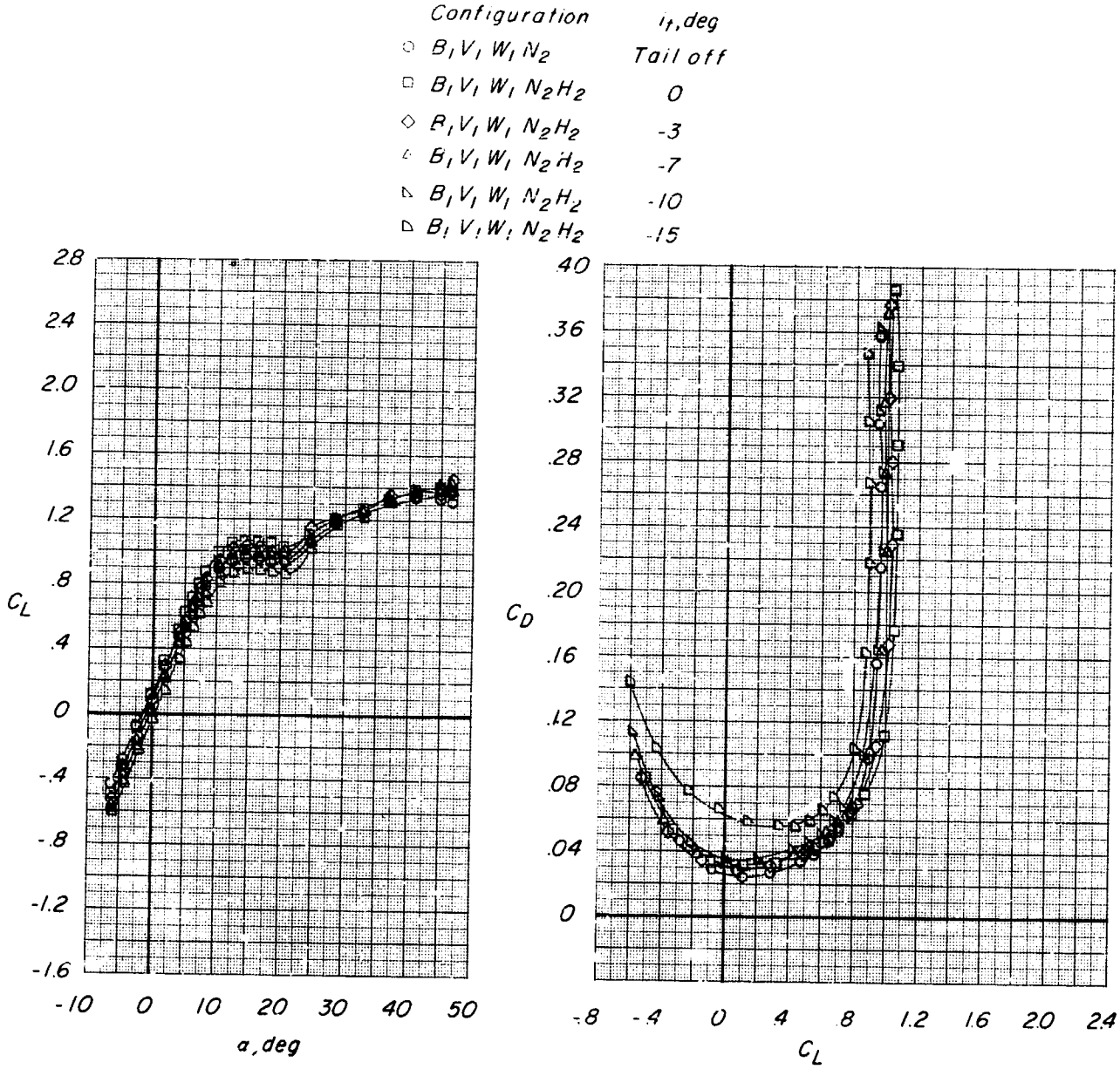

(b) Variation of C_L with α and C_D with C_L.

Figure 5.- Continued.

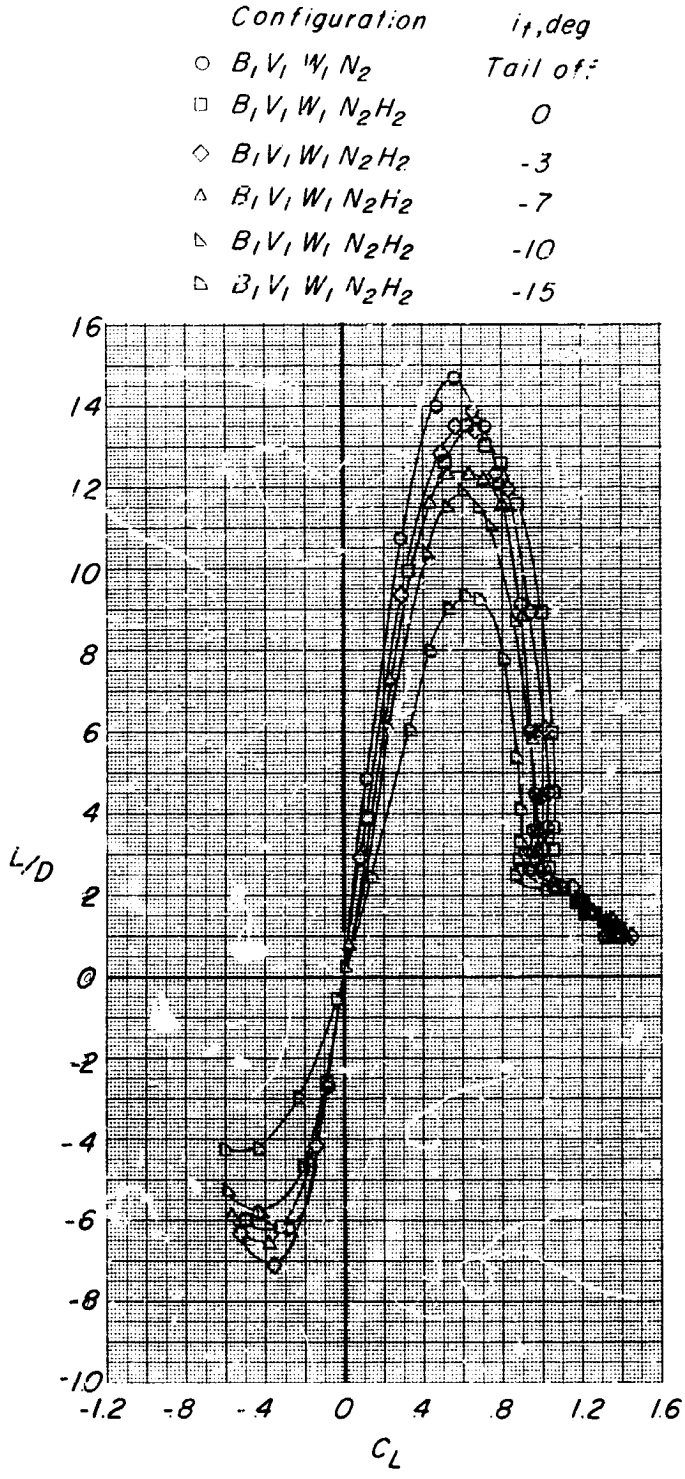

(c) Variation of L/D with C_L.

Figure 5.- Concluded.

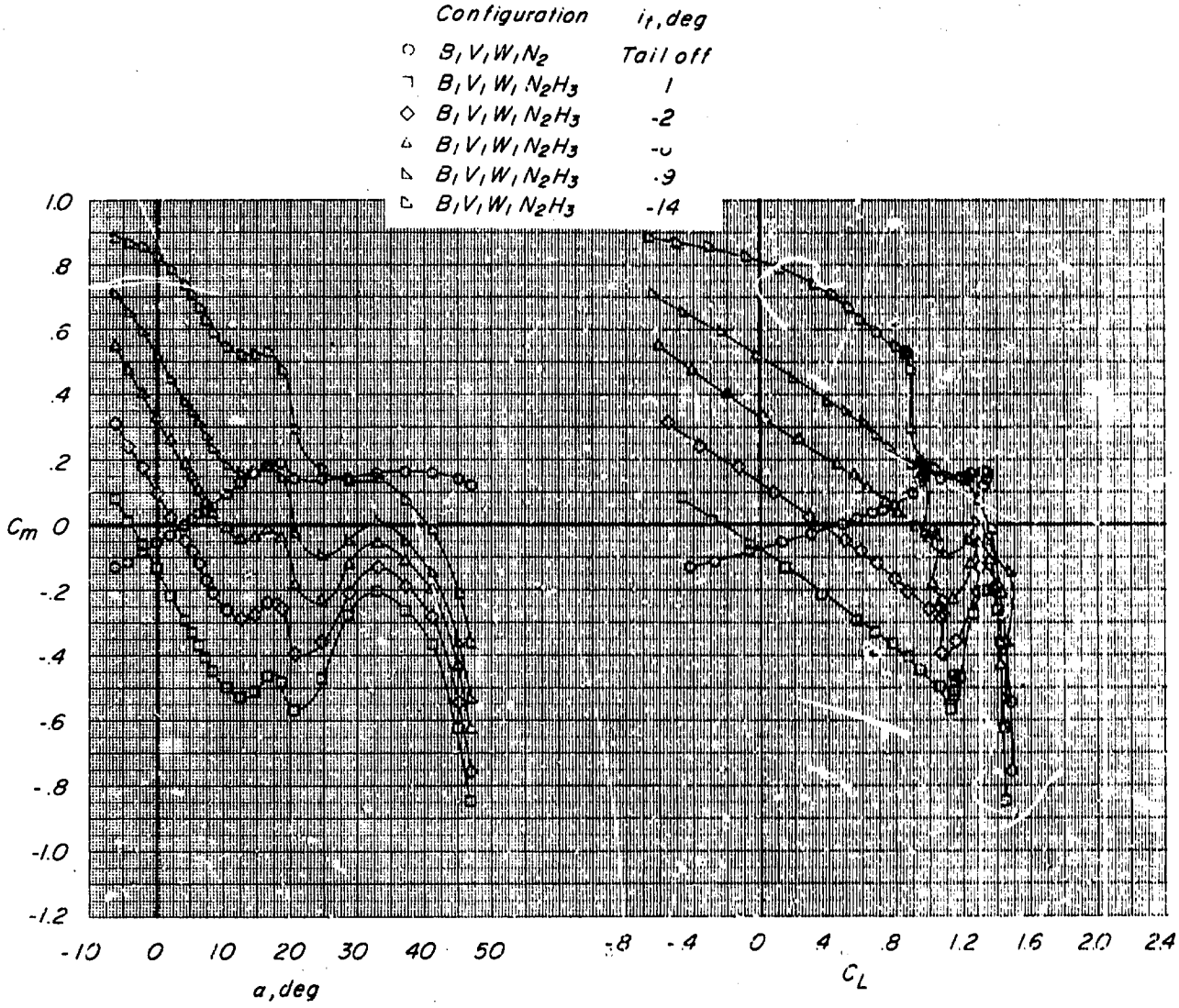

(a) Variation of C_m with α and C_L.

Figure 6.- Longitudinal control effectiveness of body 1 configuration with large horizontal tails H_3 having taper ratio of 0.29 ($B_1V_1W_1N_2H_3$). M = 0.21; R = 0.78 x 10^6.

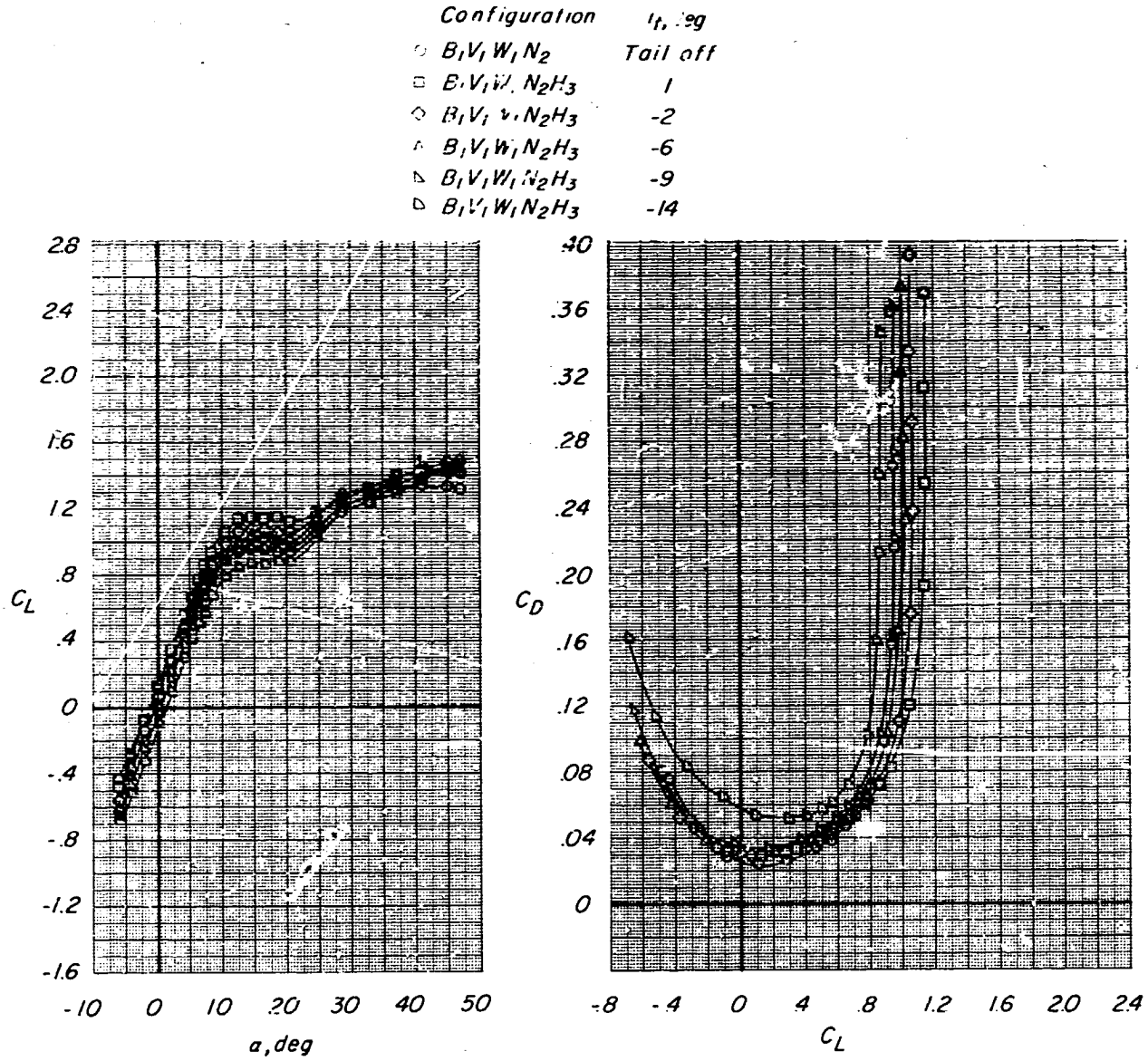

(b) Variation of C_L with α and C_D with C_L.

Figure 6.- Continued.

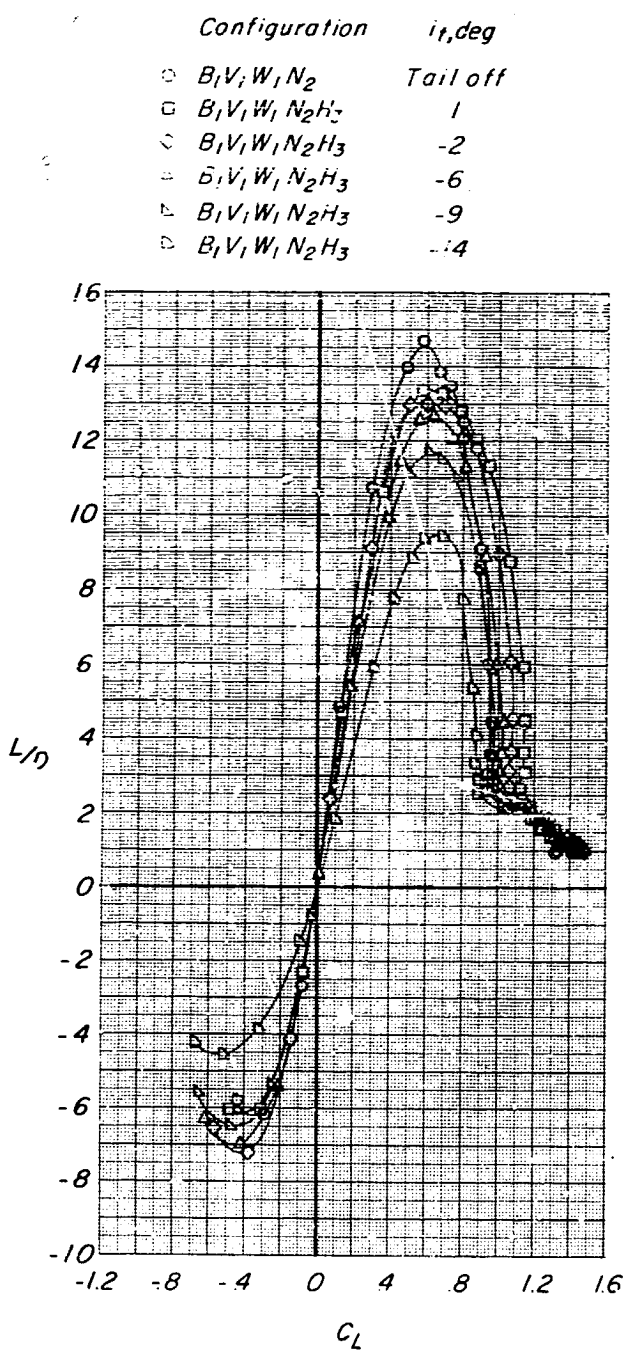

(c) Variation of L/D with C_L.

Figure 6.- Concluded.

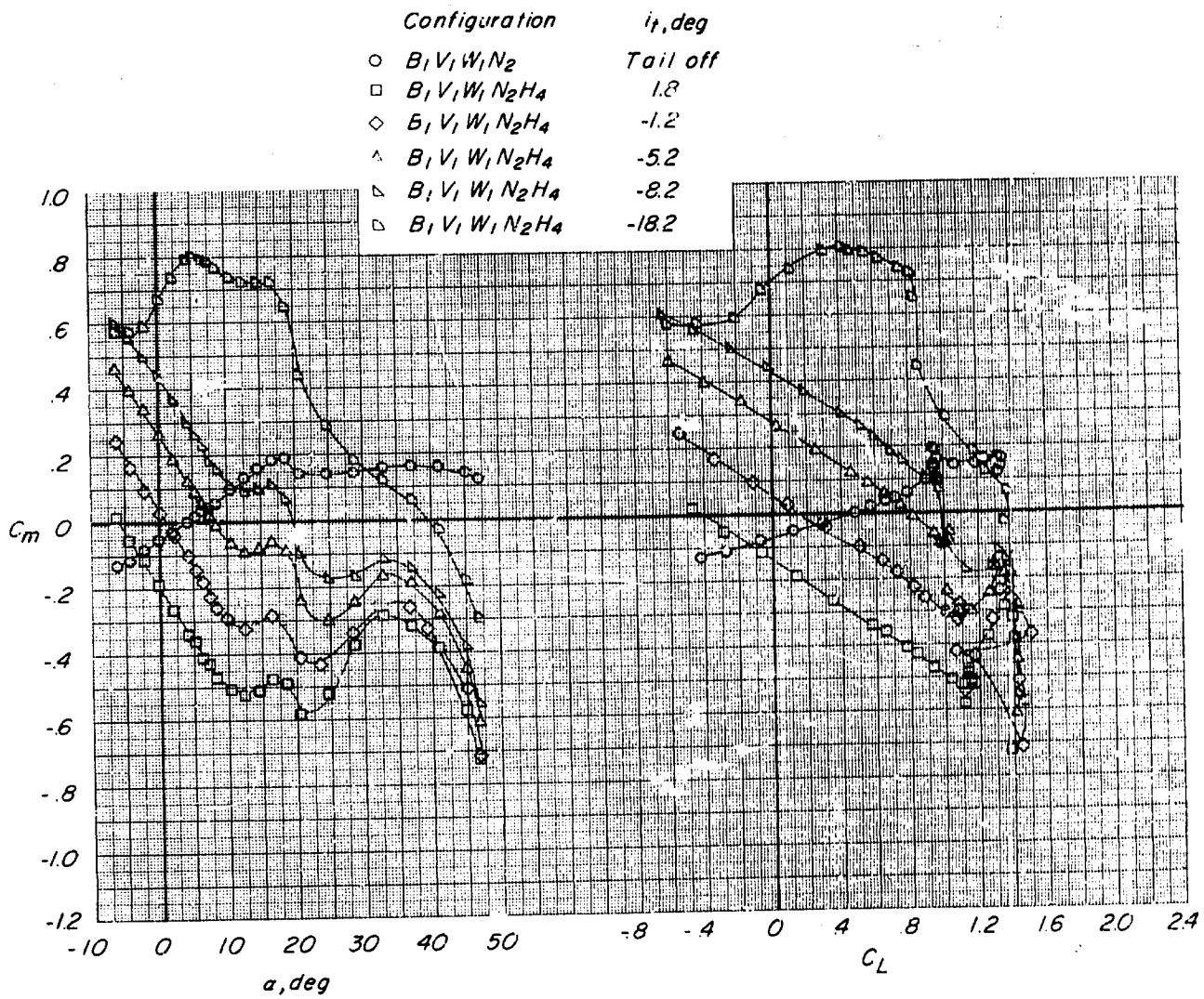

(a) Variation of C_m with α and C_L.

Figure 7.- Longitudinal control effectiveness of body 1 configuration with large horizontal tails H_4 having taper ratio of 1.00 $(B_1V_1W_1N_2H_4)$. M = 0.21; R = 0.78 × 10^6.

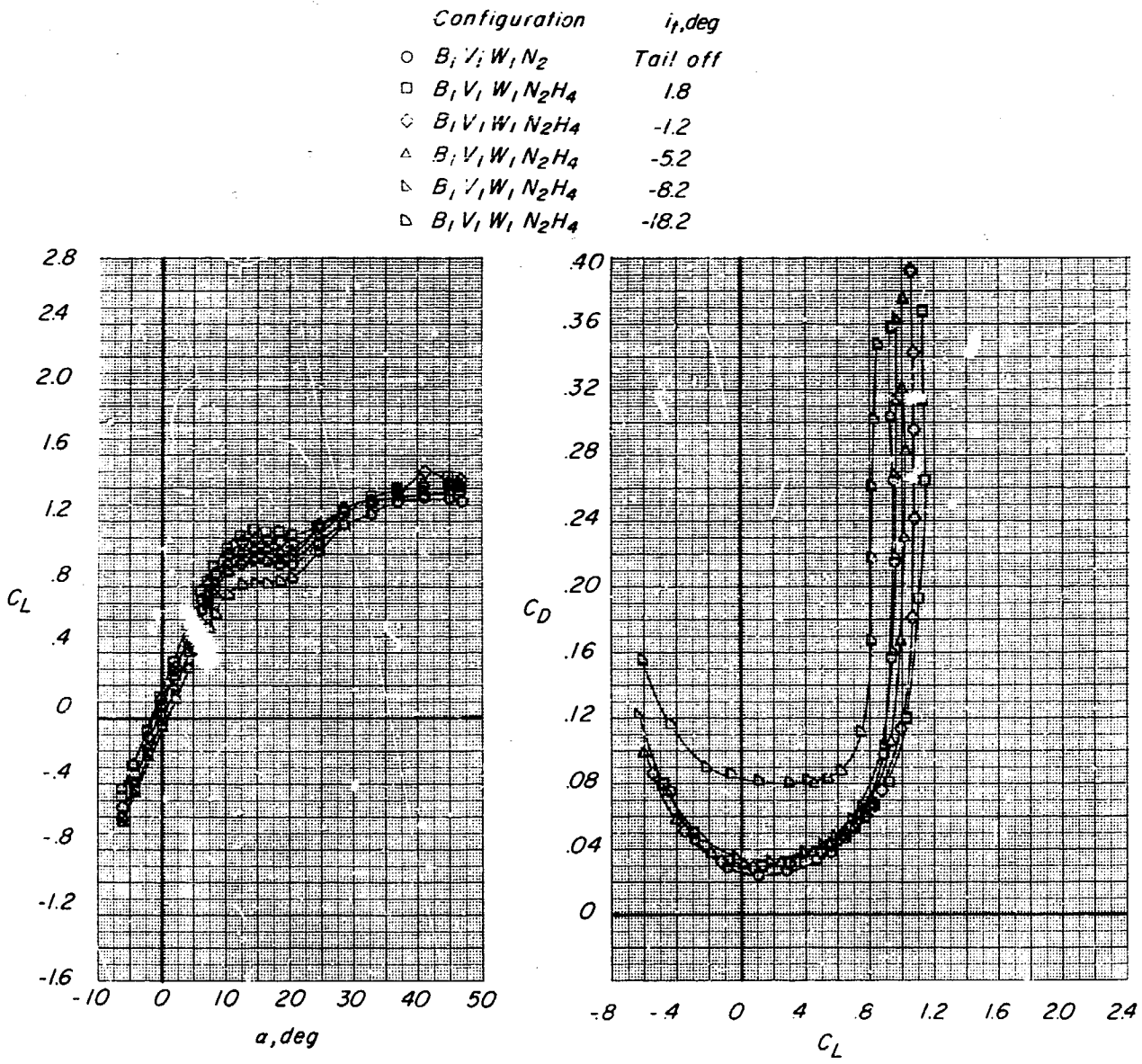

(b) Variation of C_L with α and C_D with C_L.

Figure 7.- Continued.

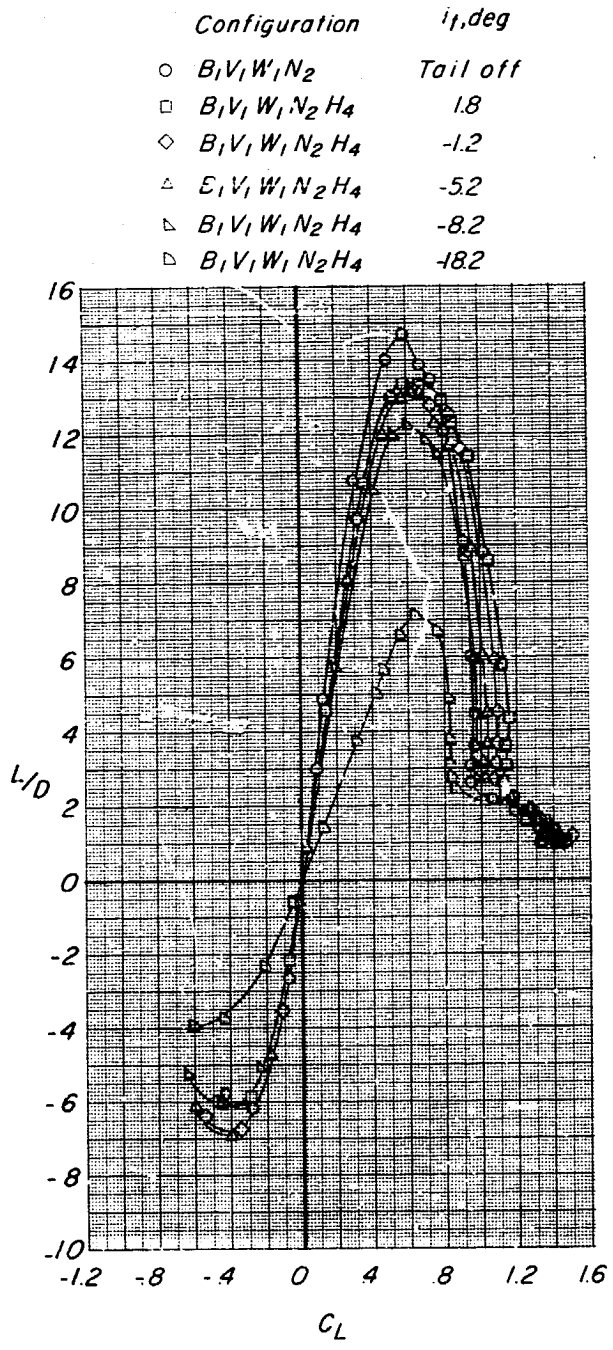

(c) Variation of L/D with C_L.

Figure 7.- Concluded.

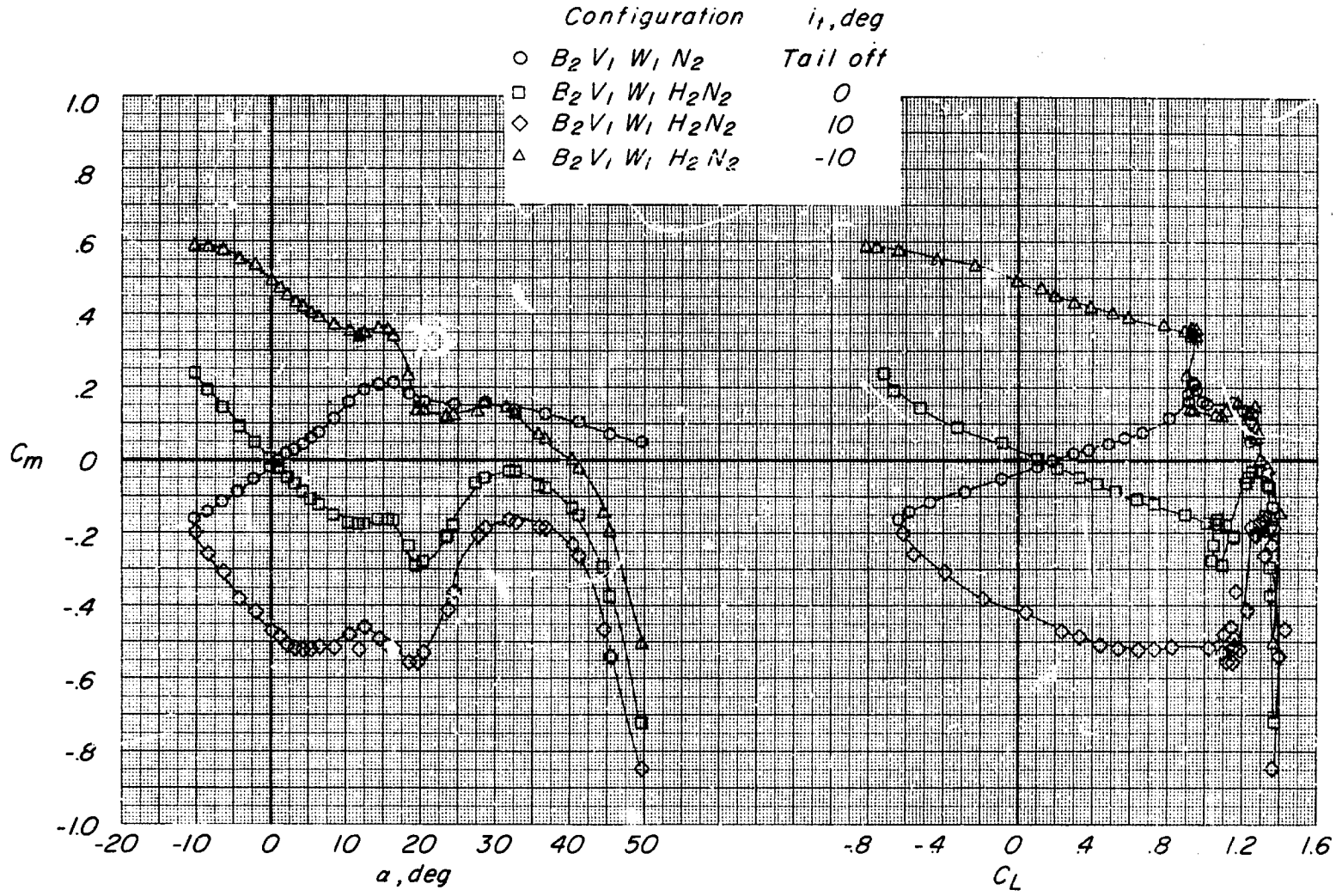

(a) Variation of C_m with α and C_L.

Figure 8.- Longitudinal control effectiveness of body 2 configuration $(B_2V_1W_1H_2N_2)$. M = 0.21; R = 0.78 x 10^6.

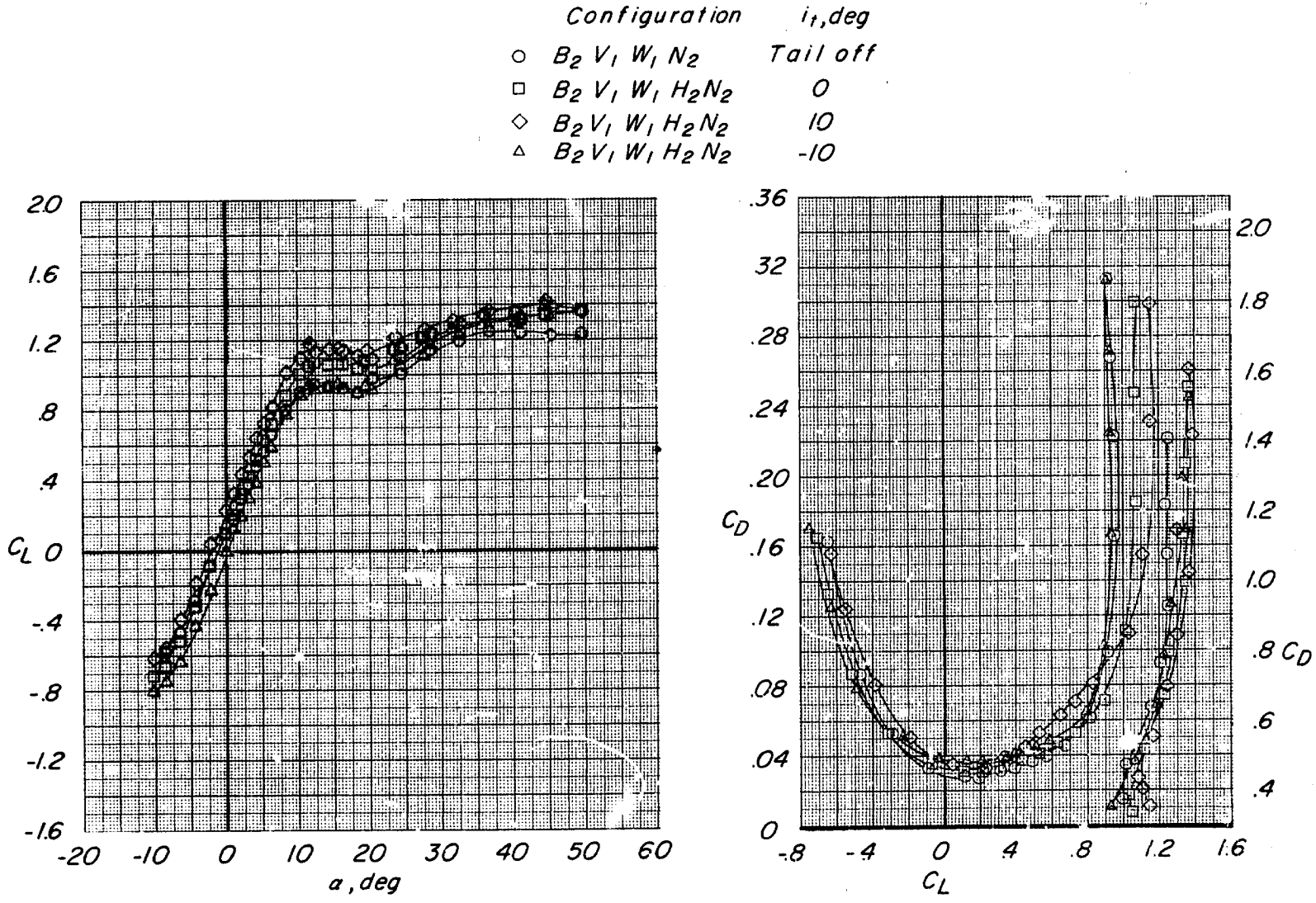

(b) Variation of C_L with α and C_D with C_L.

Figure 8.- Concluded.

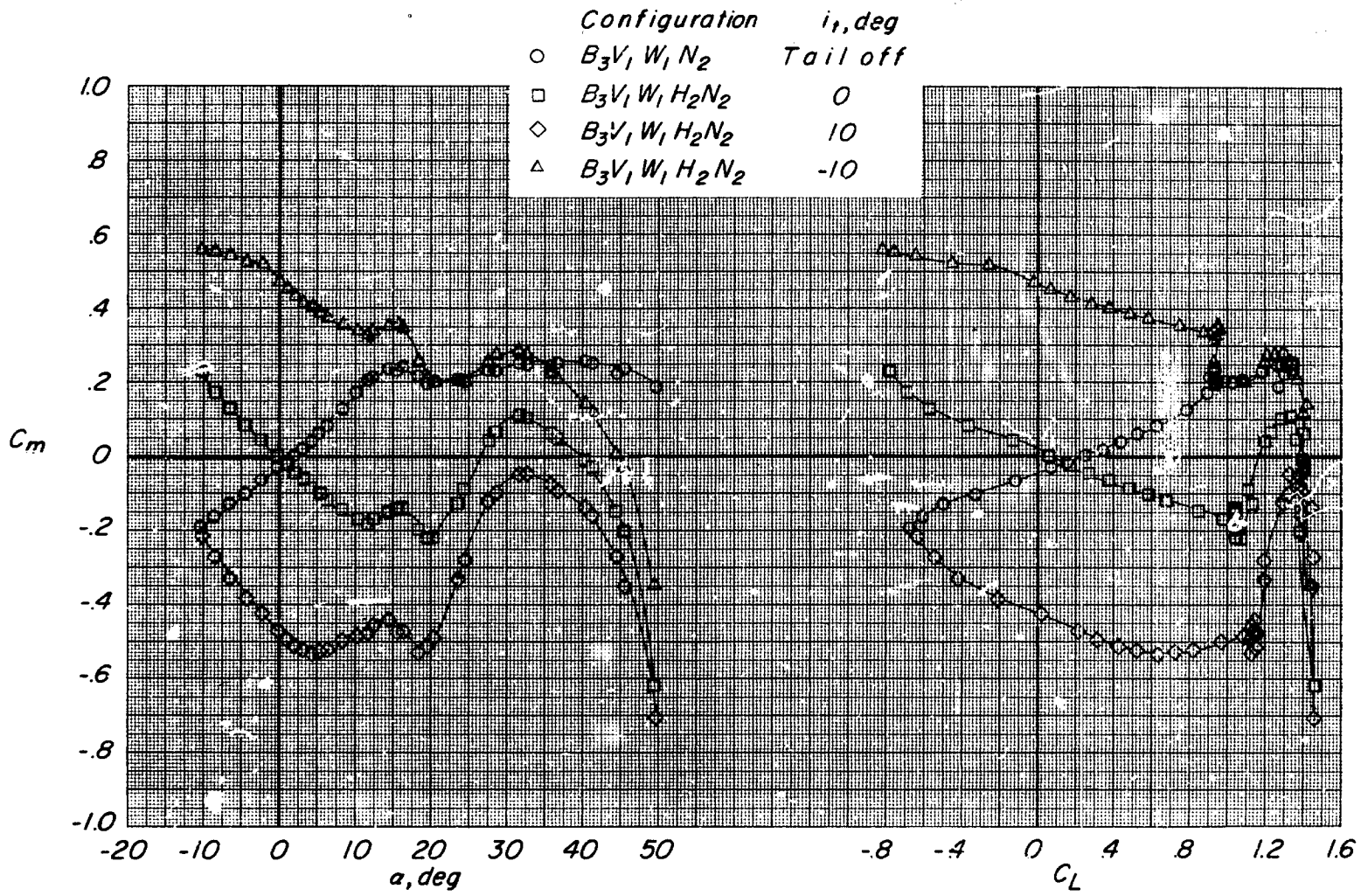

(a) Variation of C_m with α and C_L.

Figure 9.- Longitudinal control effectiveness of body 3 configuration $(B_3V_1W_1H_2N_2)$. M = 0.21; R = 0.78 × 10^6.

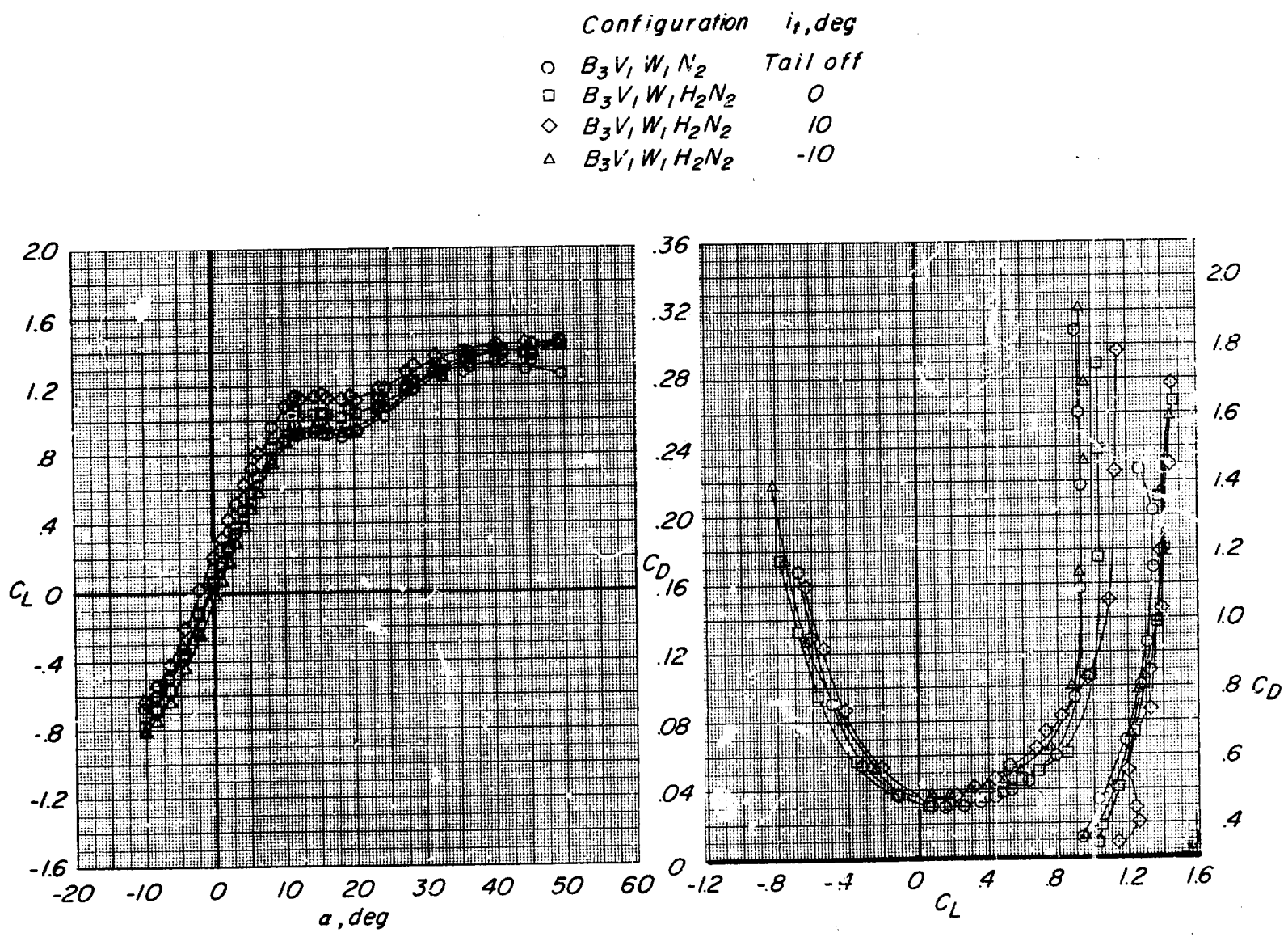

(b) Variation of C_L with α and C_D with C_L.

Figure 9.- Concluded.

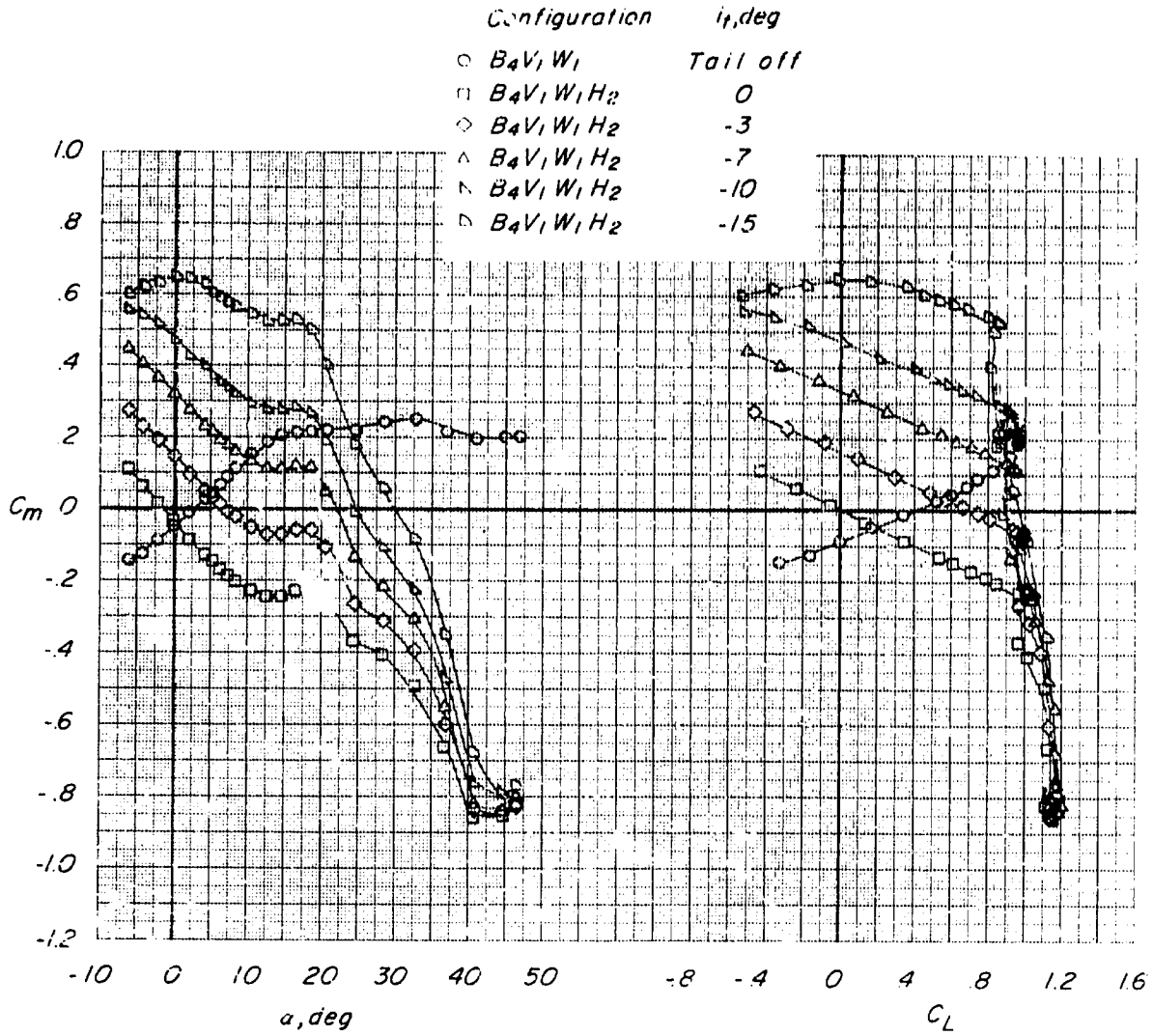

(a) Variation of C_m with α and C_L.

Figure 10.- Longitudinal control effectiveness of body 4 configuration without nacelles $(B_4V_1W_1H_2)$. M = 0.21; R = 0.78×10^6.

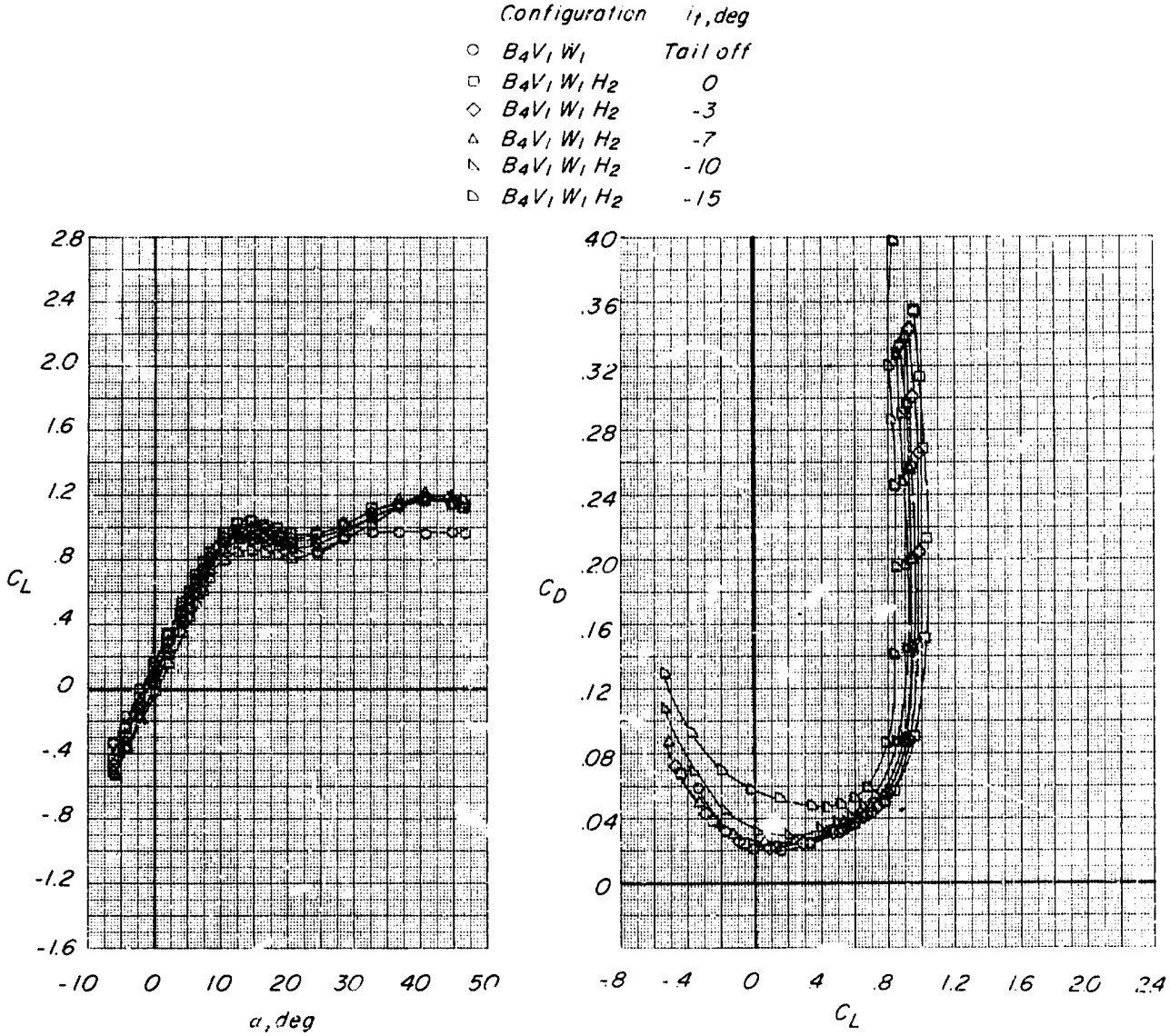

(b) Variation of C_L with α and C_D with C_L.

Figure 10.- Concluded.

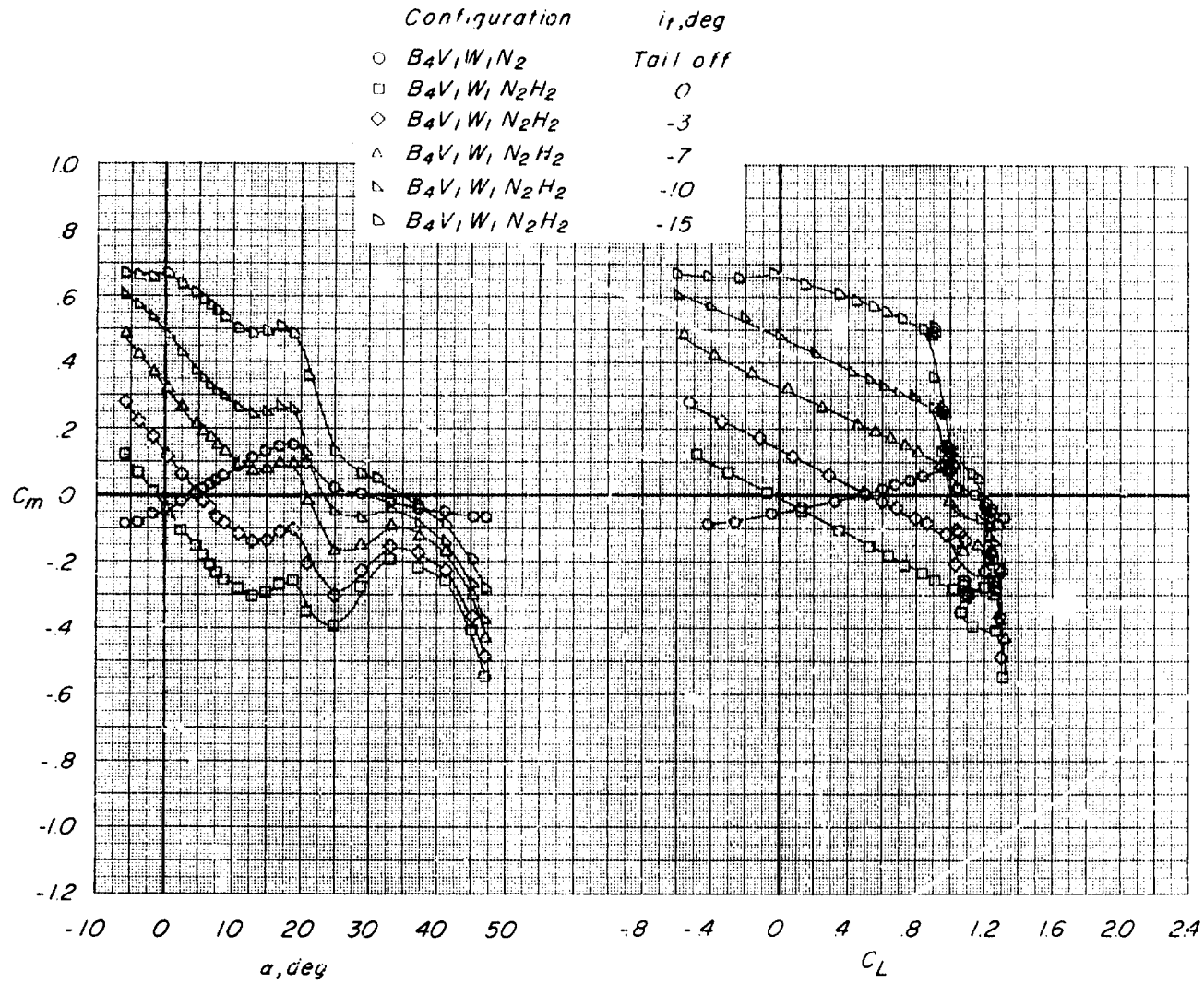

(a) Variation of C_m with α and C_L.

Figure 11.- Longitudinal control effectiveness of body 4 configuration with nacelles $\left(B_4V_1W_1N_2H_2\right)$. M = 0.21; R = 0.78×10^6.

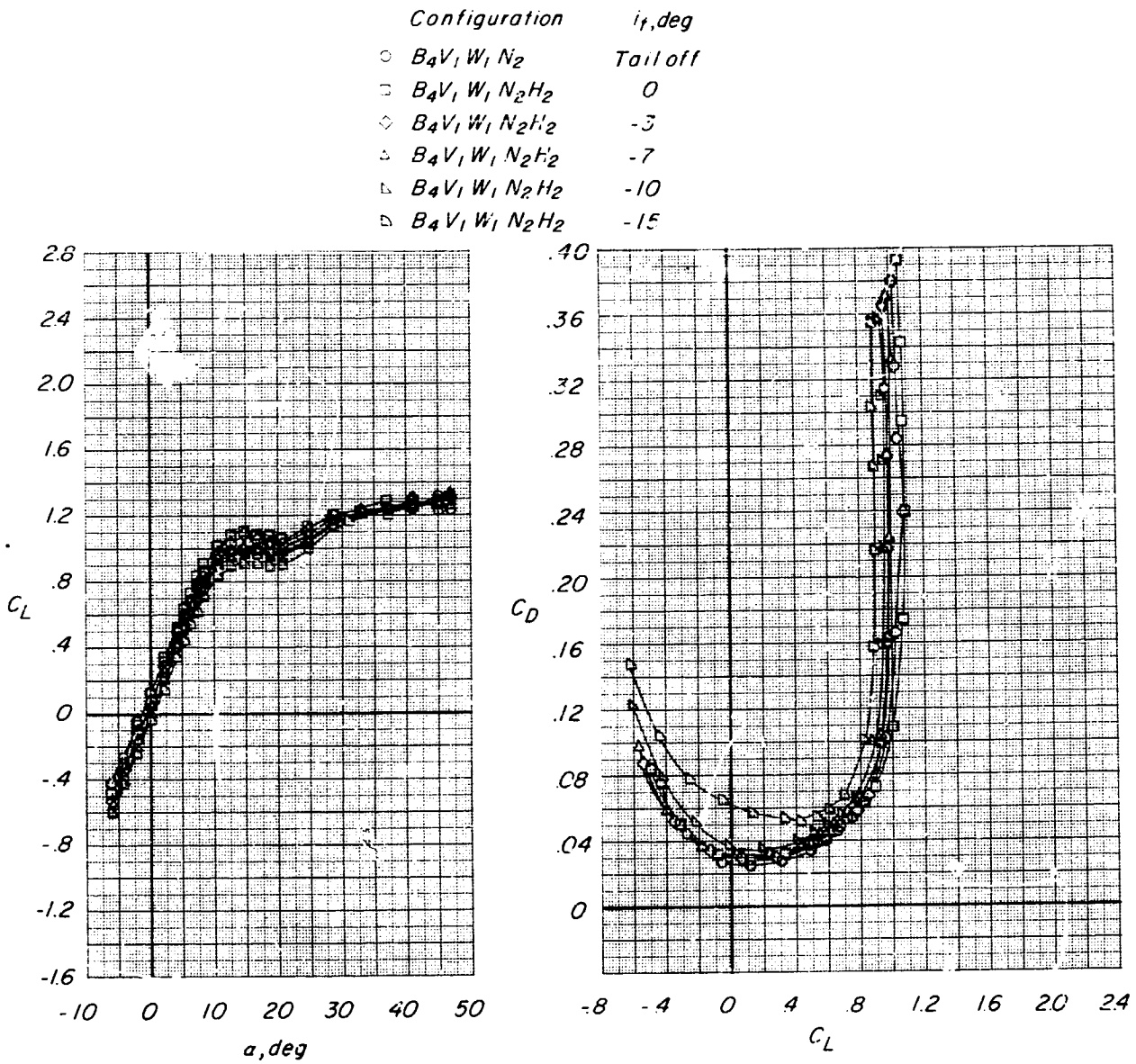

(b) Variation of C_L with α and C_D with C_L.

Figure 11.- Continued.

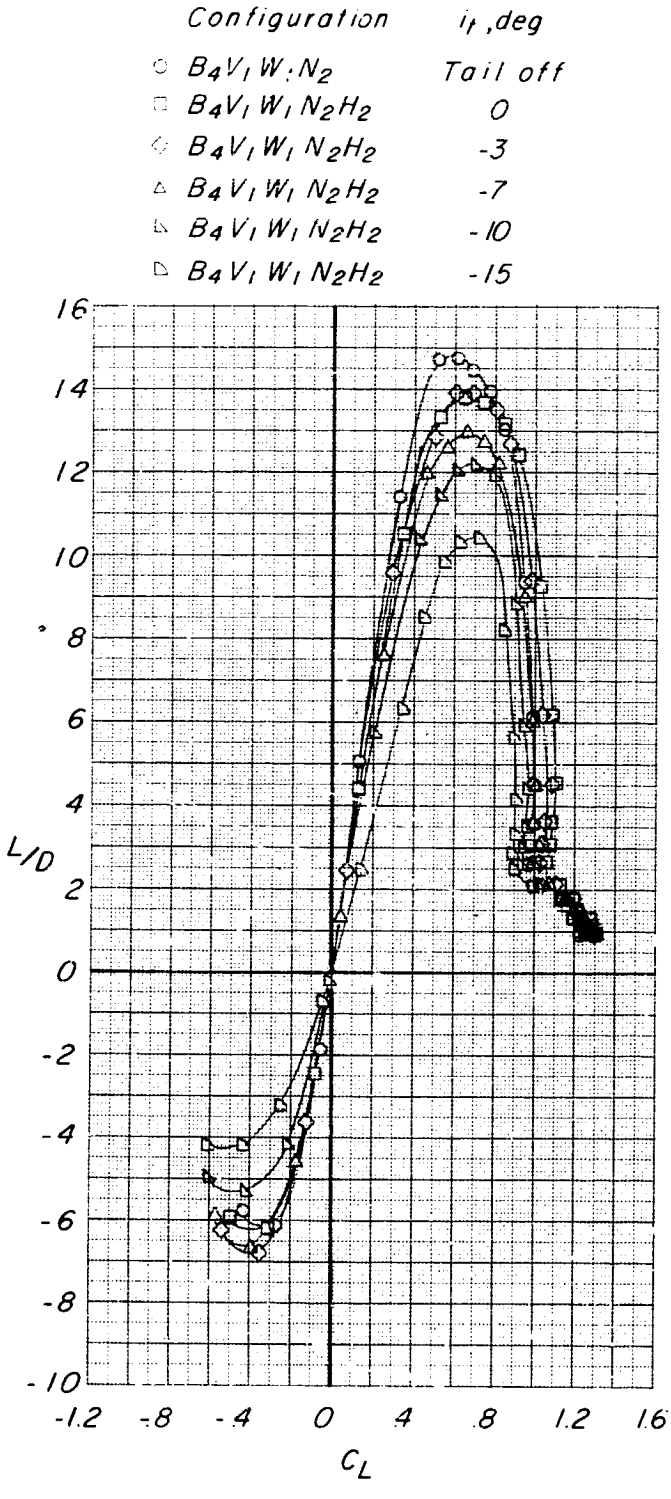

(c) Variation of L/D with C_L.

Figure 11.- Concluded.

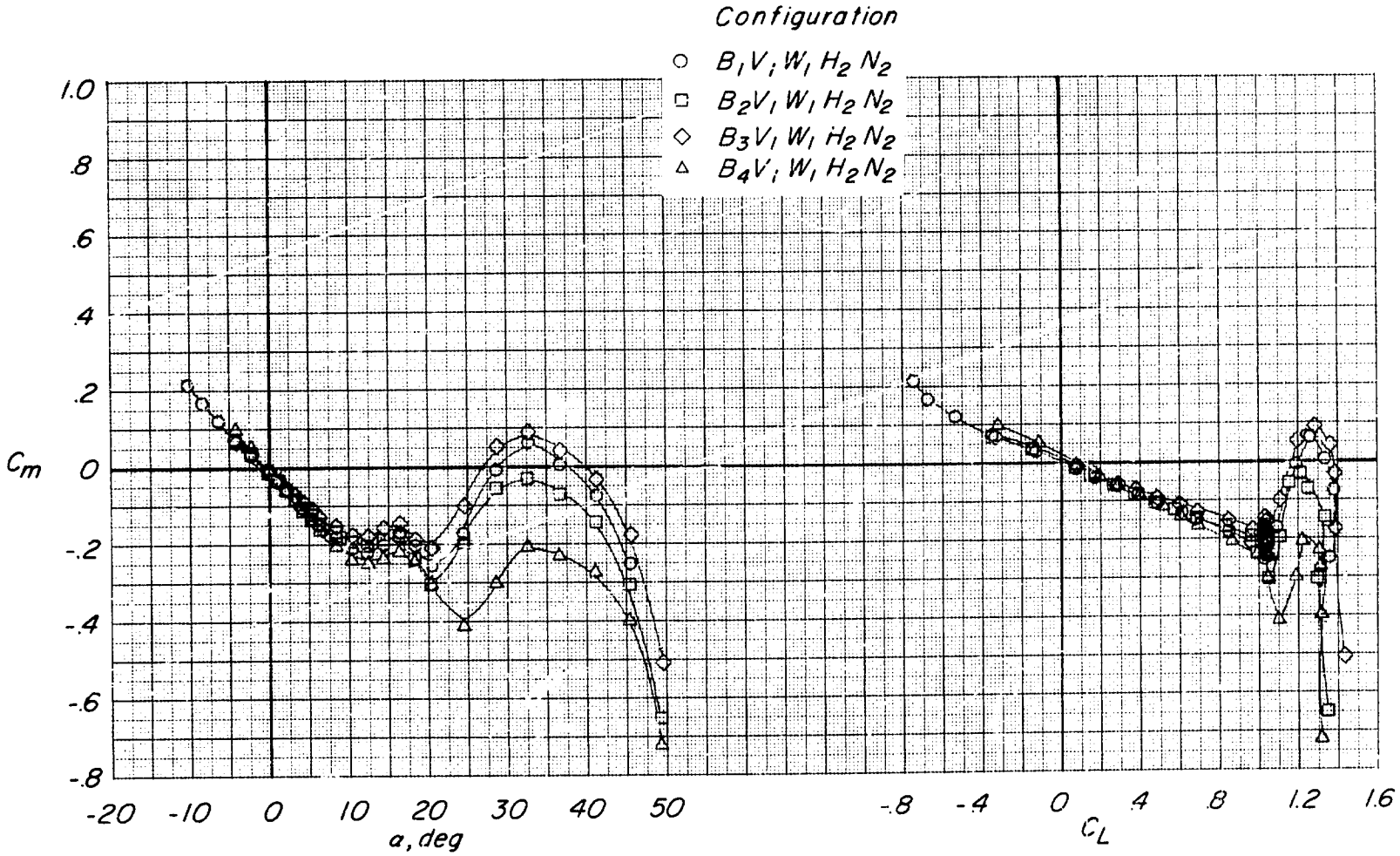

(a) Bodies 1, 2, 3, and 4.

Figure 12.- Effect of body size and shape on longitudinal stability characteristics. M = 0.21; R = 0.78×10^6.

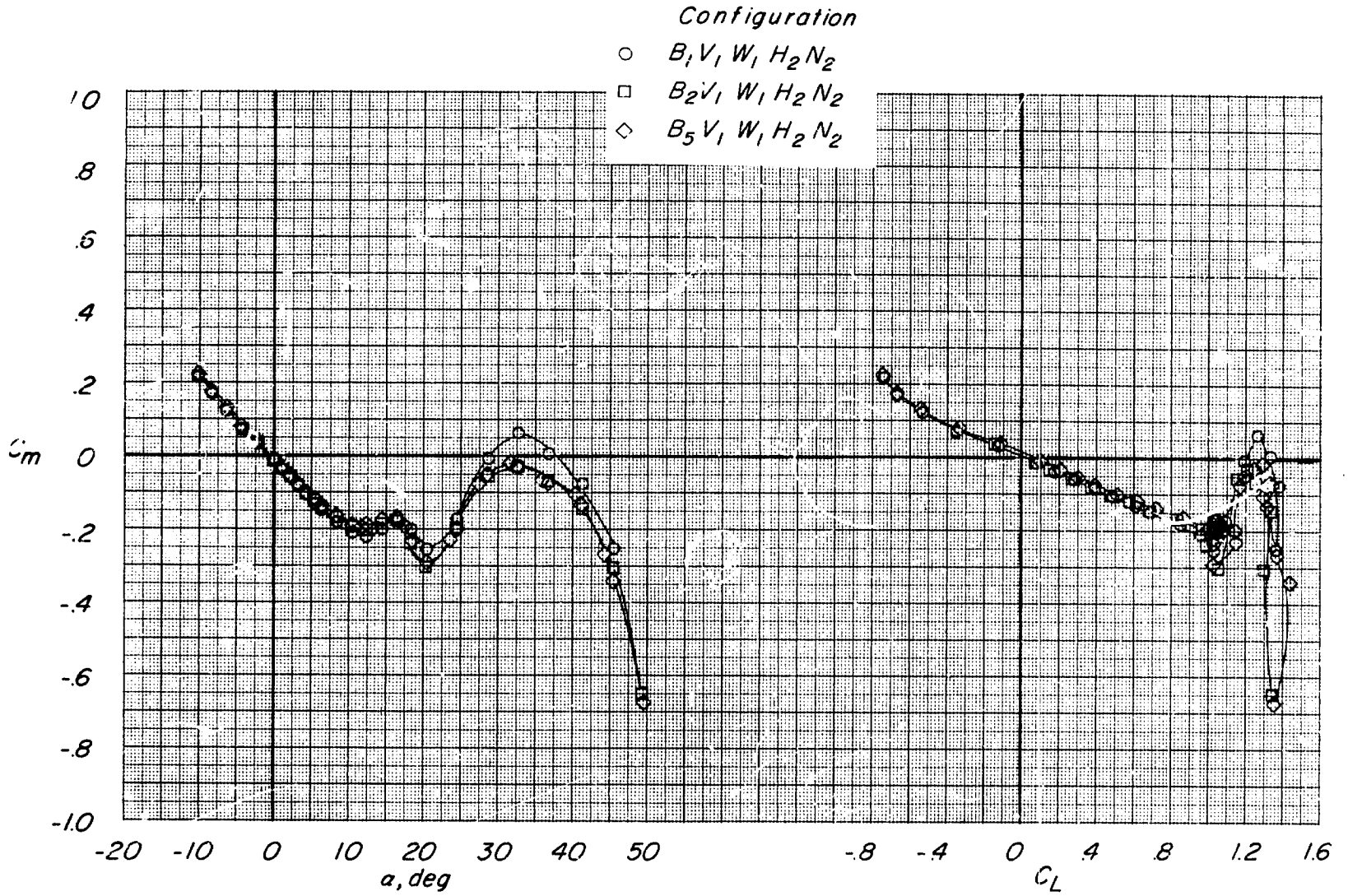

(b) Bodies 1, 2, and 5.

Figure 12.- Concluded.

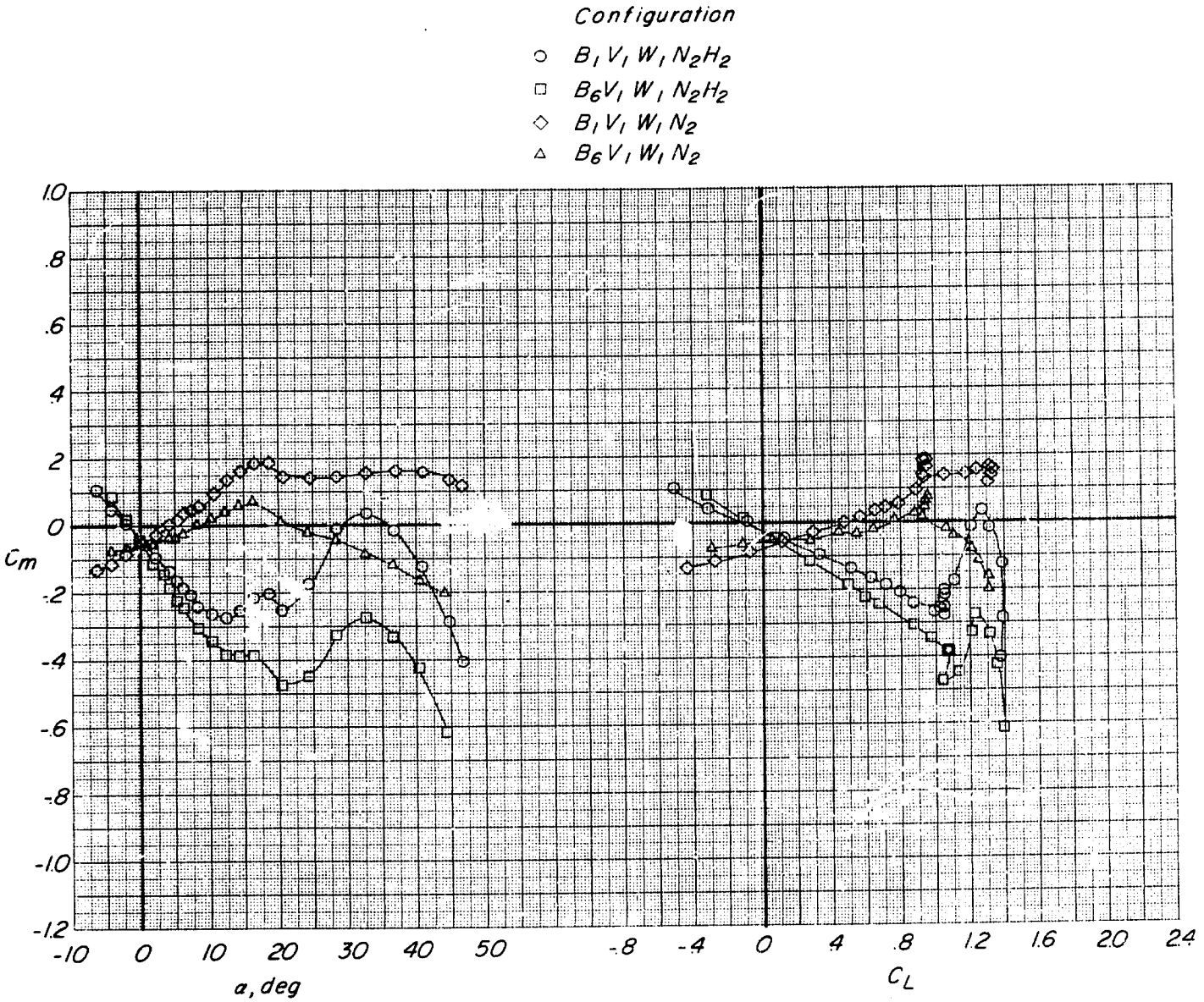

Figure 13.- Effect of fuselage length on longitudinal stability characteristics of basic configuration ($B_1V_1W_1H_2N_2$). M = 0.21; R = 0.78 × 10^6.

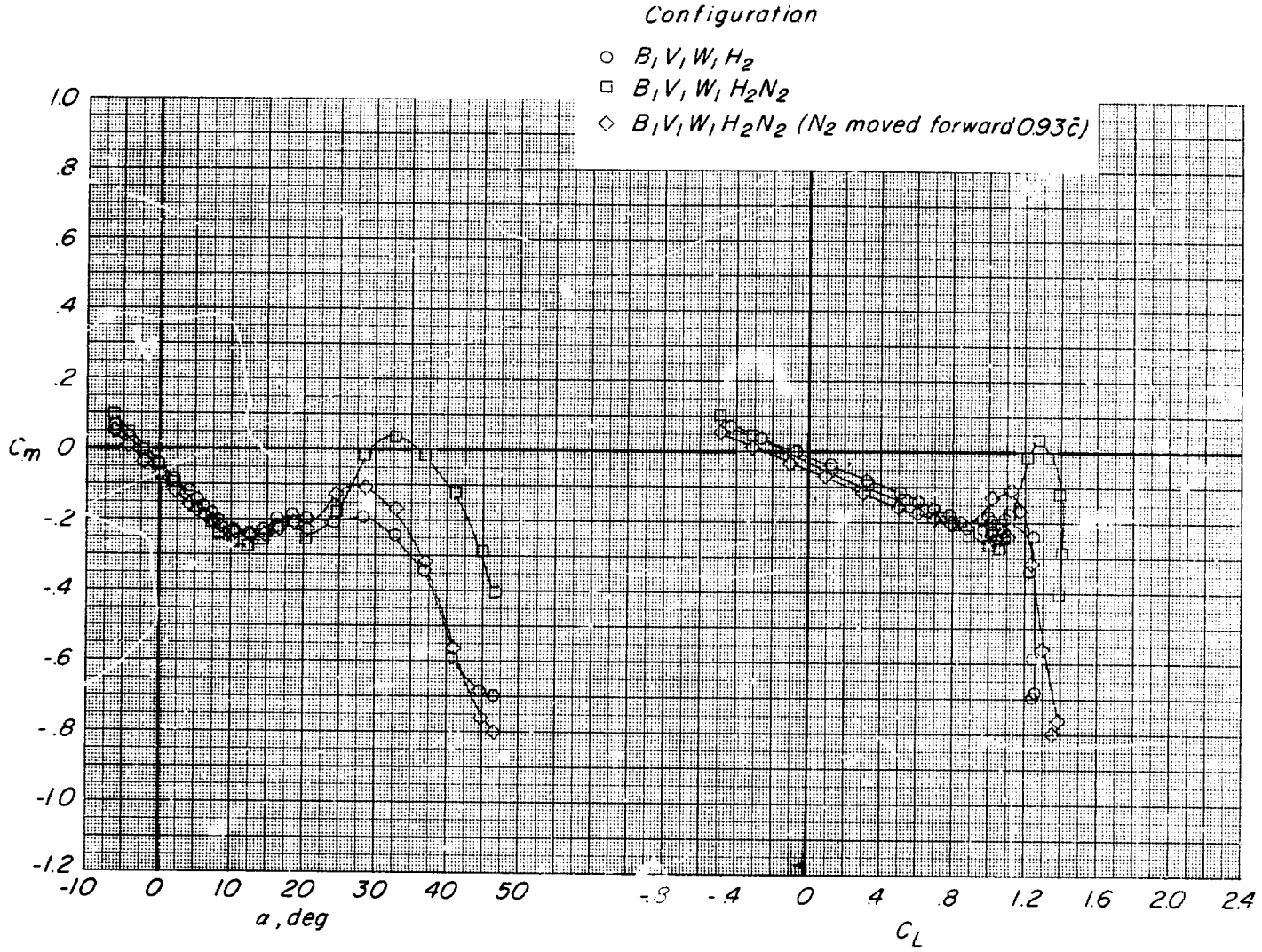

(a) Basic configuration with nacelles without nacelles, and with nacelles moved forward 0.93$\bar{c}$.

Figure 14.- Effect of nacelle position on longitudinal stability characteristics of basic configuration ($B_1V_1W_1H_2N_2$). M = 0.21; R = 0.78 × 10^6.

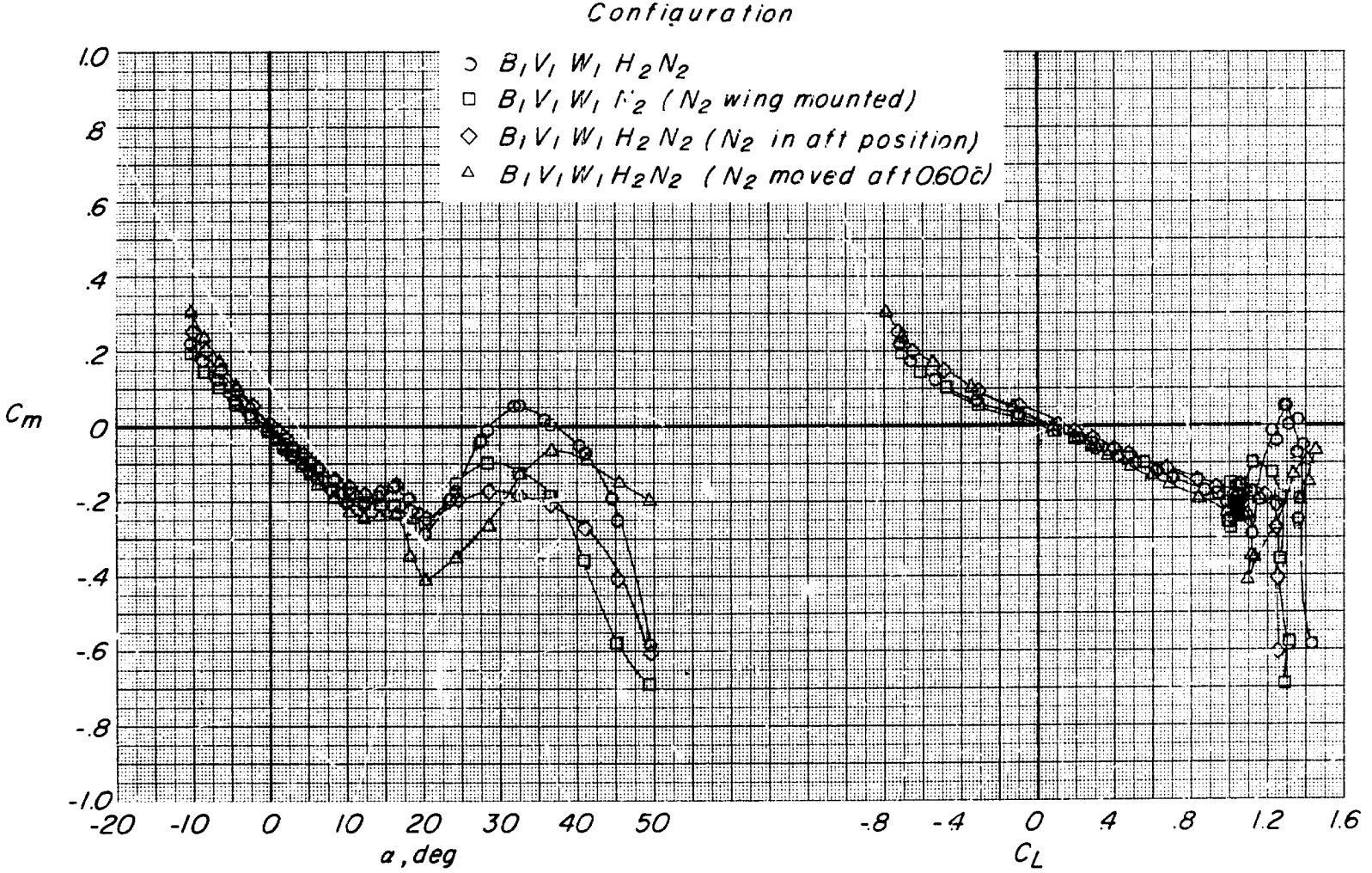

(b) Basic configuration with nacelles, with nacelles wing-mounted, with nacelles in aft position, and with nacelles moved aft 0.60c̄.

Figure 14.- Concluded.

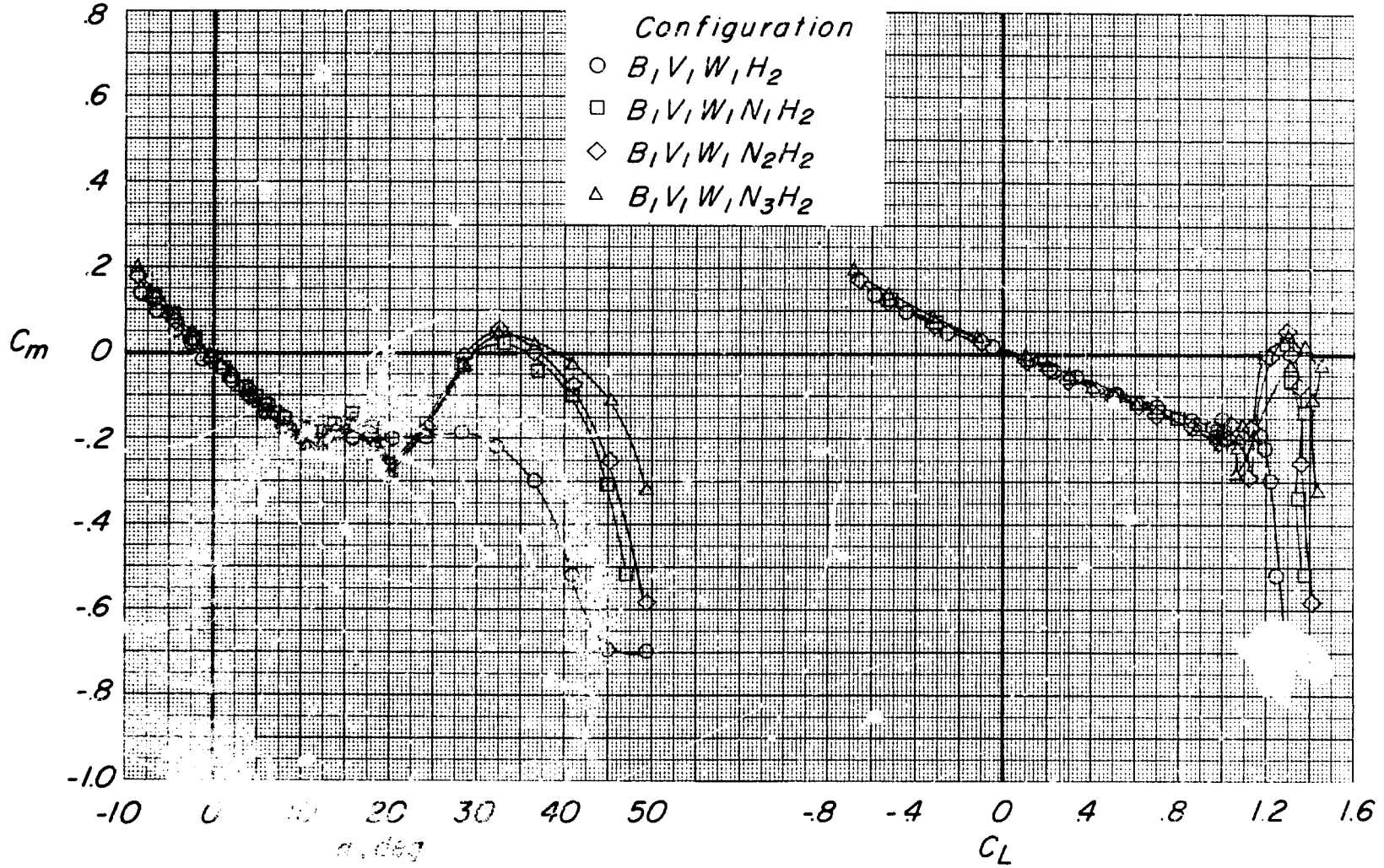

Figure 15.- Effect of nacelle size on longitudinal stability characteristics of basic configuration ($B_1V_1W_1H_2N_2$). M = 0.21; R = 0.78×10^6.

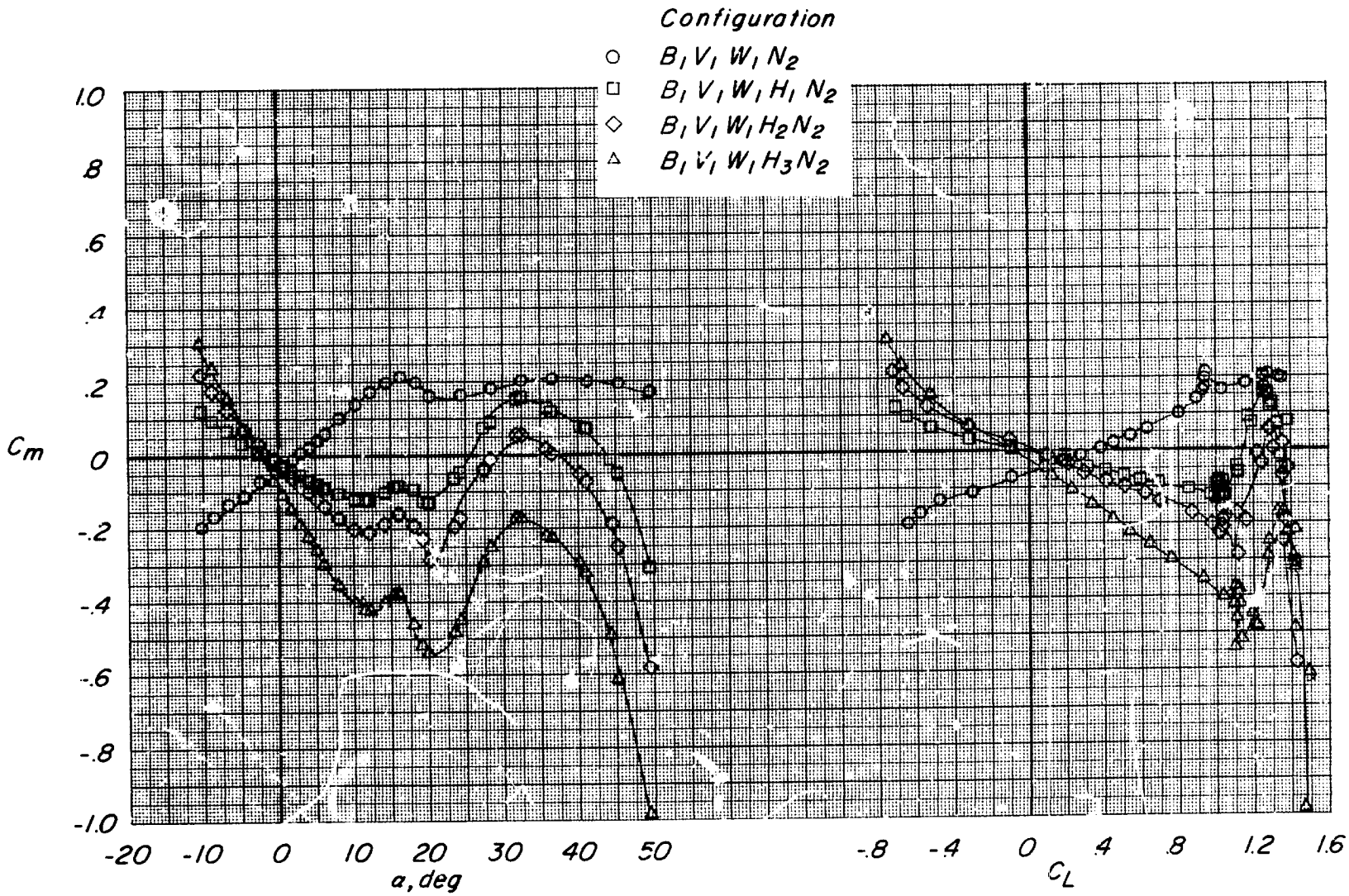

Figure 16.- Effect of horizontal-tail size on longitudinal stability characteristics of basic configuration ($B_1V_1W_1H_2N_2$). M = 0.21; R = 0.78 × 10^6.

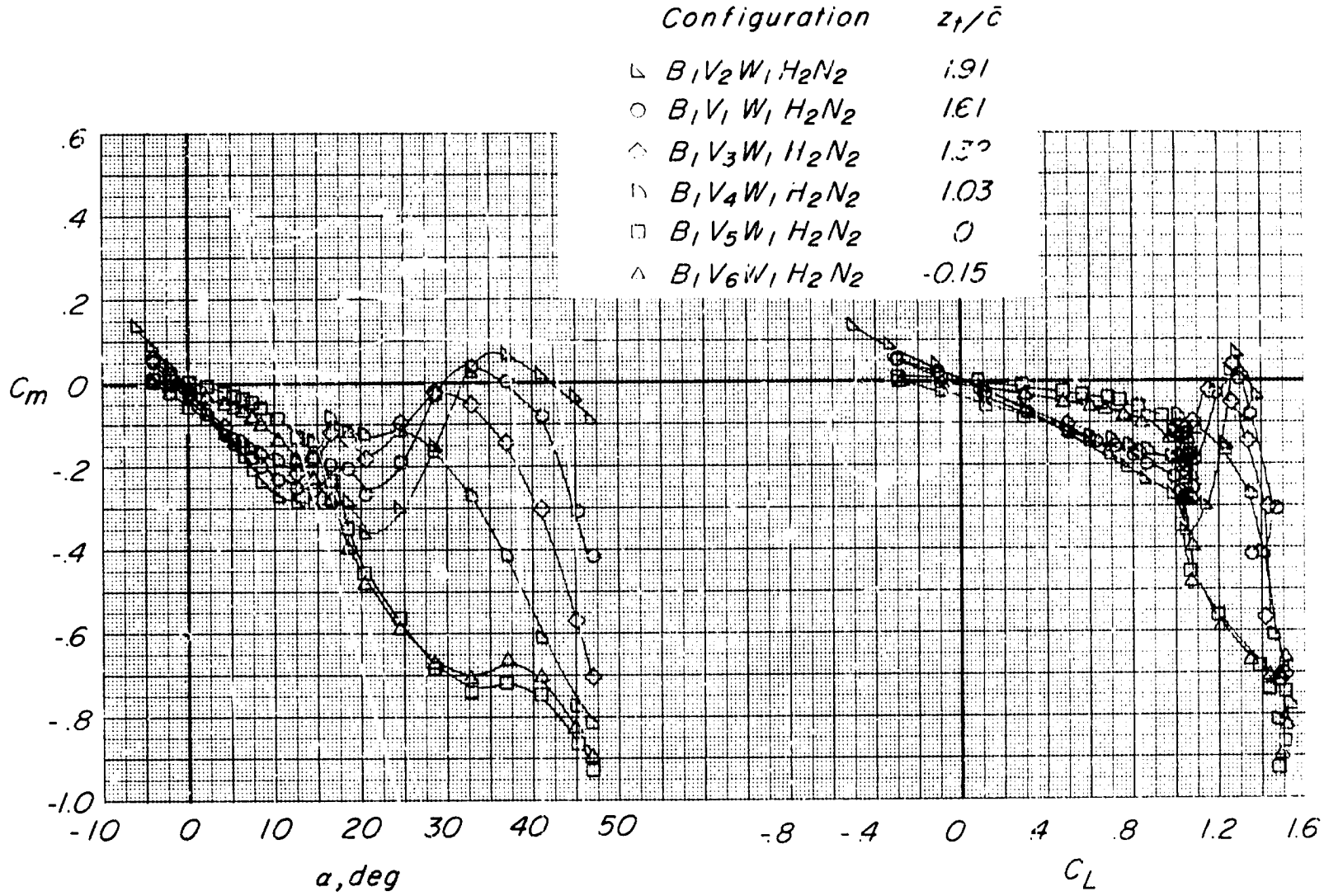

Figure 17.- Effect of horizontal-tail height on longitudinal stability characteristics of basic configuration ($B_1V_1W_1H_2N_2$). M = 0.21; R = 0.78 × 10^6.

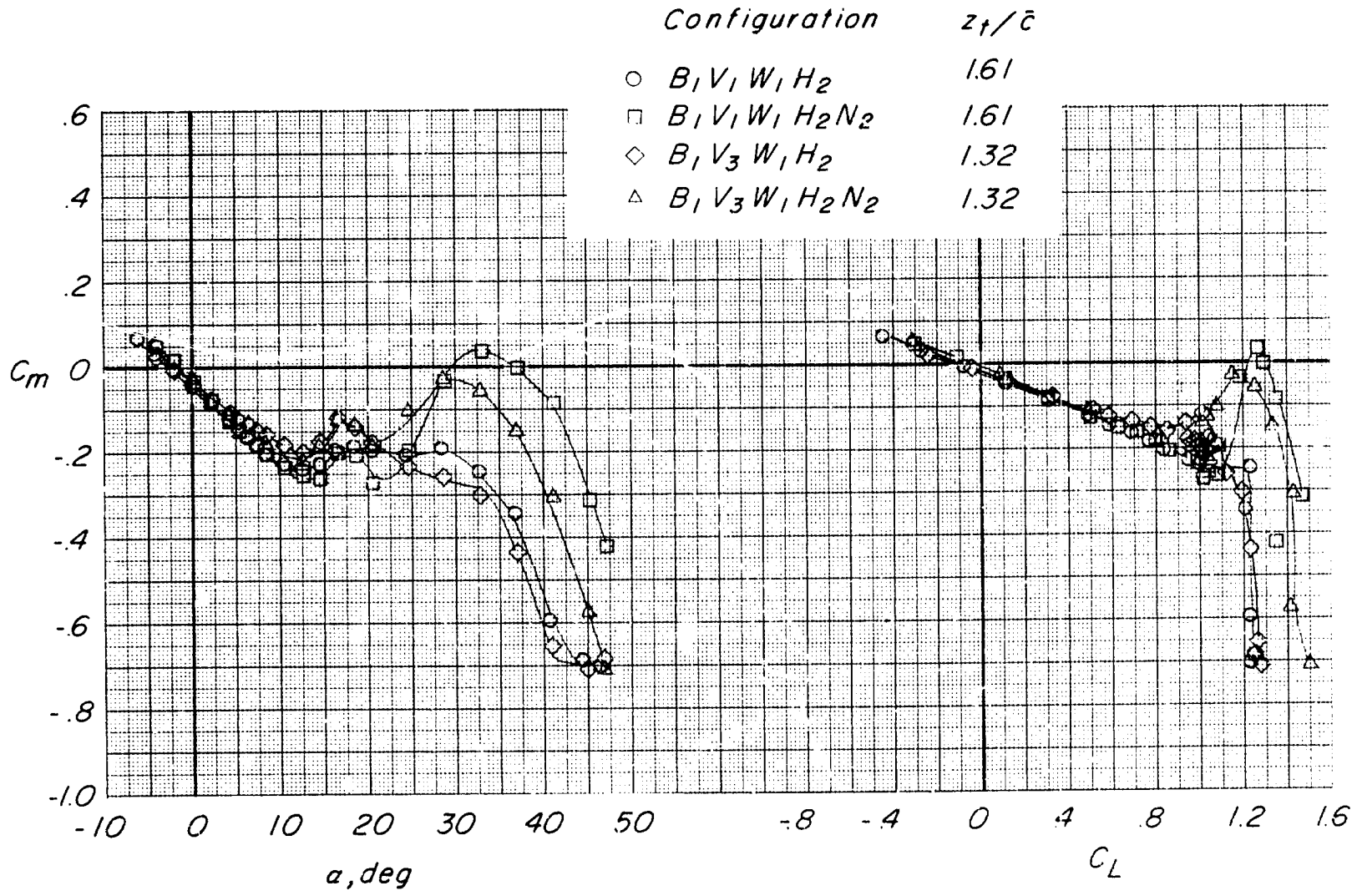

(a) V_1 and V_3.

Figure 18.- Effect of nacelles on longitudinal stability characteristics of basic configuration having various horizontal-tail heights. M = 0.21; R = 0.78×10^6.

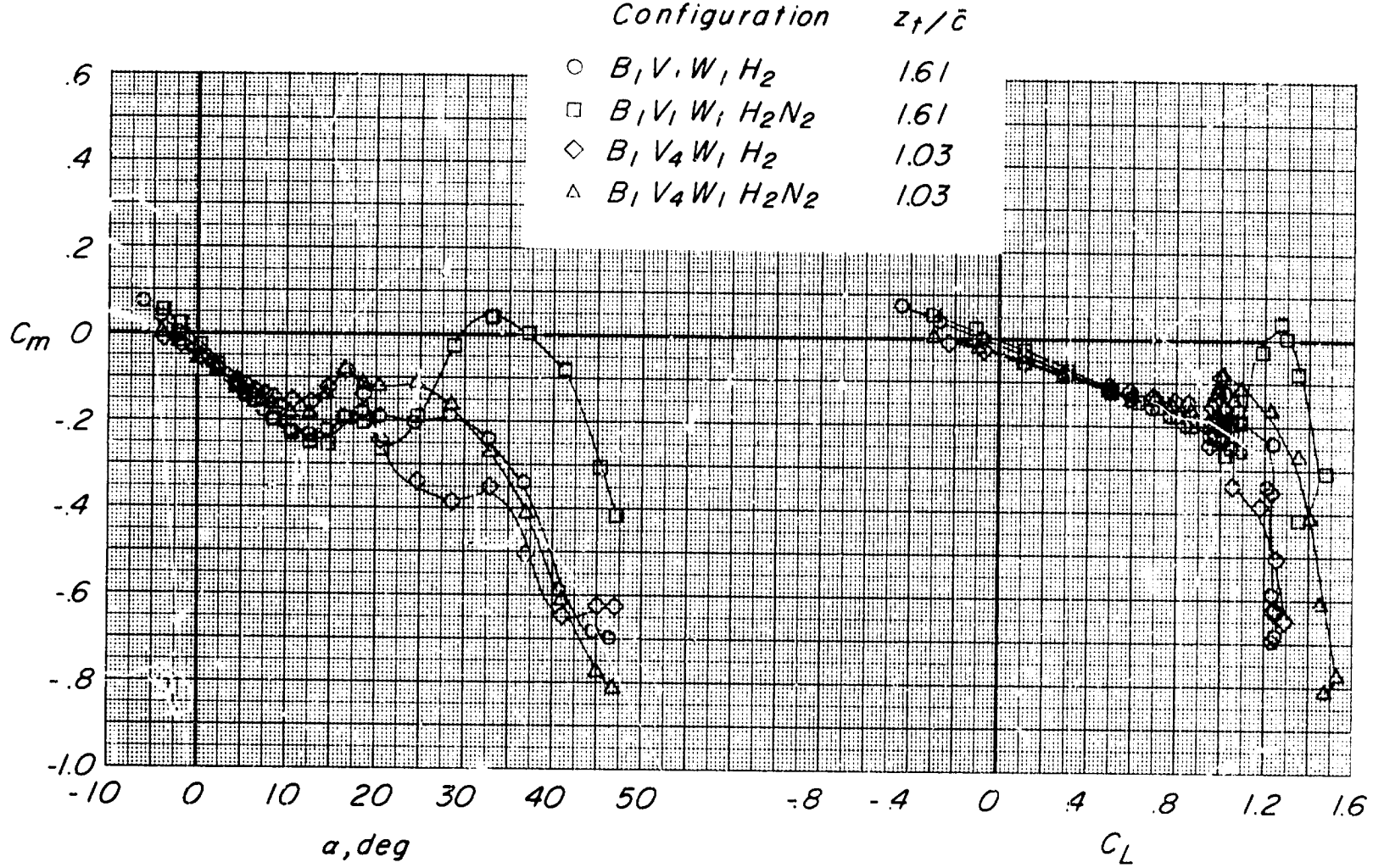

(b) V_1 and V_4.

Figure 18.- Continued.

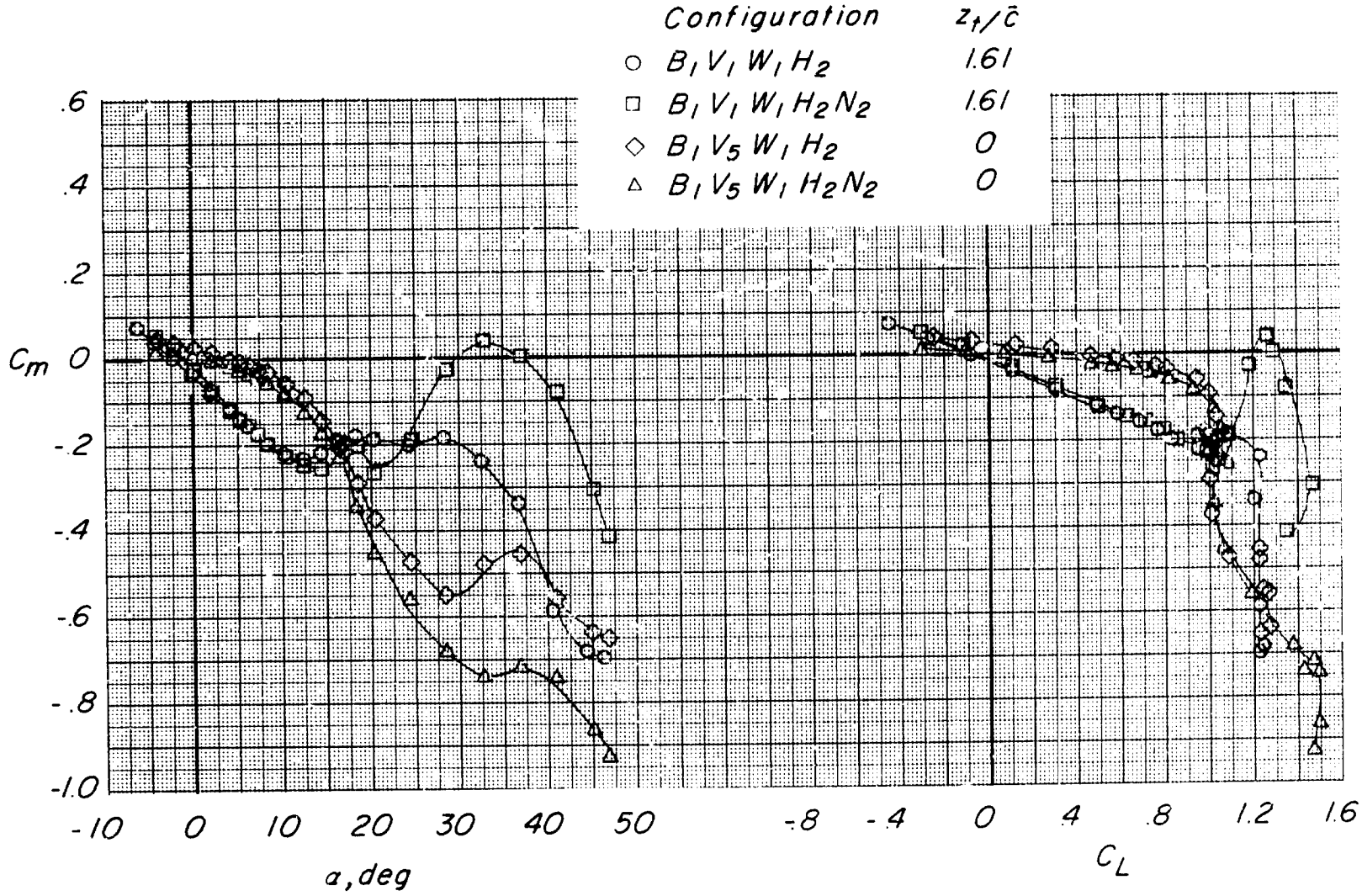

(c) V_1 and V_5.

Figure 18.- Concluded.

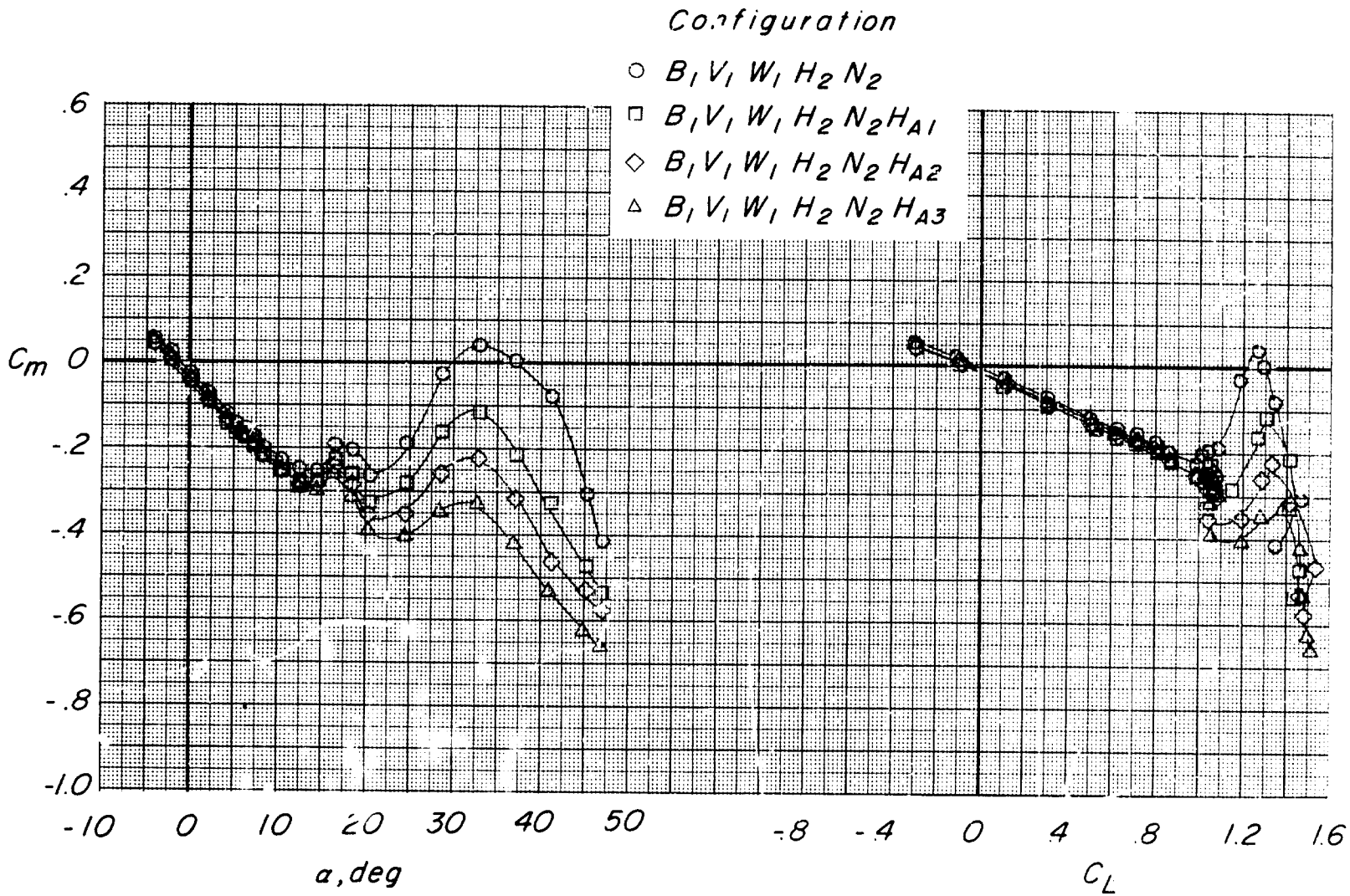

Figure 19.- Effect of auxiliary horizontal tails on longitudinal stability characteristics of basic configuration $(B_1V_1W_1H_2N_2)$. M = 0.21; R = 0.78 × 10^6.

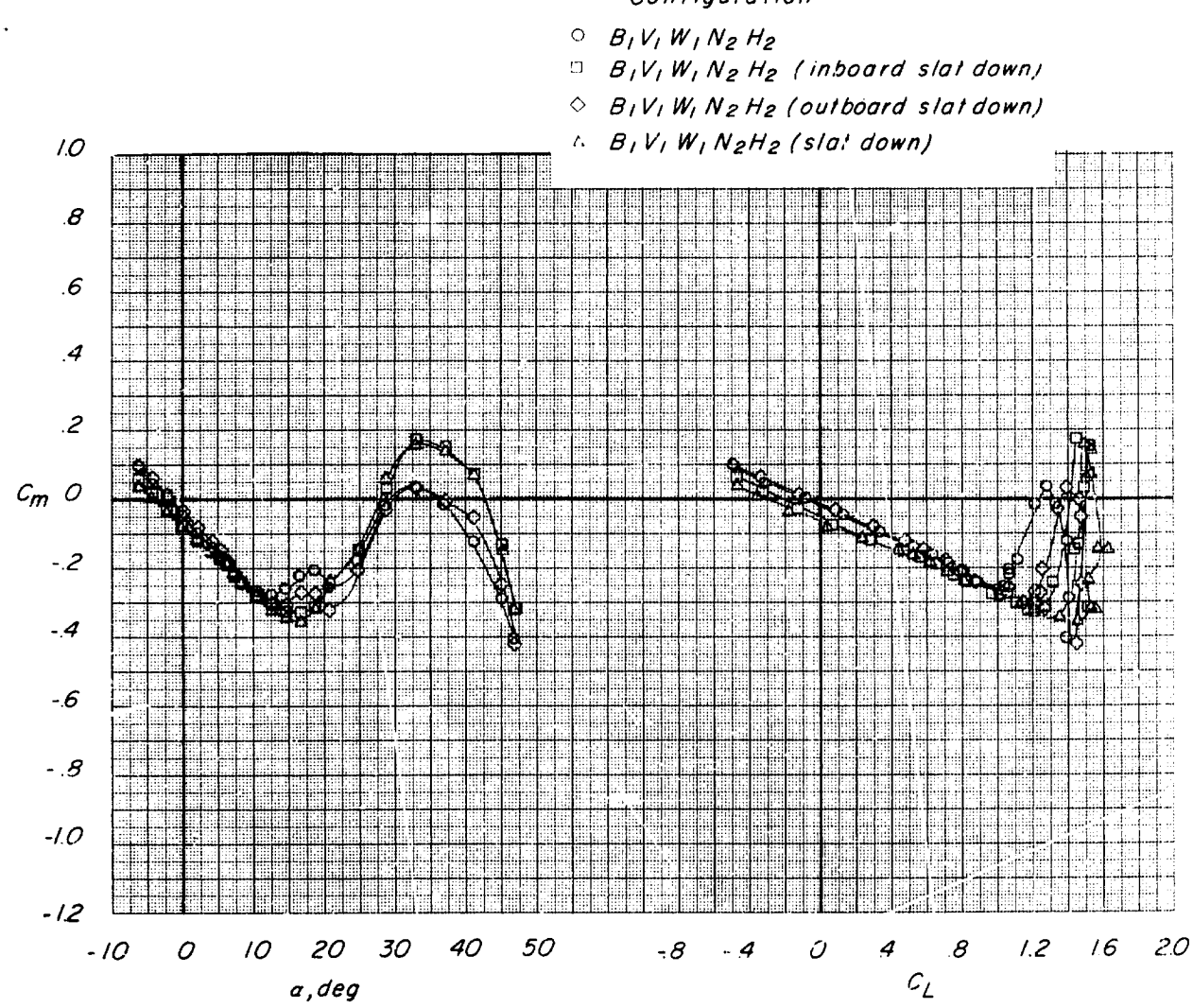

(a) Variation of C_m with α and C_L.

Figure 20.- Effect of wing slats on longitudinal aerodynamic characteristics of basic configuration ($B_1V_1W_1N_2H_2$). M = 0.21; R = 0.78 × 10^6.

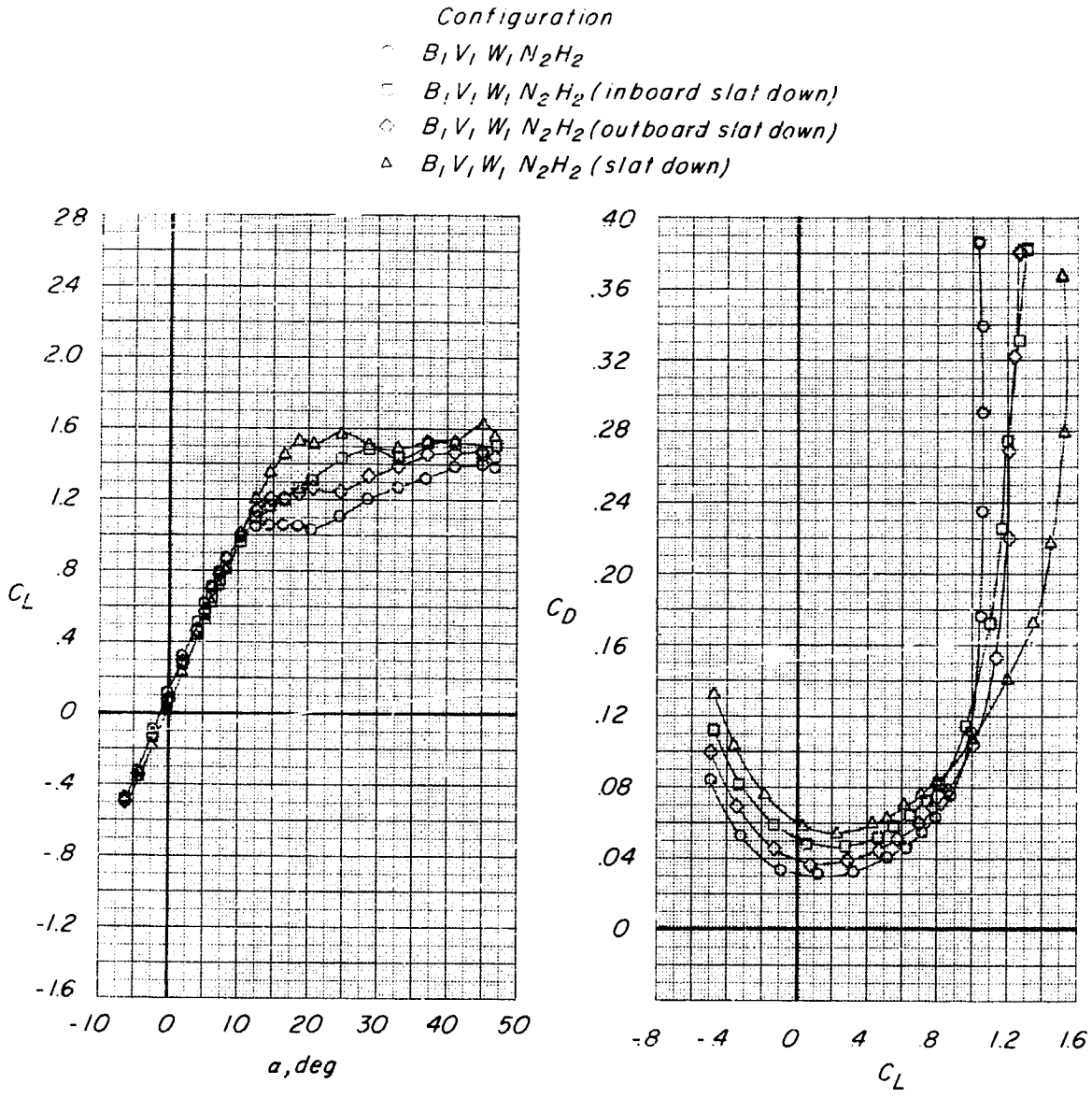

(b) Variation of C_L with α and C_D with C_L.

Figure 20.- Continued.

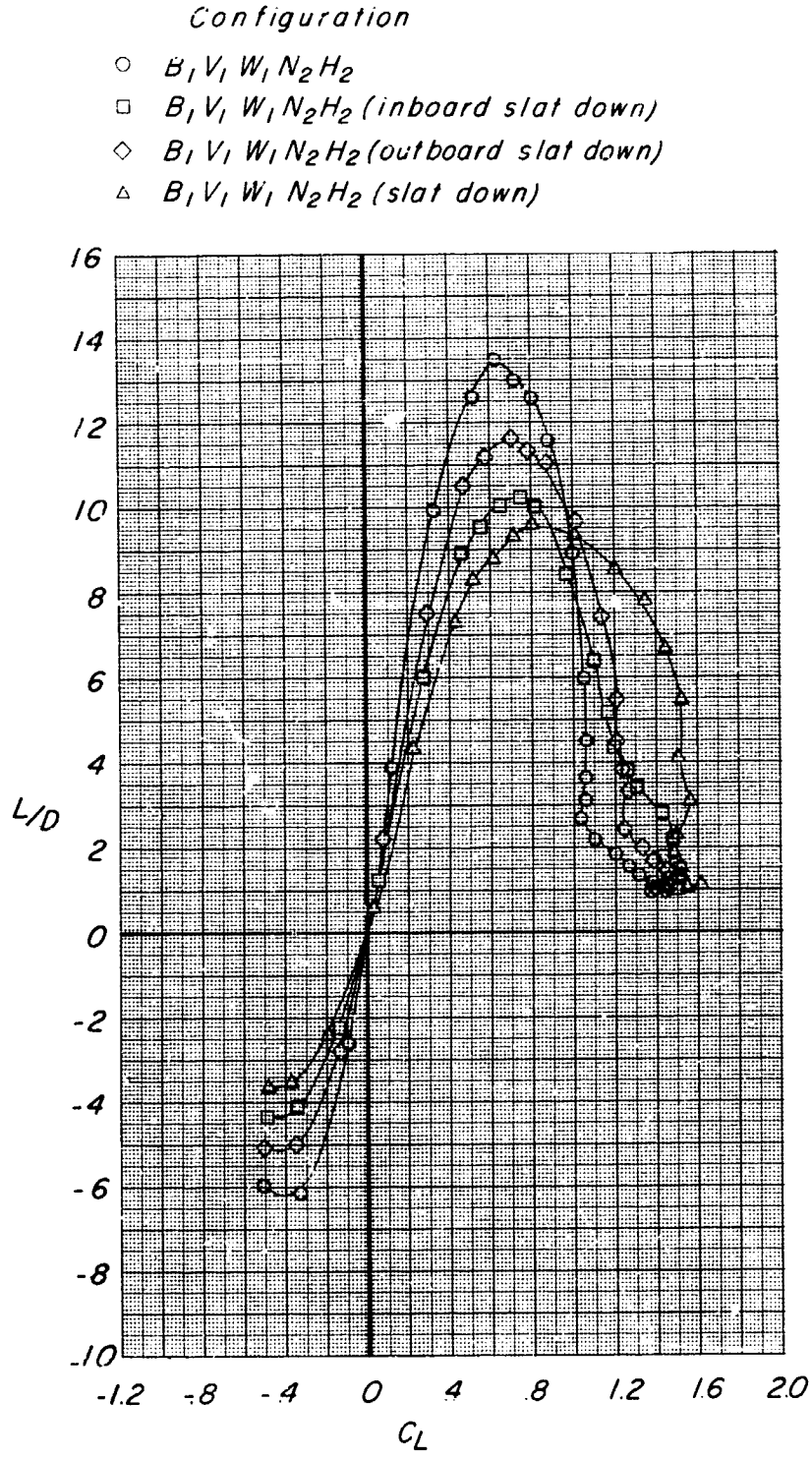

(c) Variation of L/D with C_L.

Figure 20.- Concluded.

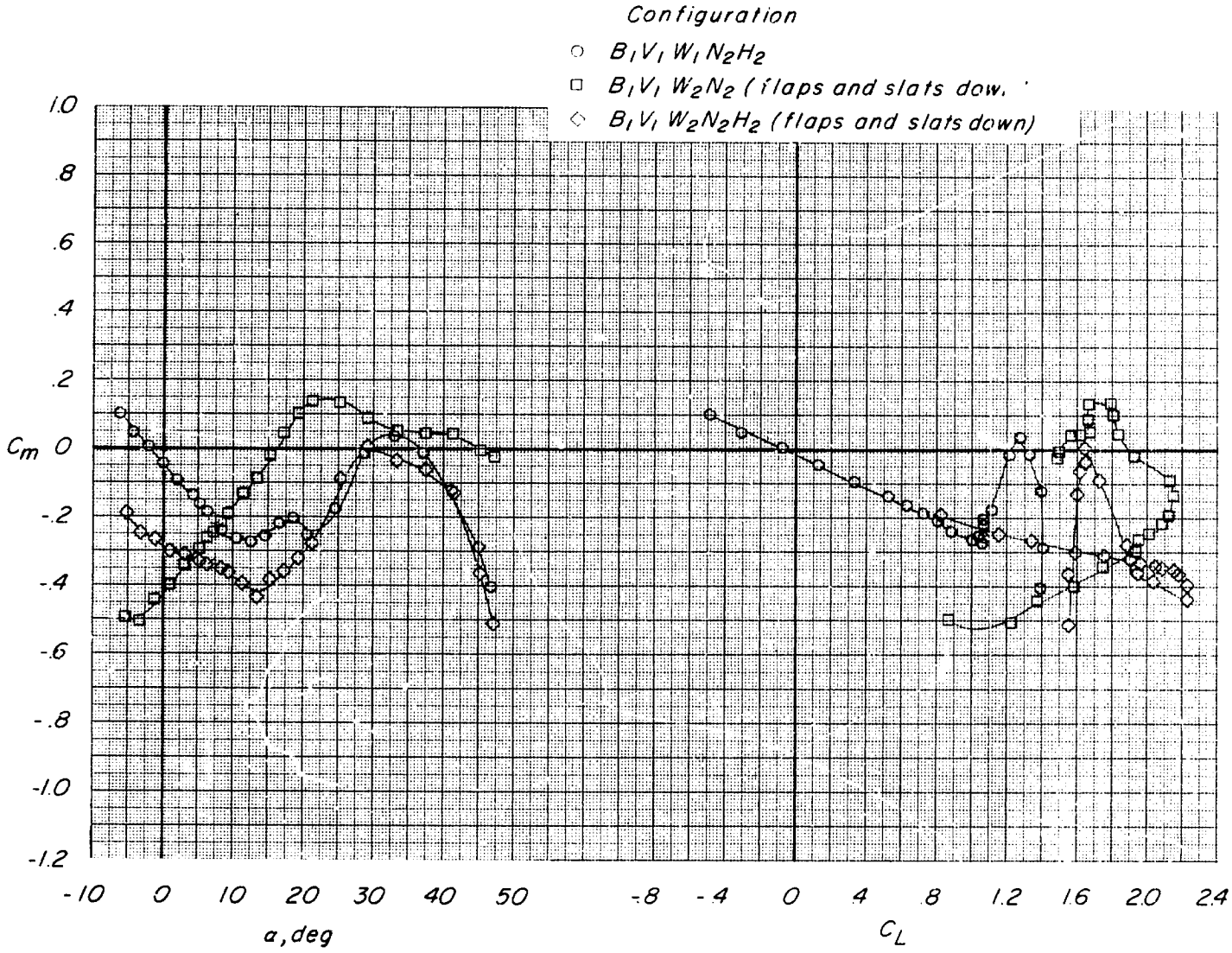

(a) Variation of C_m with α and C_L.

Figure 21.- Effect of wing flaps and slats on longitudinal aerodynamic characteristics of basic configuration ($B_1V_1W_1N_2H_2$). M = 0.21; R = 0.78 x 10^6.

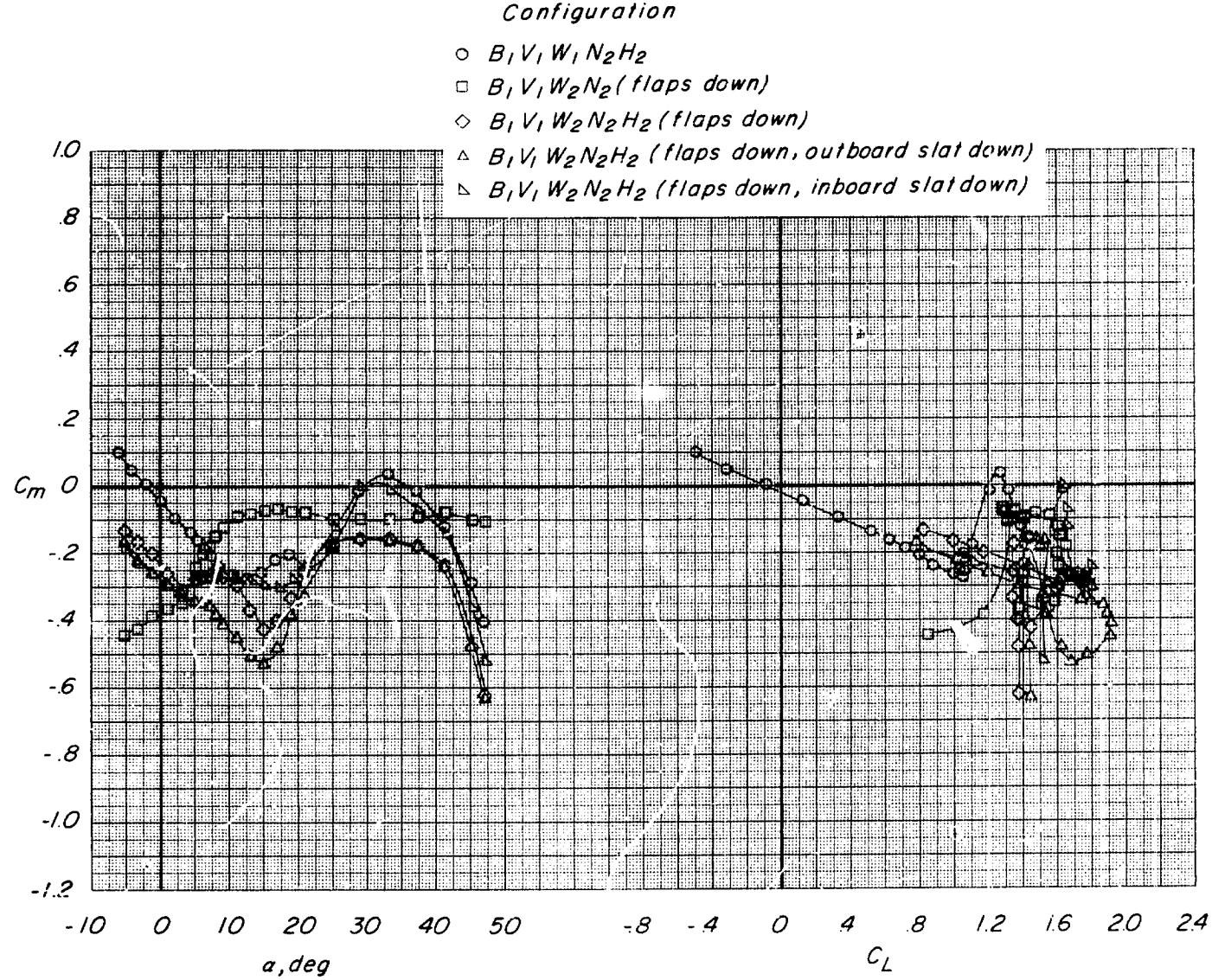

(a) Concluded.

Figure 21.- Continued.

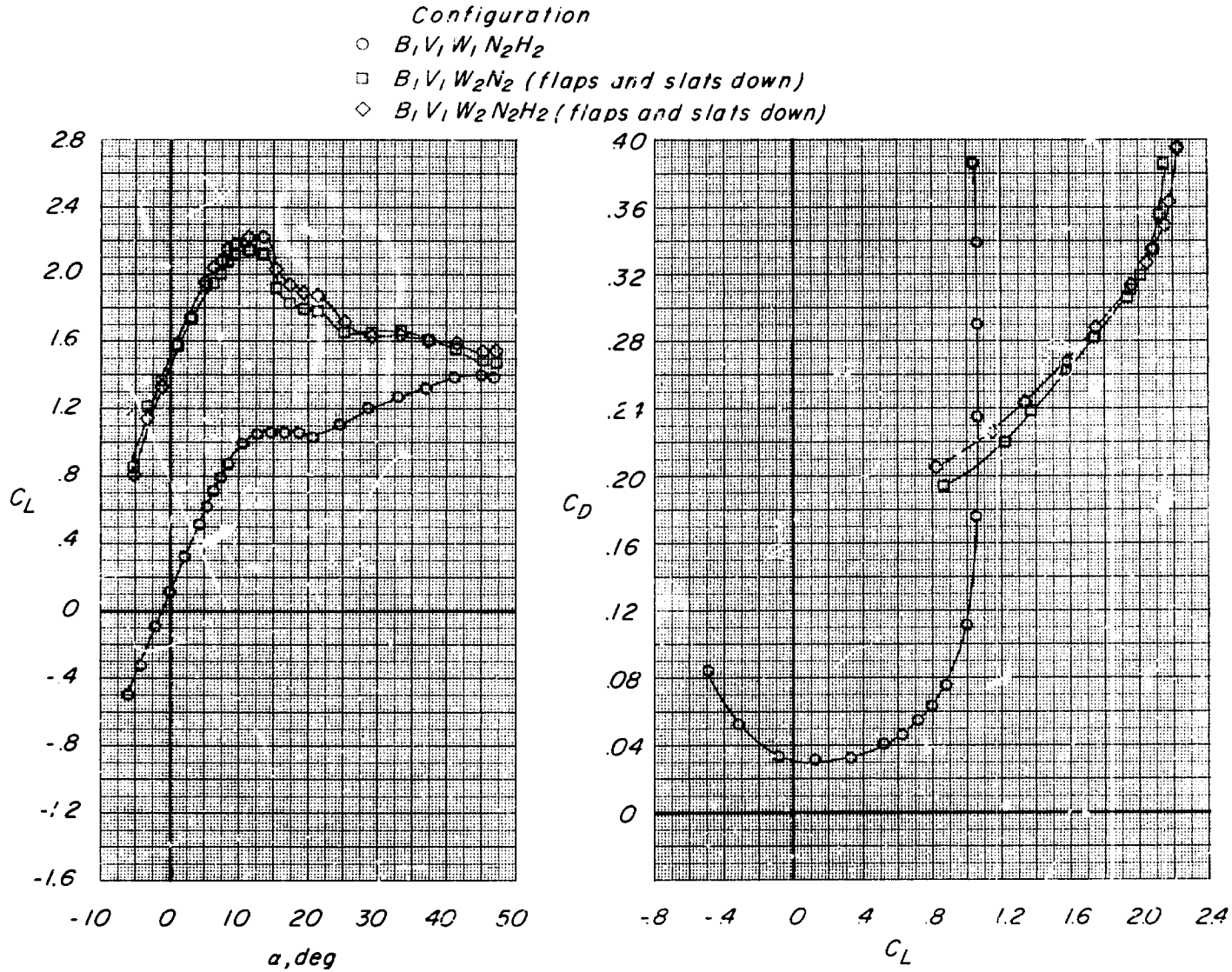

(b) Variation of C_L with α and C_D with C_L.

Figure 21.- Continued.

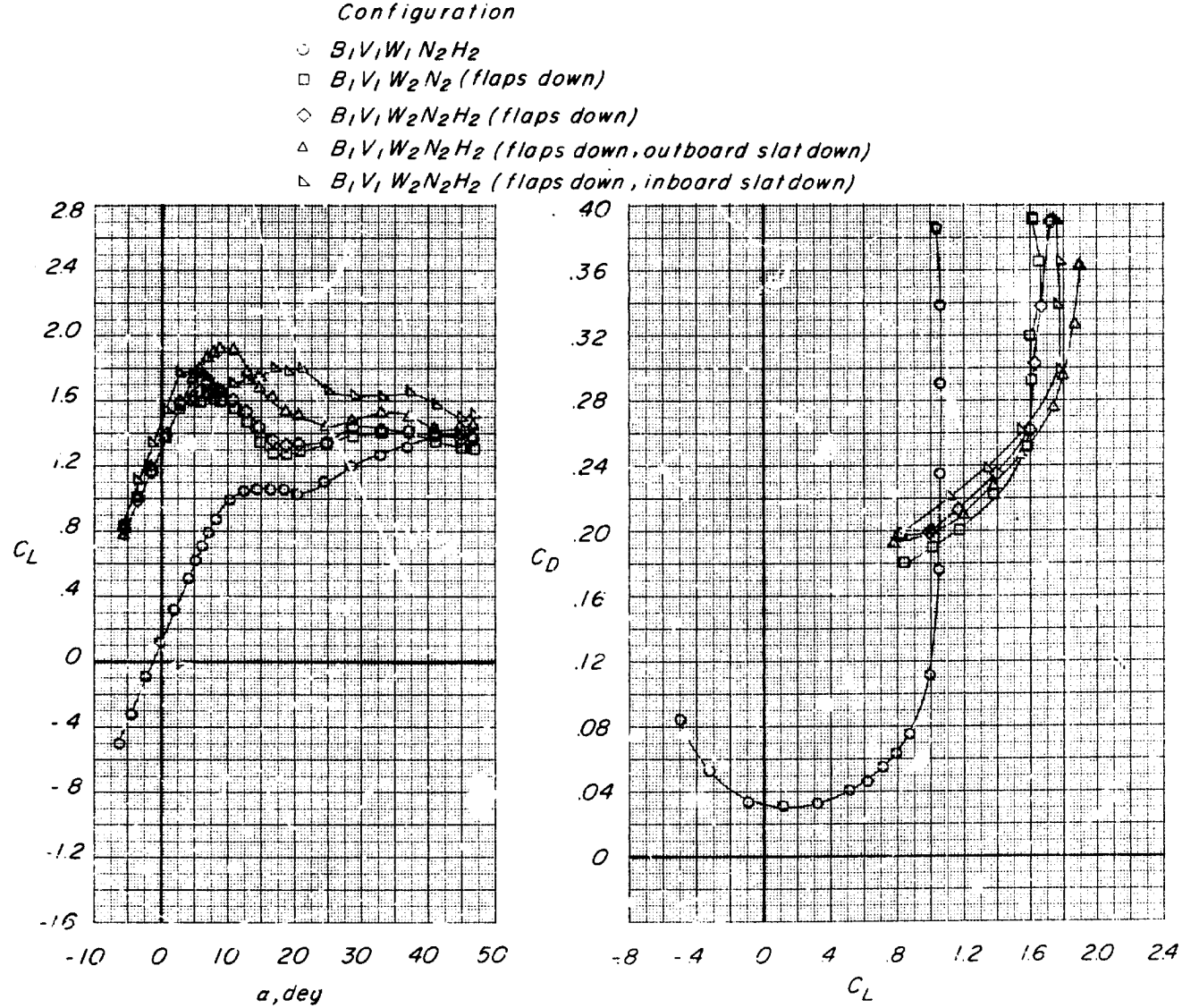

(b) Concluded.

Figure 21.- Concluded.

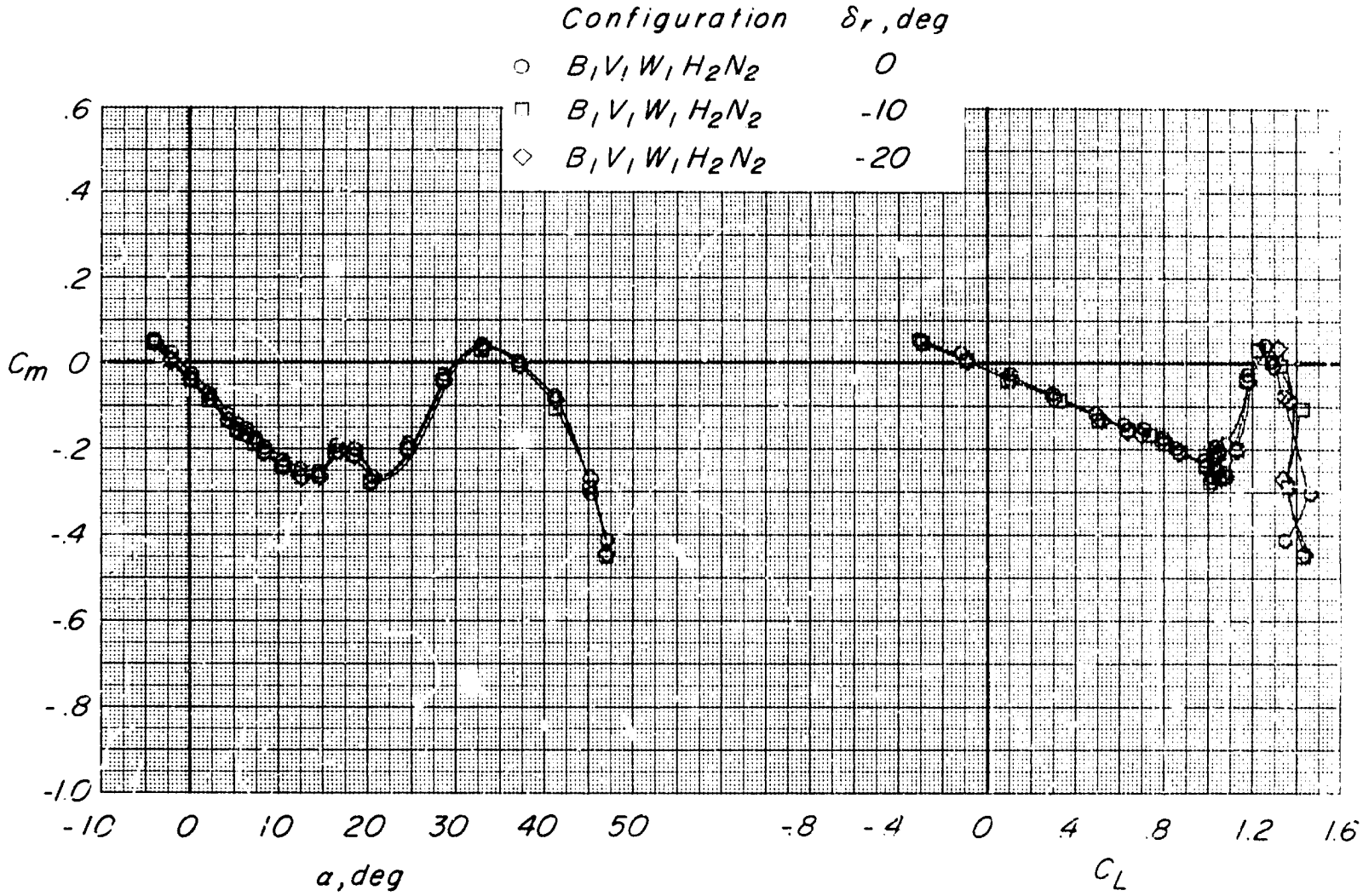

(a) Variation of C_m with α and C_L.

Figure 22.- Effect of rudder deflection on longitudinal and lateral stability characteristics of basic configuration $(B_1V_1W_1H_2N_2)$. M = 0.21; R = 0.78 × 10^6.

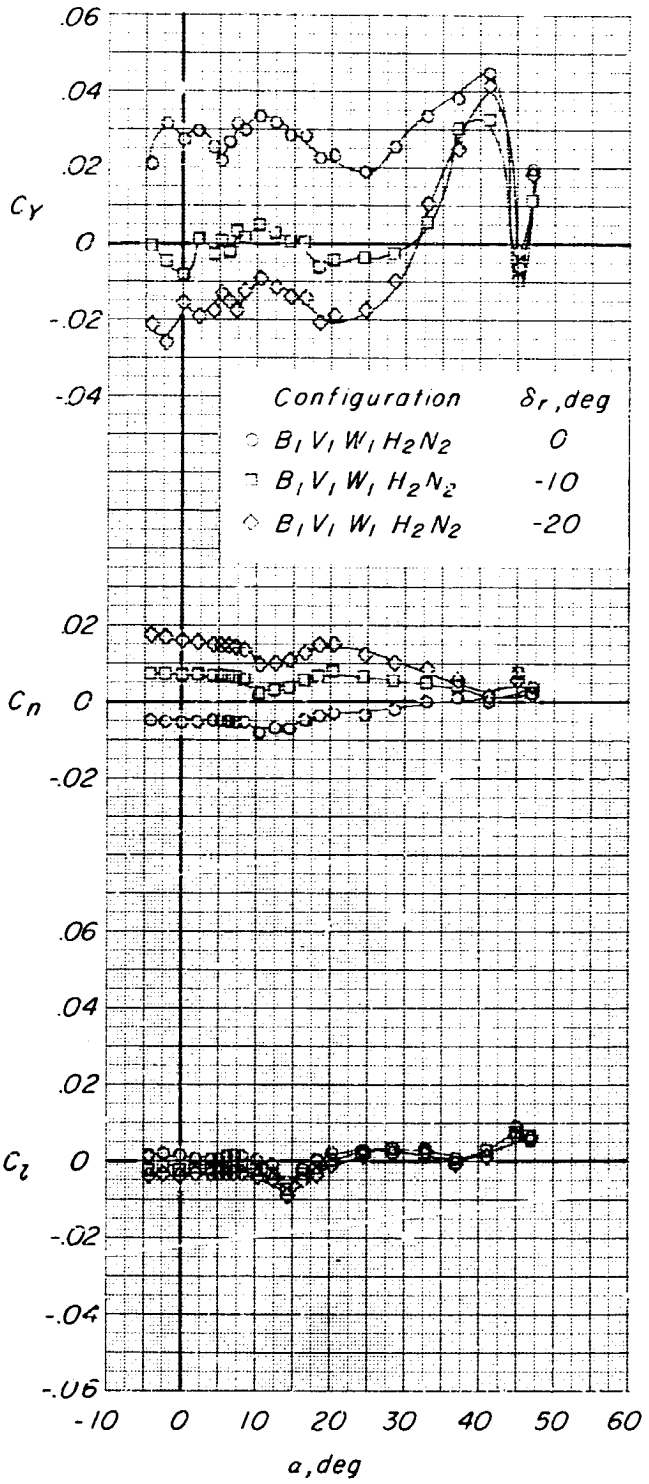

(b) Variation of C_Y, C_n, and C_l with α.

Figure 22.- Concluded.

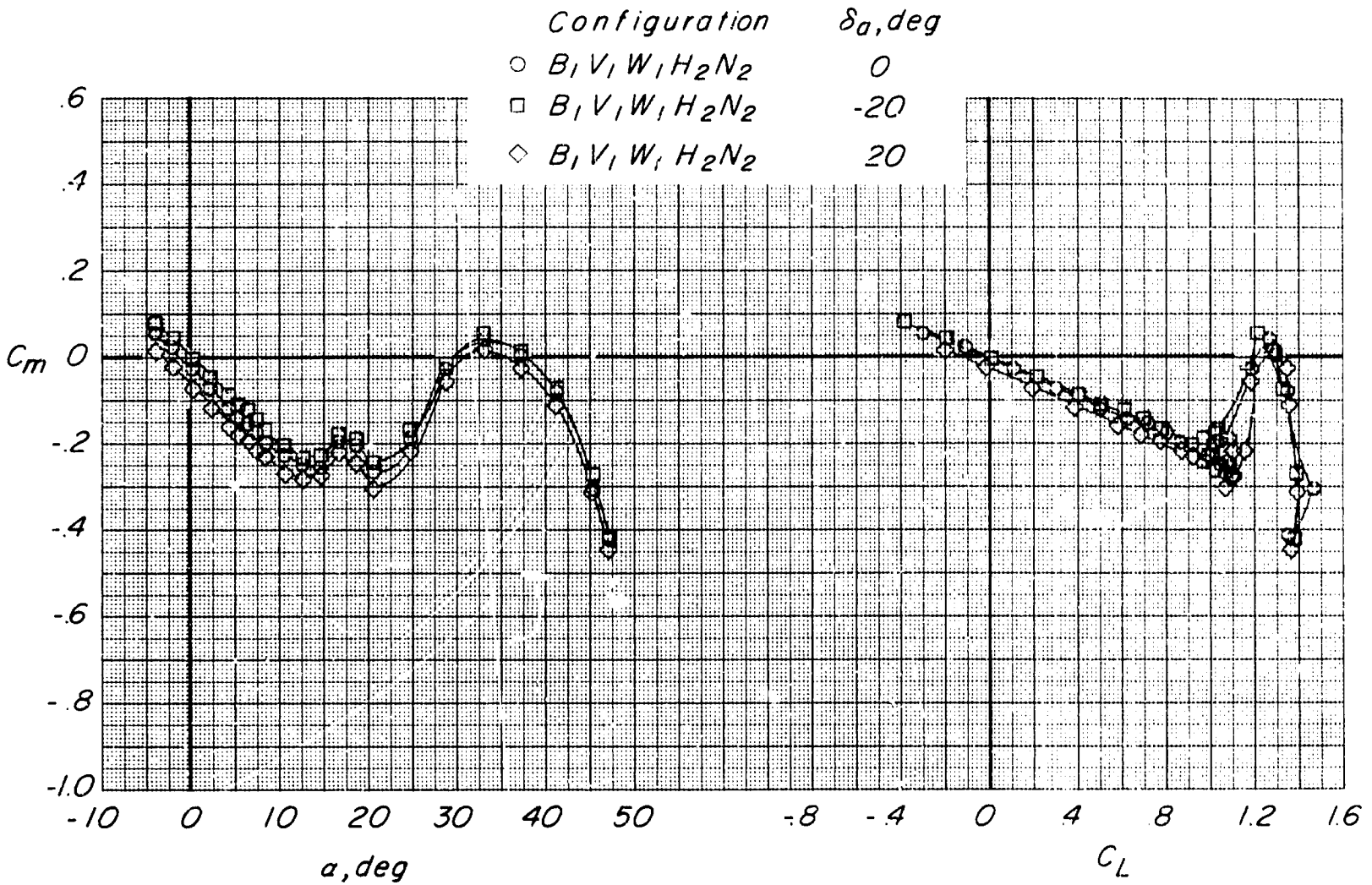

(a) Variation of C_m with α and C_L.

Figure 23.- Effect of right wing aileron deflection on longitudinal and lateral stability characteristics of basic configuration ($B_1V_1W_1H_2N_2$). M = 0.21; R = 0.78 × 10^6.

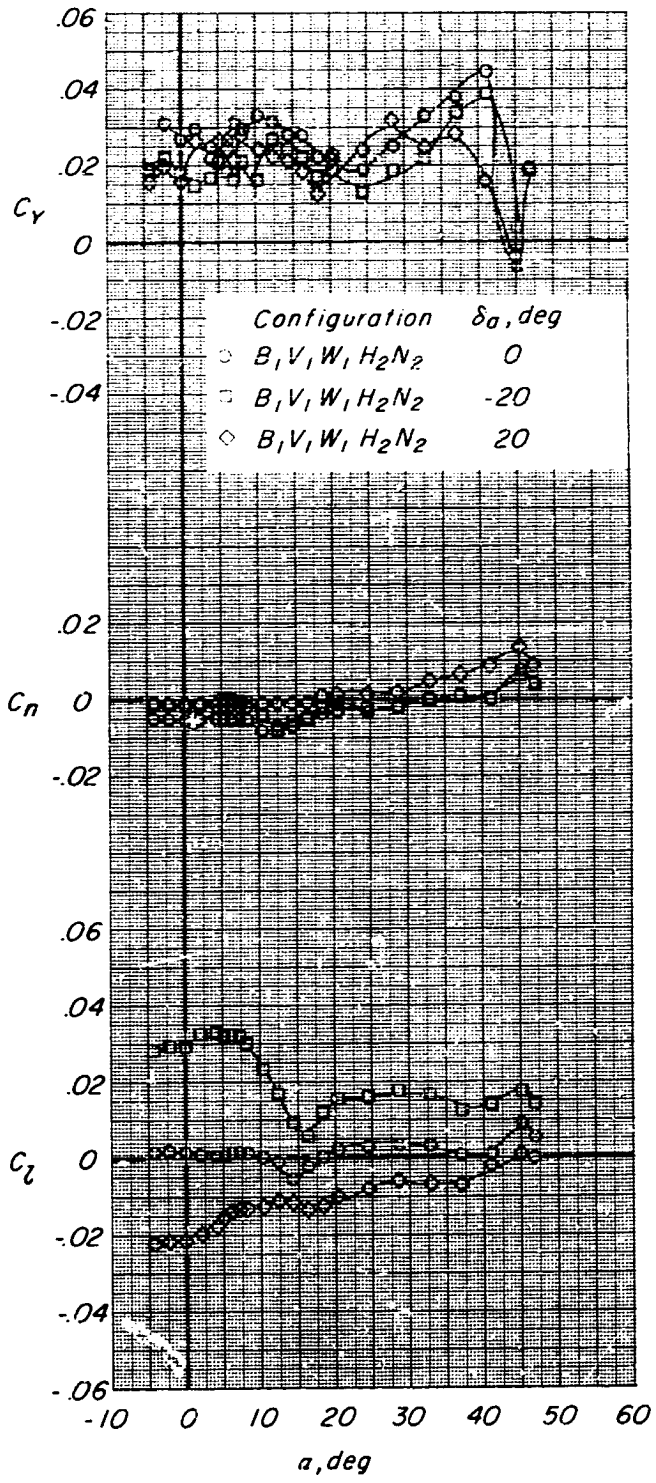

(b) Variation of C_Y, C_n, and C_l with α.

Figure 23.- Concluded.

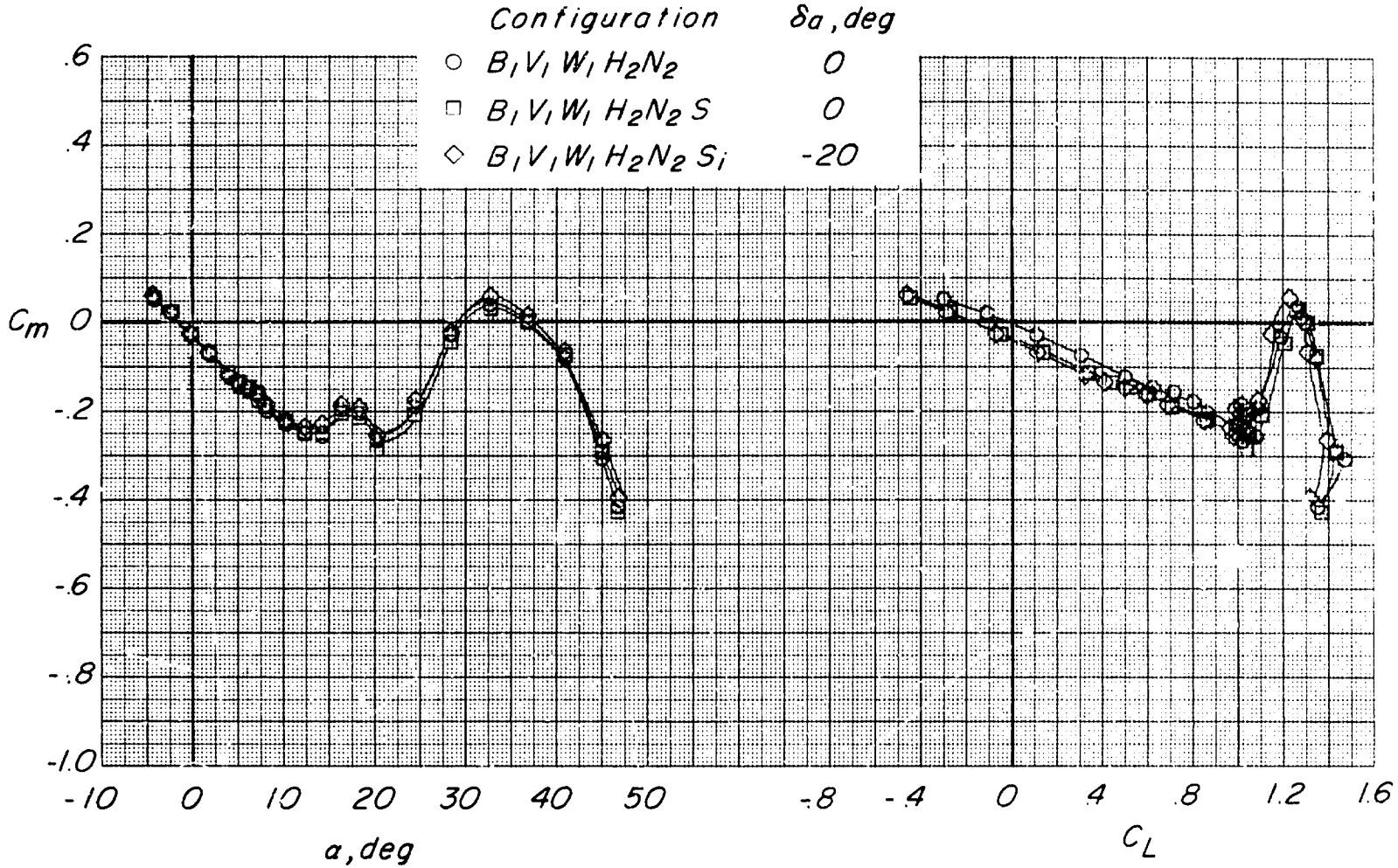

(a) Variation of C_m with α and C_L

Figure 24.- Effect of right wing aileron and spoiler deflections on longitudinal and lateral stability characteristics of basic configuration $(B_1V_1W_1H_2N_2)$. M = 0.21; R = 0.78 × 10^6.

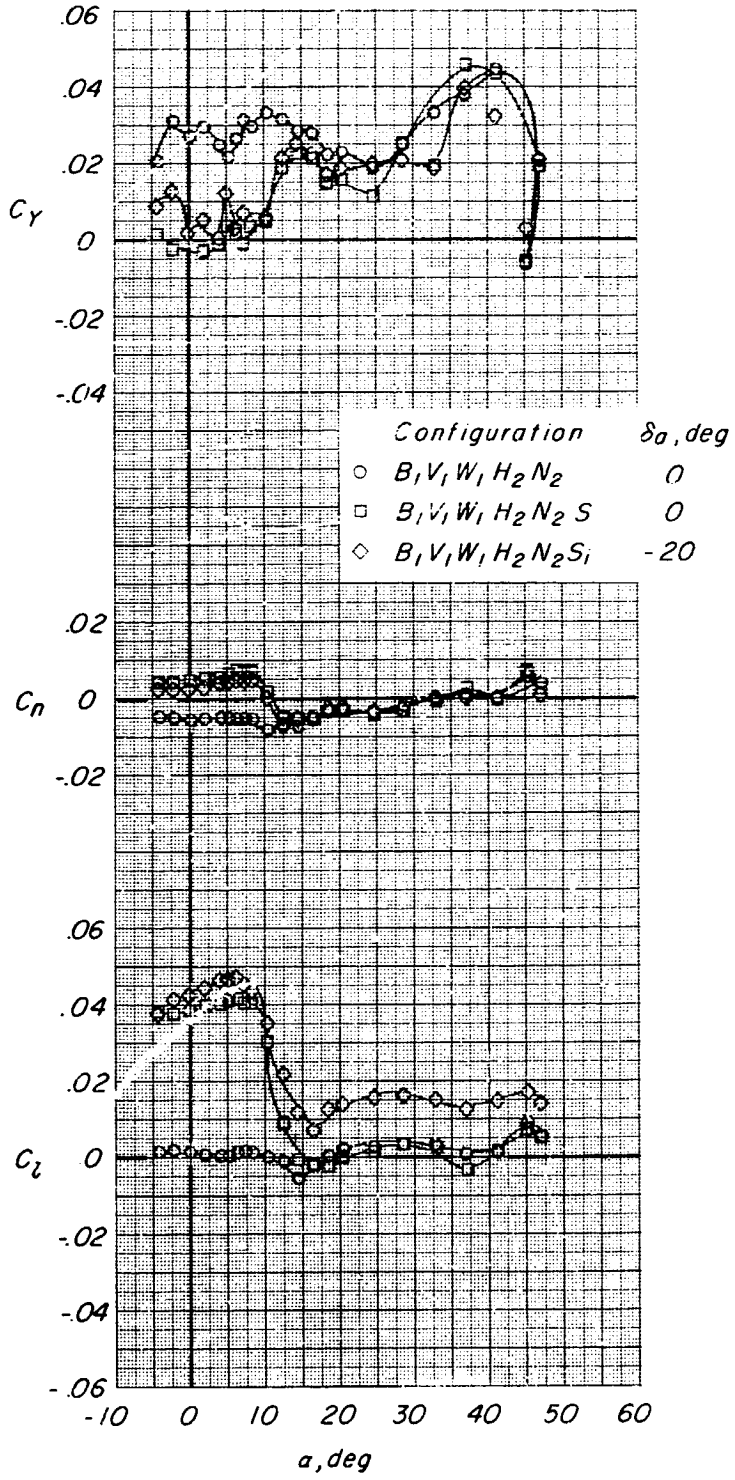

(b) Variation of C_Y, C_n, and C_l with α.

Figure 24.- Concluded.

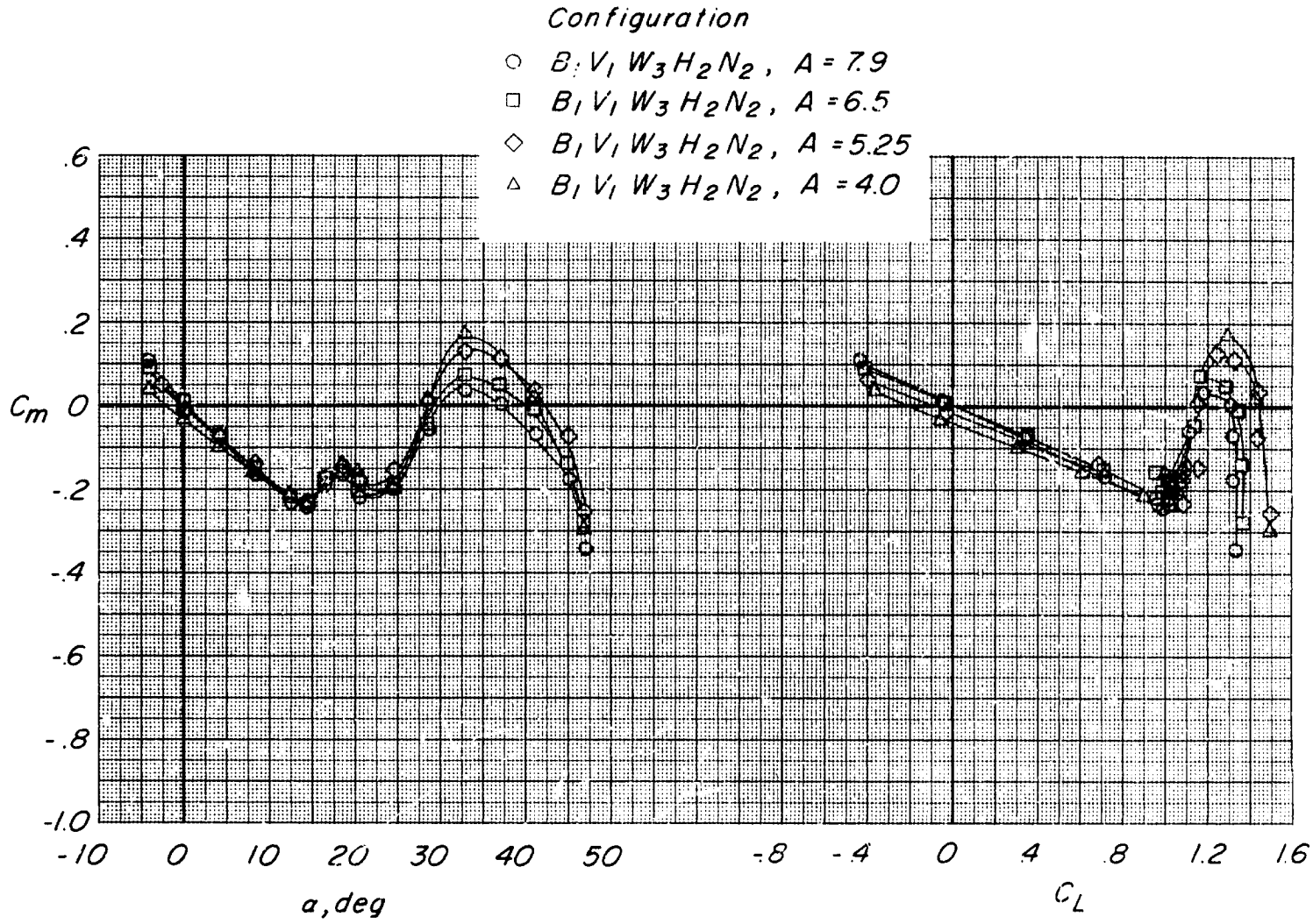

(a) Variation of C_m with α and C_L.

Figure 25.- Effect of wing aspect ratio on longitudinal aerodynamic characteristics of basic configuration with wing 3 ($B_1V_1W_3H_2N_2$). M = 0.21; R = 0.78 x 10^6.

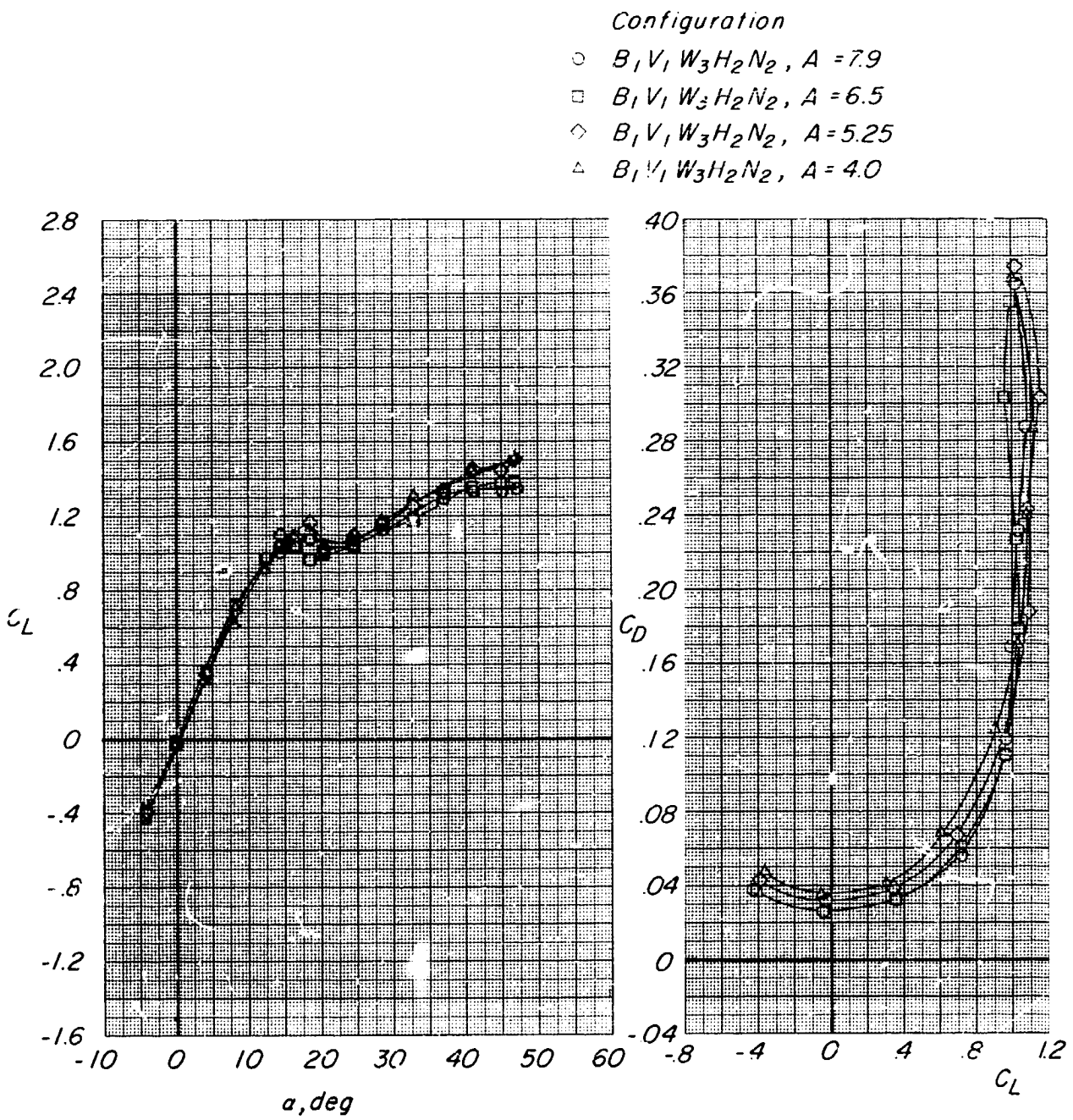

(b) Variation of C_L with α and C_D with C_L.

Figure 25.- Continued.

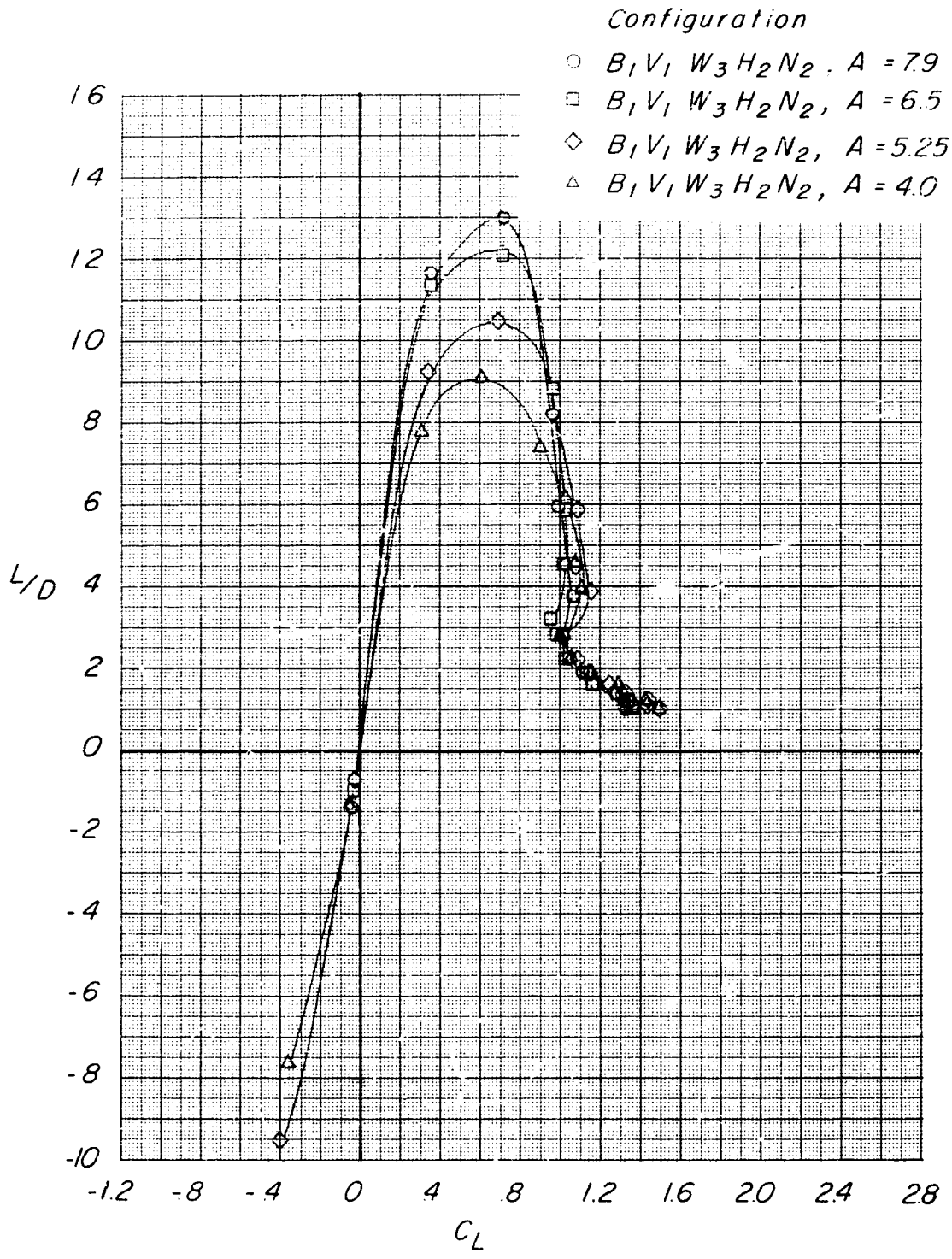

(c) Variation of L/D with C_L.

Figure 25 - Concluded.

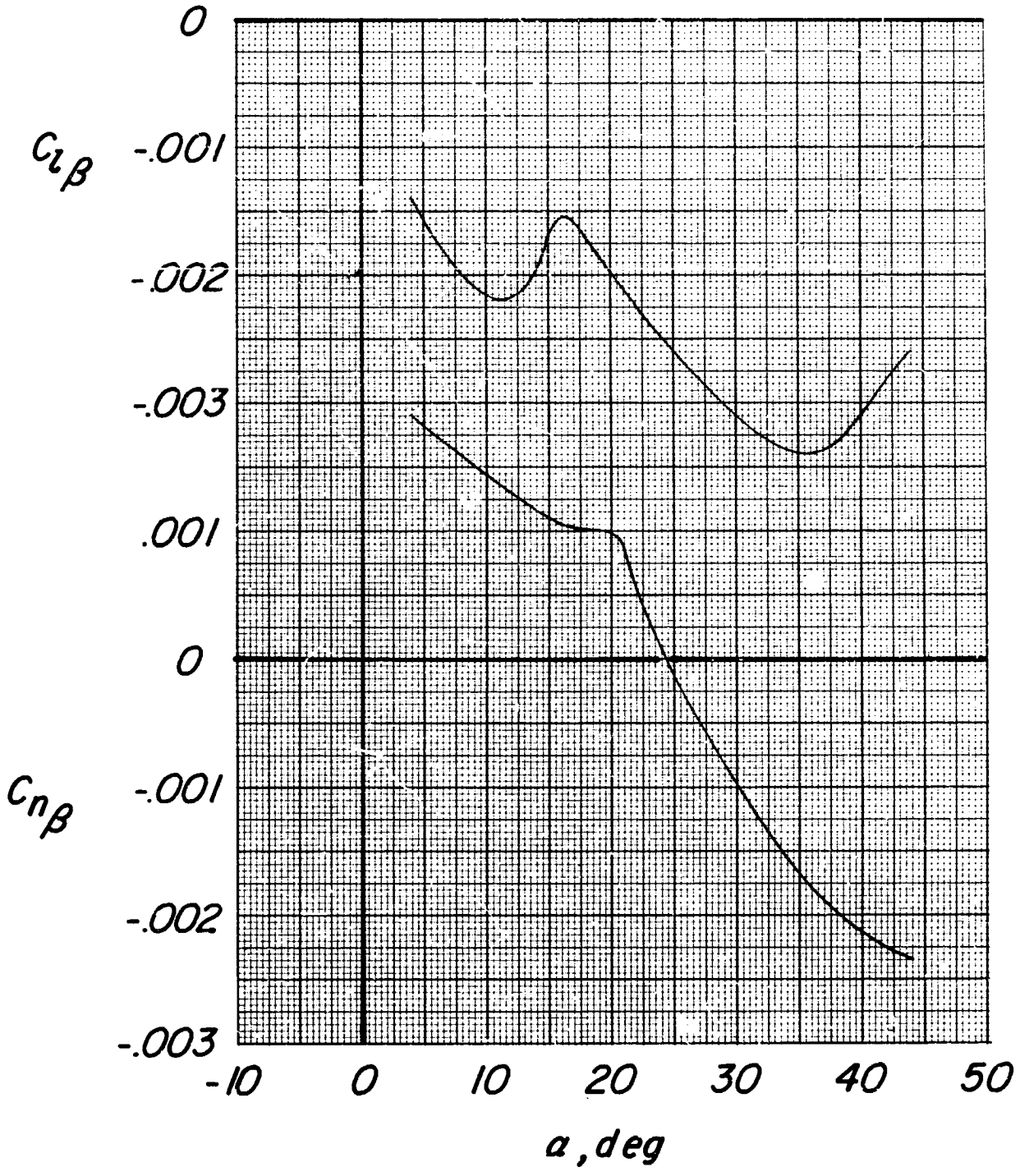

Figure 26.- Static lateral and directional stability characteristics of basic configuration $(B_1V_1W_1H_2N_2)$. M = 0.21; R = 0.78 × 10^6.

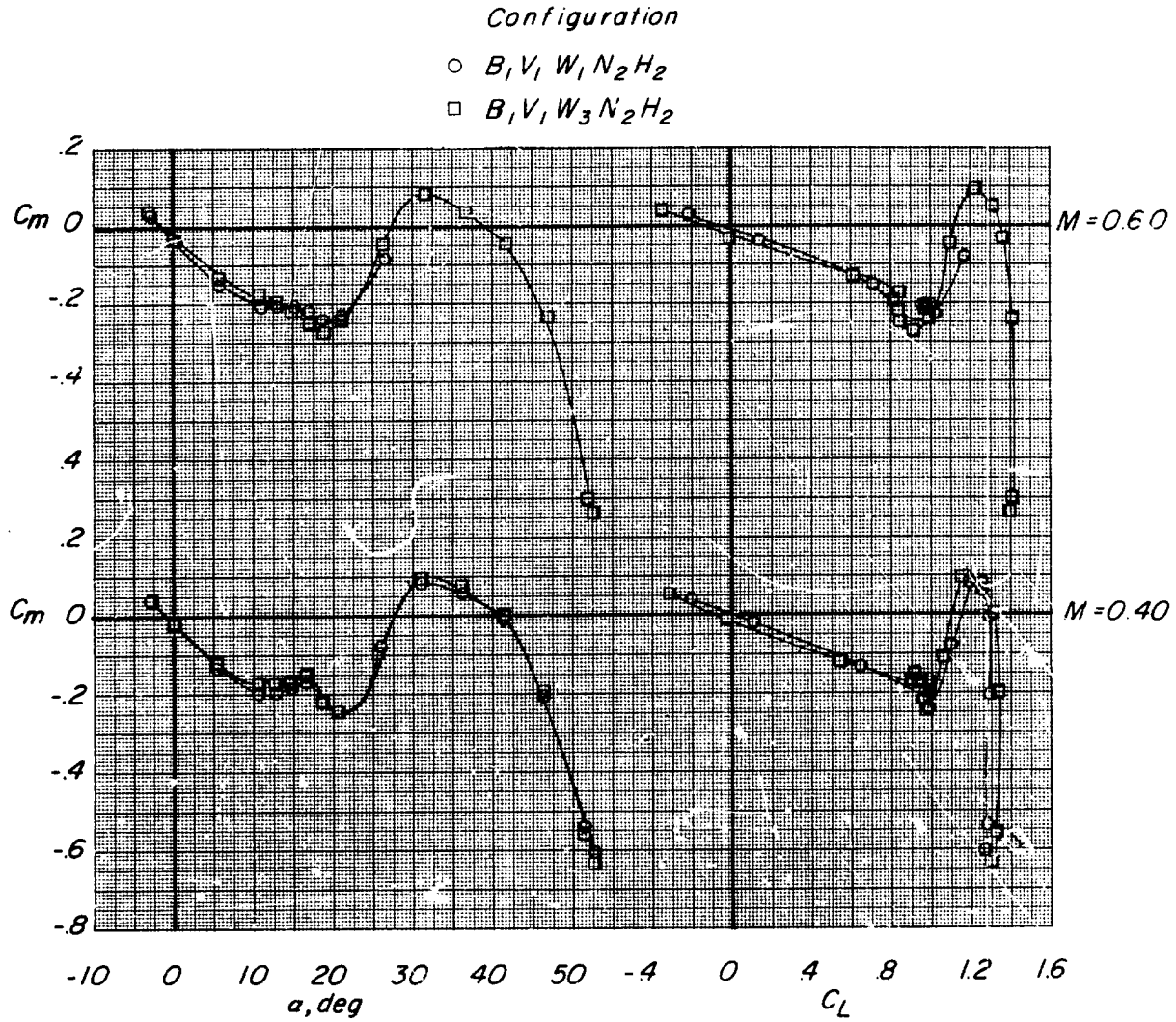

(a) Variation of C_m with α and C_L.

Figure 27.- Effect of wing airfoil section on longitudinal aerodynamic characteristics of basic configuration $(B_1V_1W_1N_2H_2)$. R = 0.71 × 10^6 at M = 0.40 and 0.60, R = 0.43 × 10^6 at M = 0.80, 0.86, and 0.91.

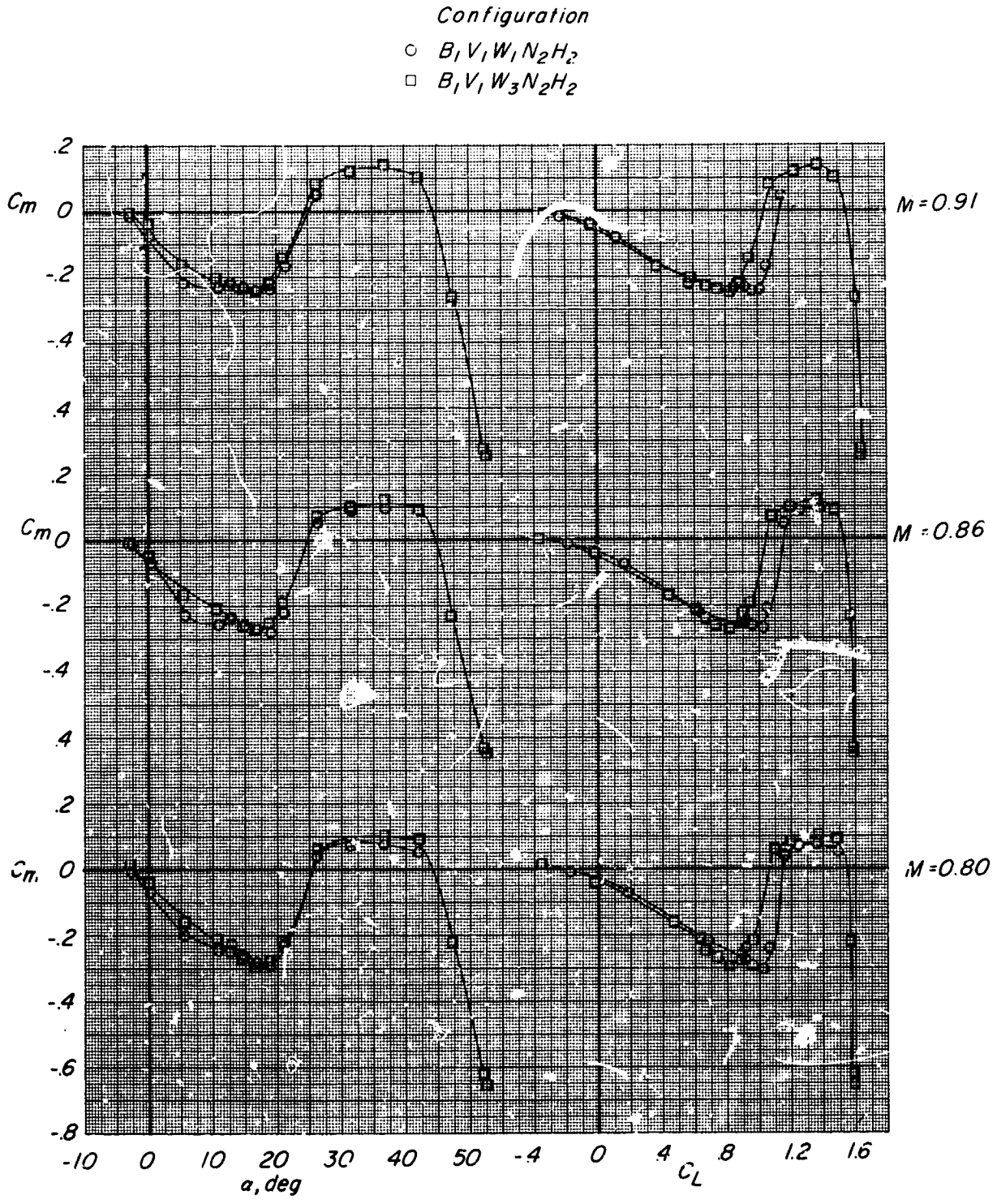

(a) Concluded.

Figure 27.- Continued.

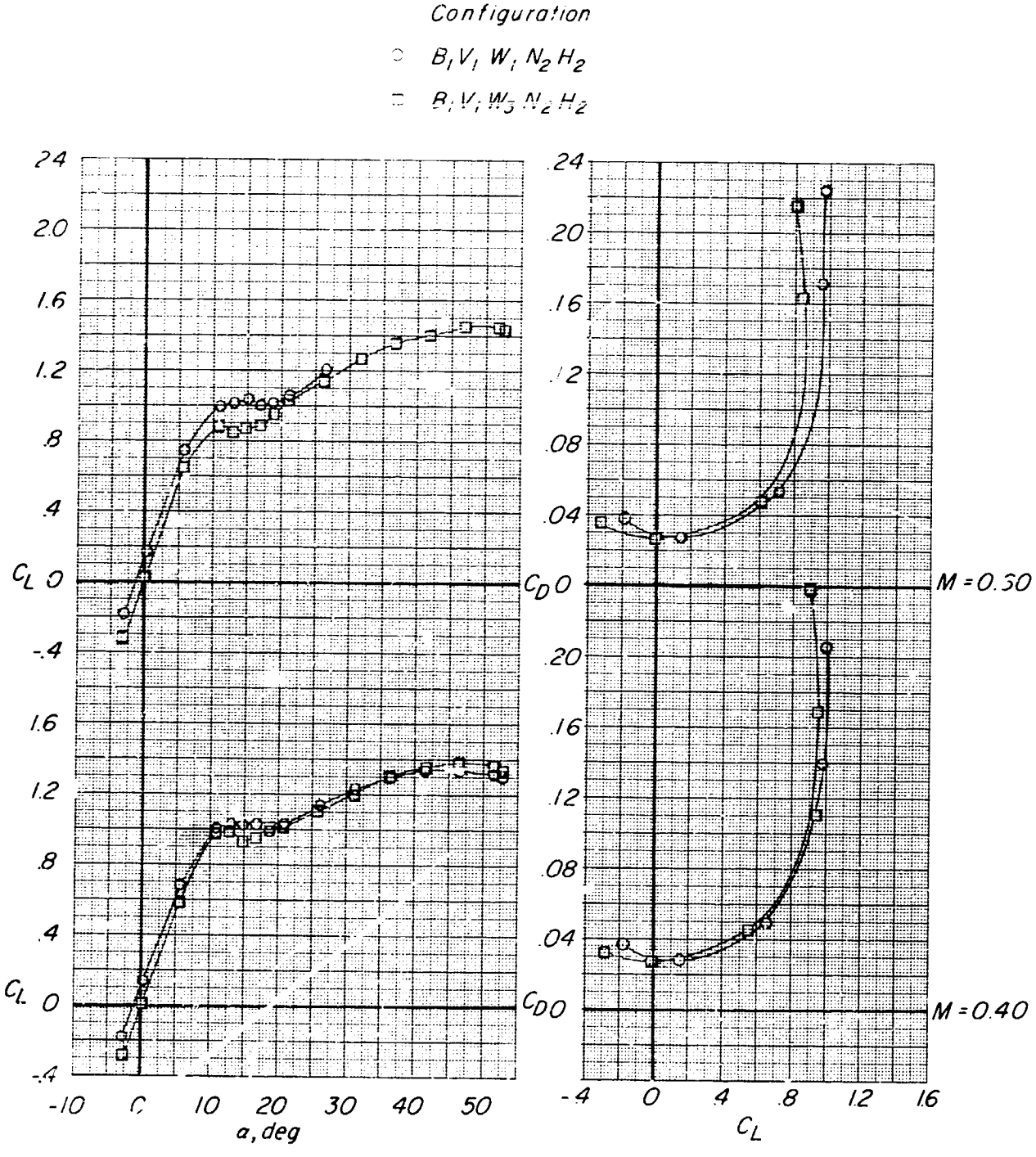

(b) Variation of C_L with α and C_D with C_L.

Figure 27.- Continued.

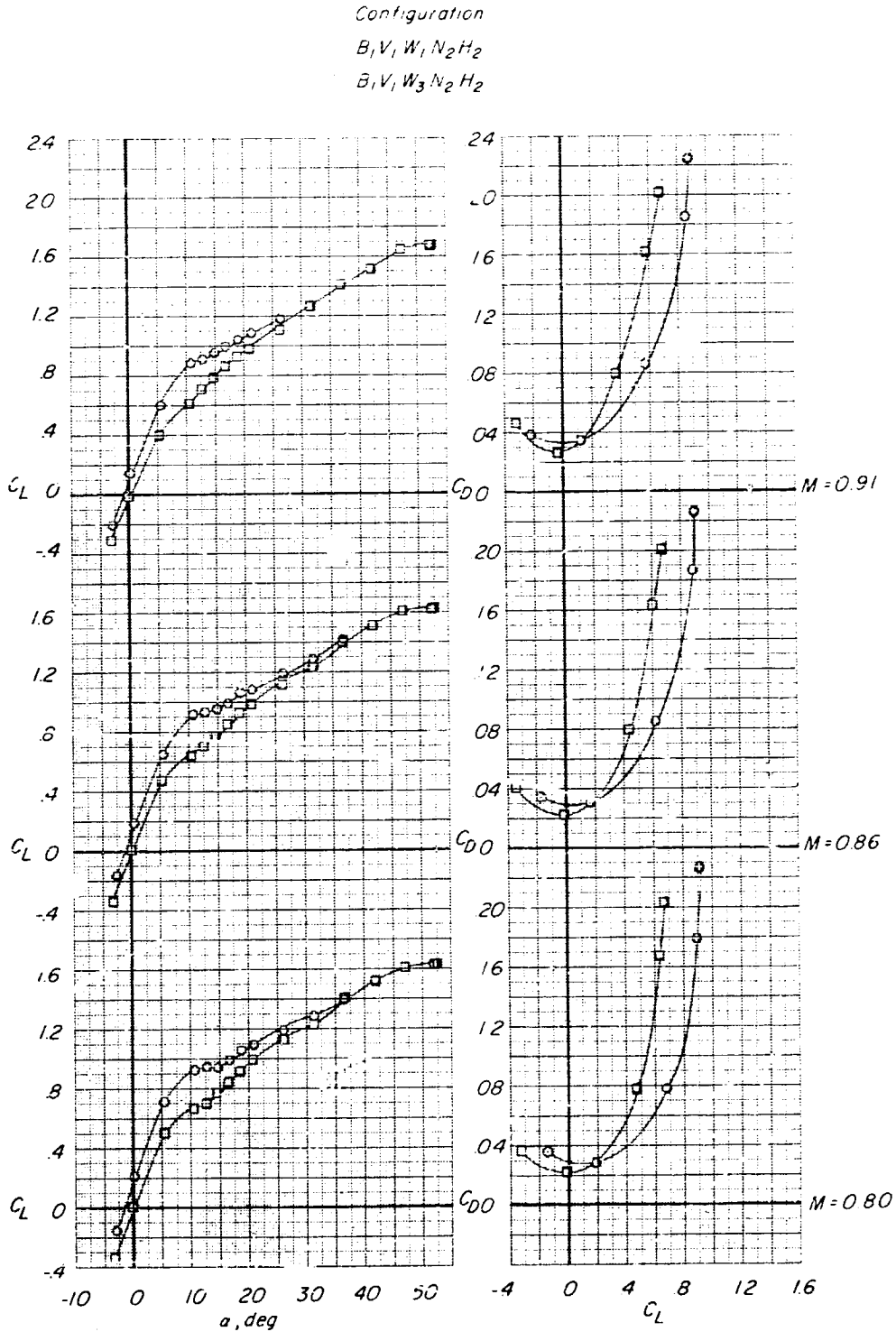

(b) Concluded.

Figure 27.- Continued.

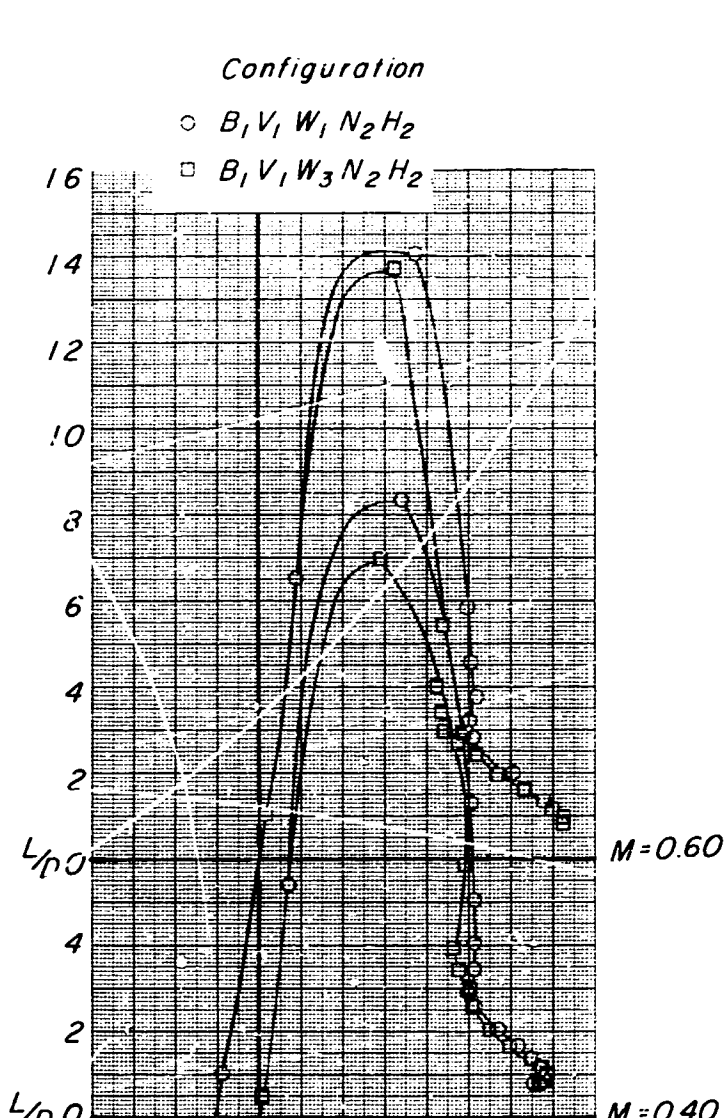

(c) Variation of L/D with C_L.

Figure 27.- Continued.

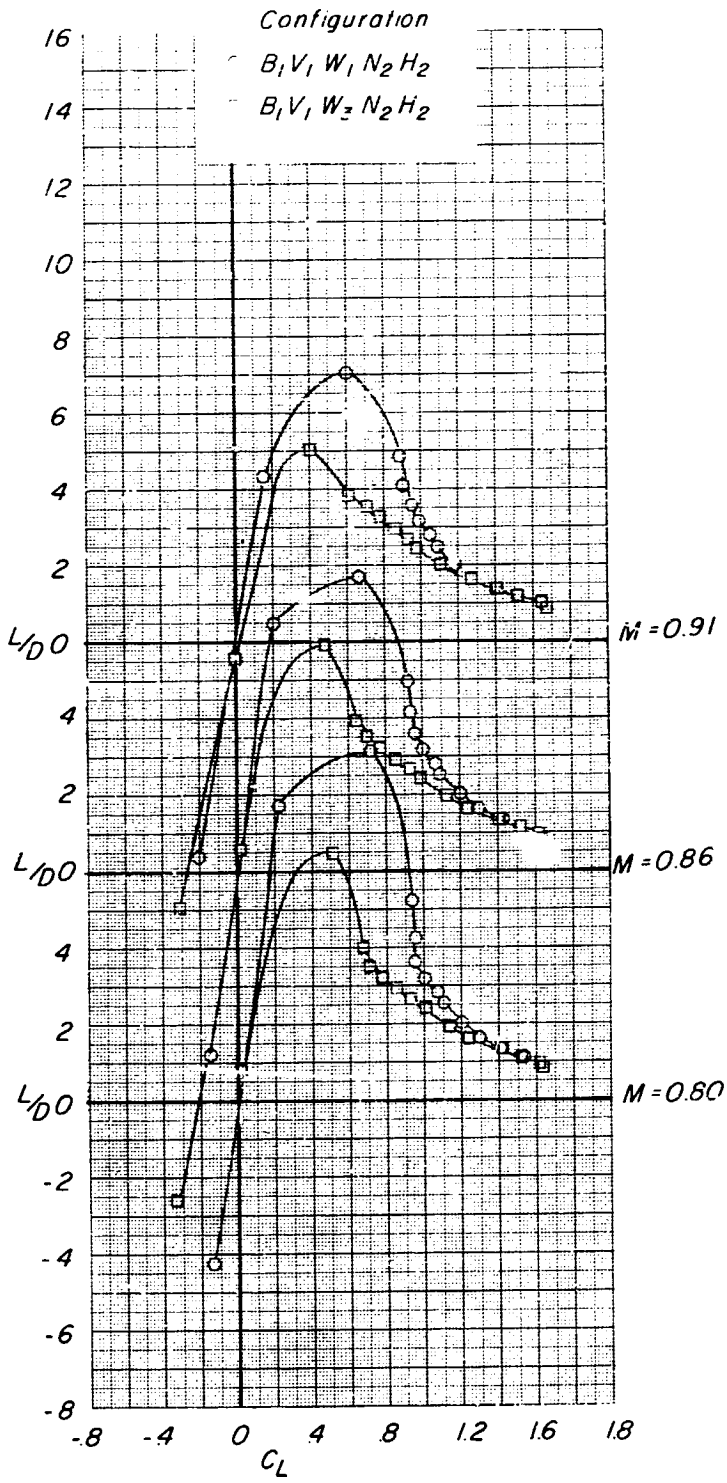

(c) Concluded.

Figure 27.- Concluded.

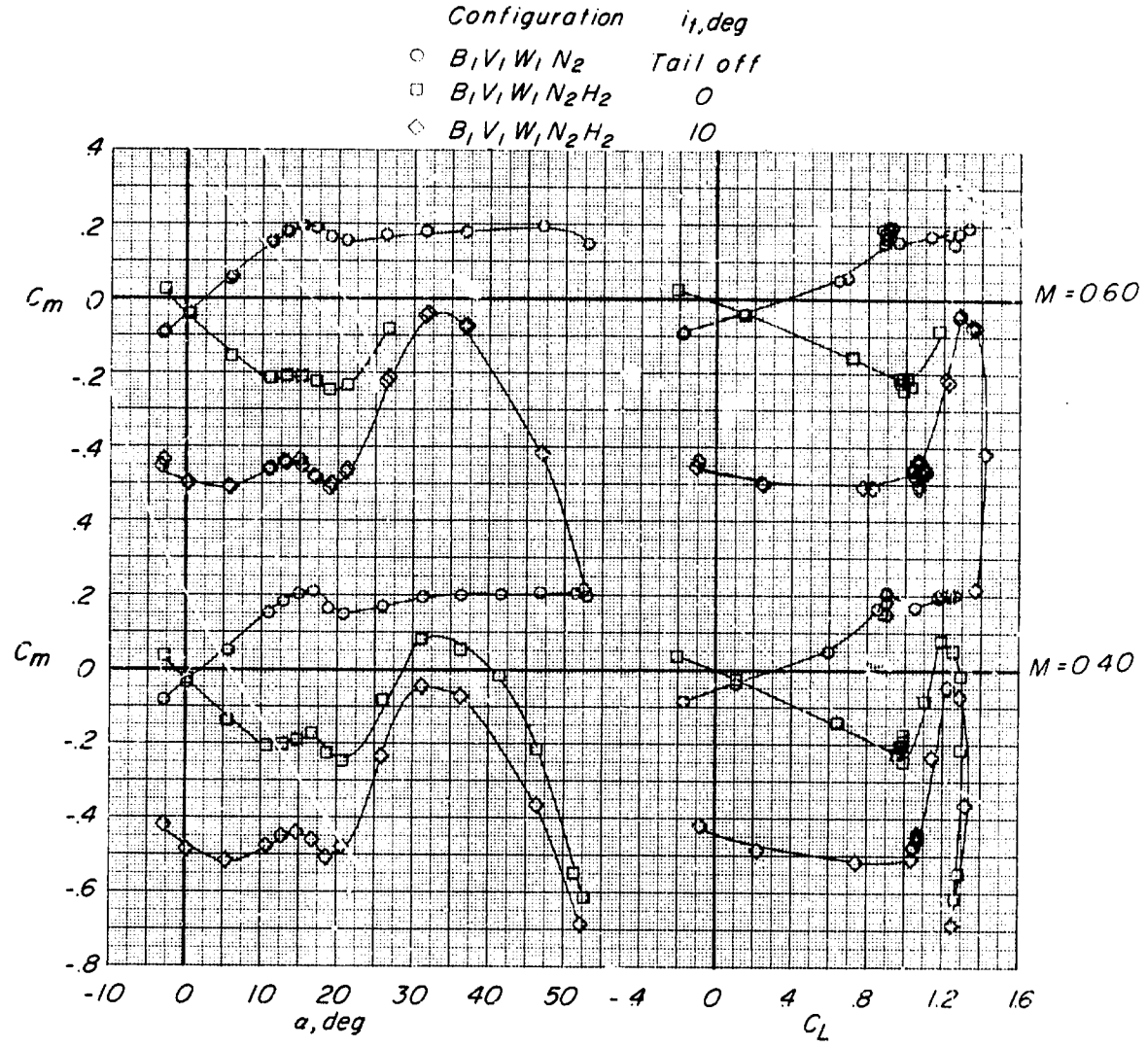

(a) Variation of C_m with α and C_L.

Figure 28.- Effect of Mach number on longitudinal control effectiveness of basic configuration ($B_1V_1W_1N_2H_2$). R = 0.71 × 10^6 at M = 0.40 and 0.60; R = 0.43 × 10^6 at M = 0.80, 0.86, and 0.91.

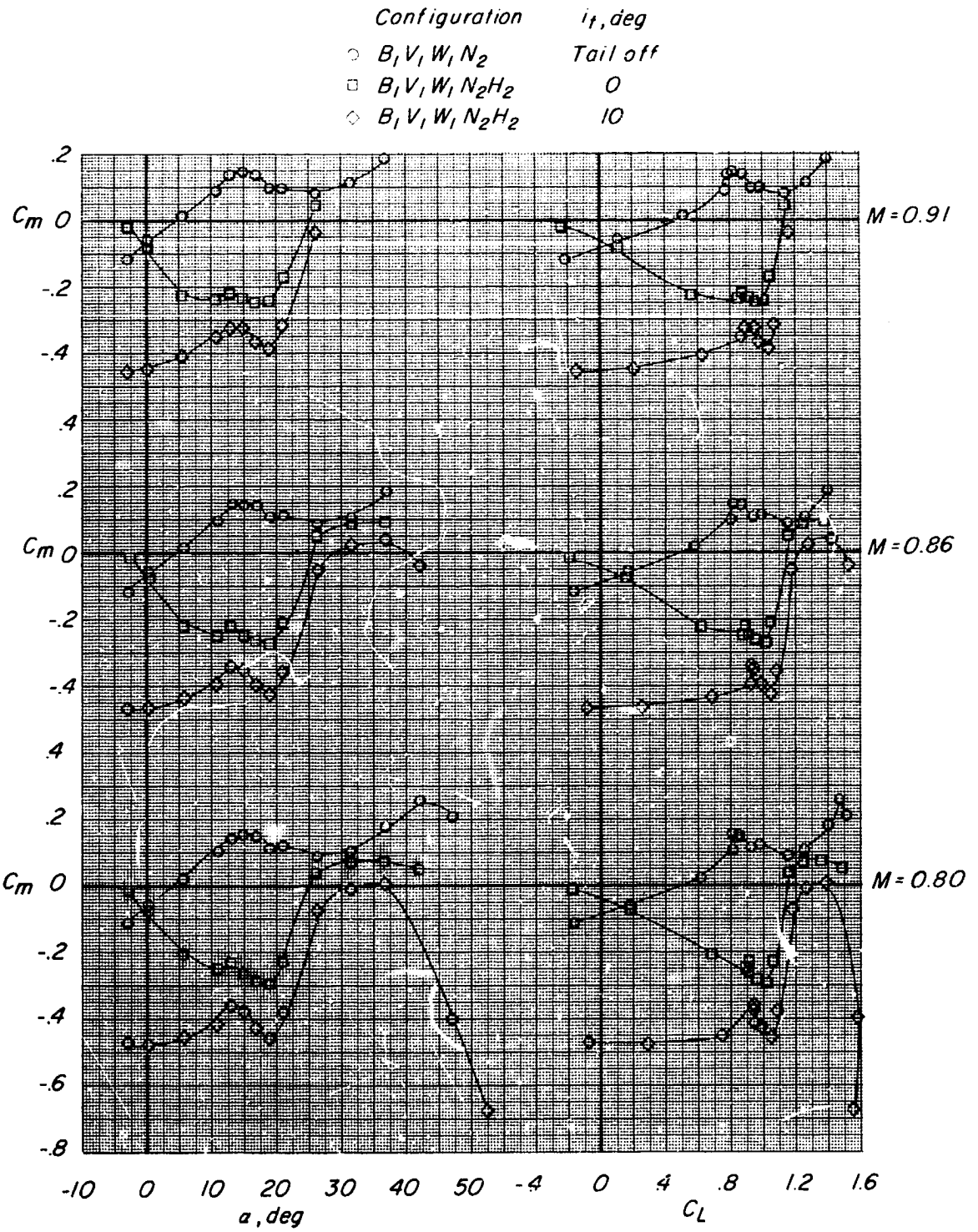

(a) Concluded.

Figure 28.- Continued.

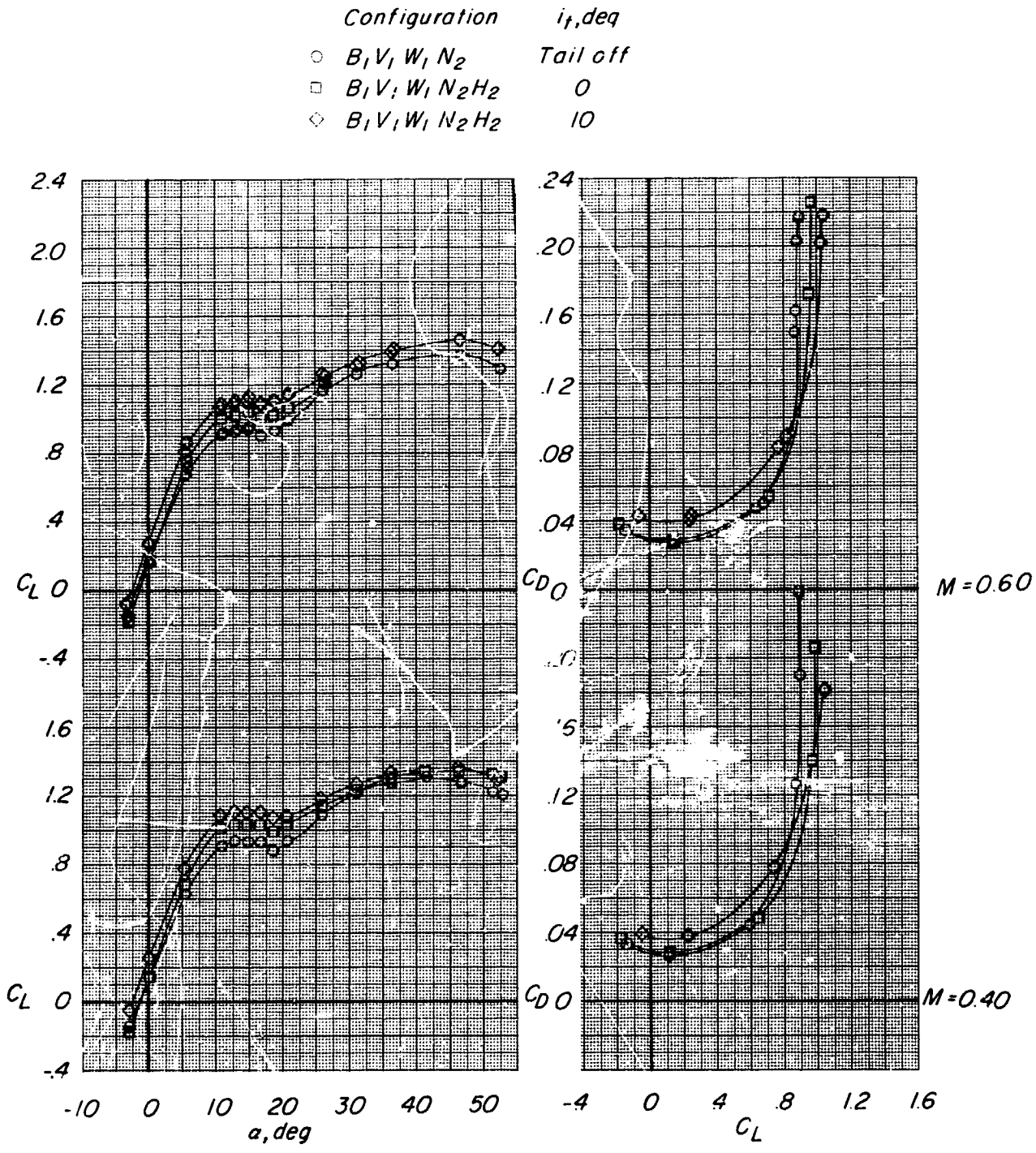

(b) Variation of C_L with α and C_D with C_L.

Figure 28.- Continued.

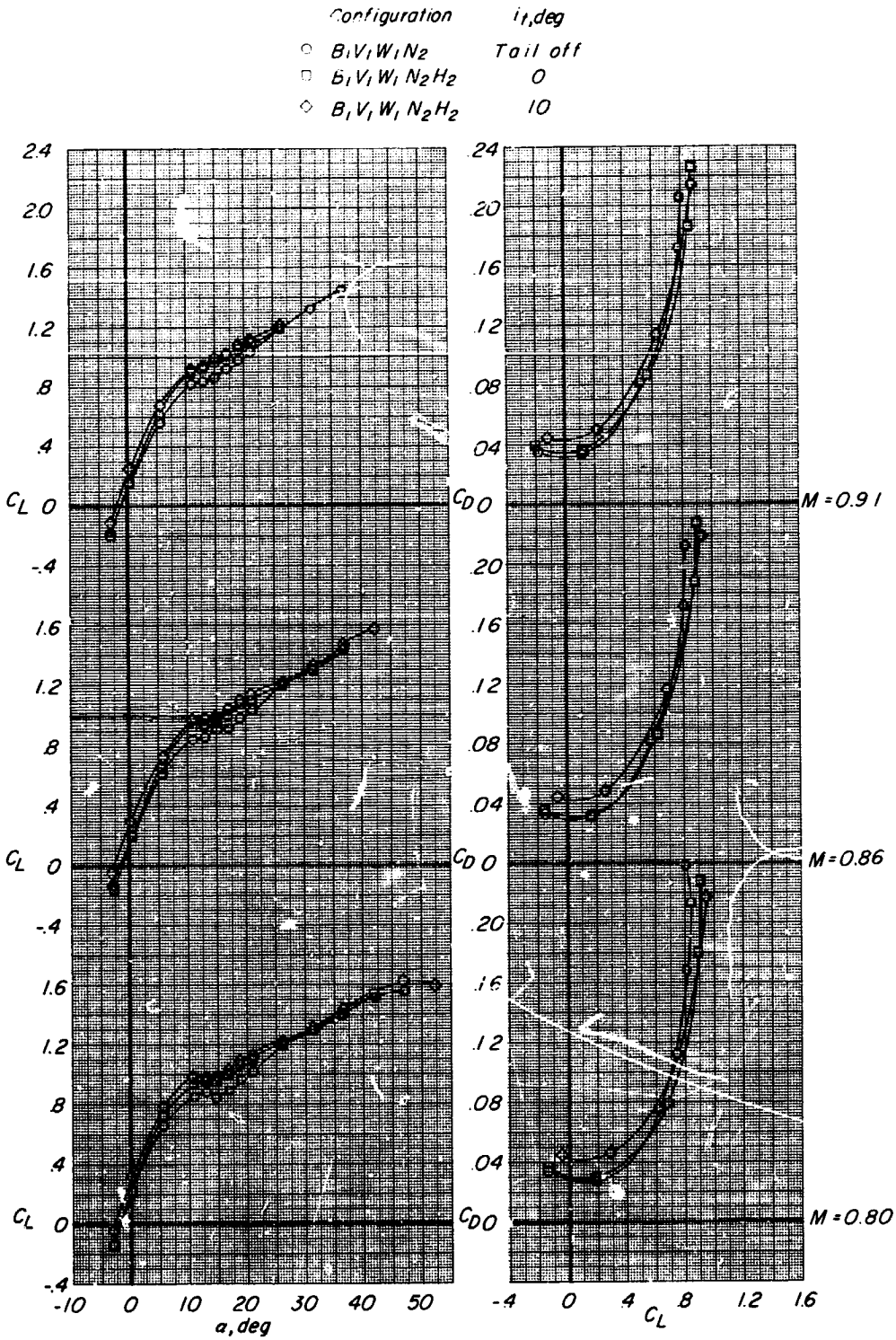

(b) Concluded.

Figure 28.- Continued.

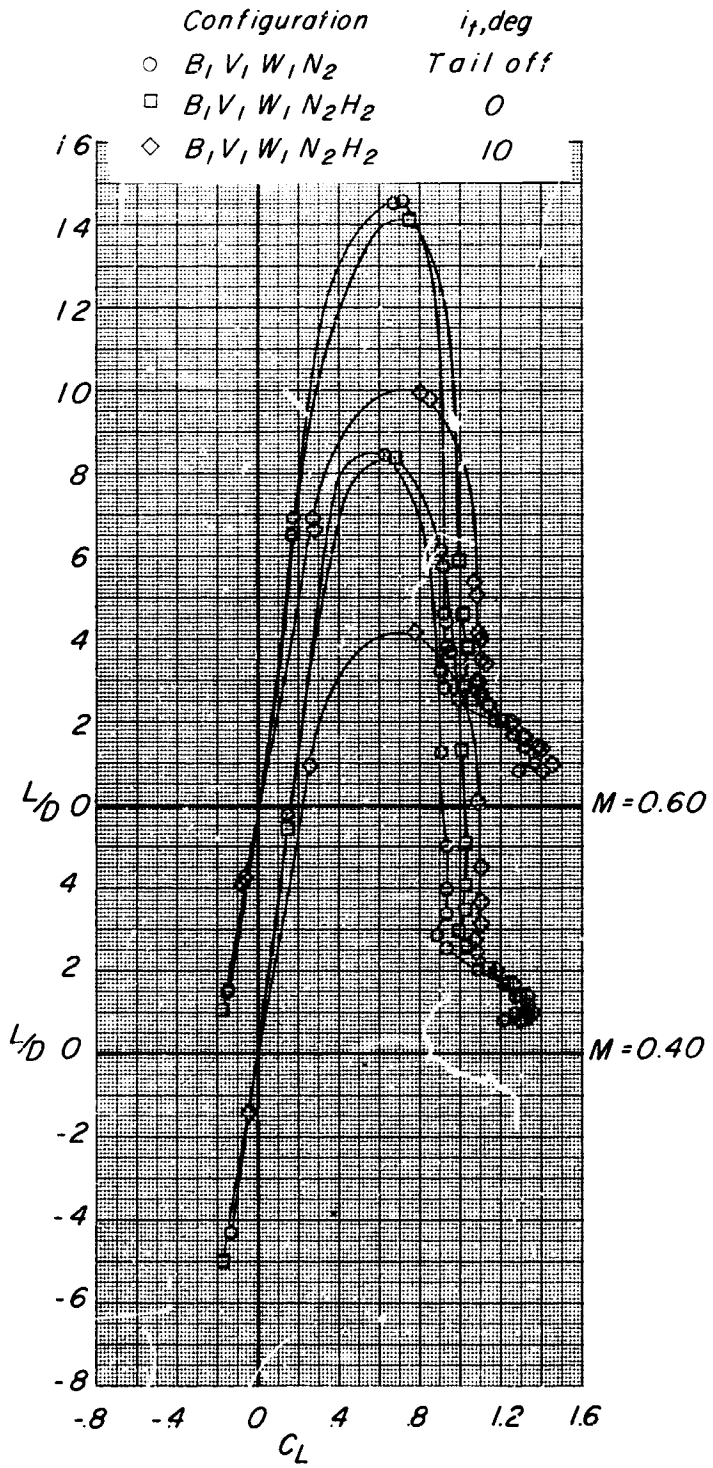

(c) Variation of L/D with C_L.

Figure 28.- Continued.

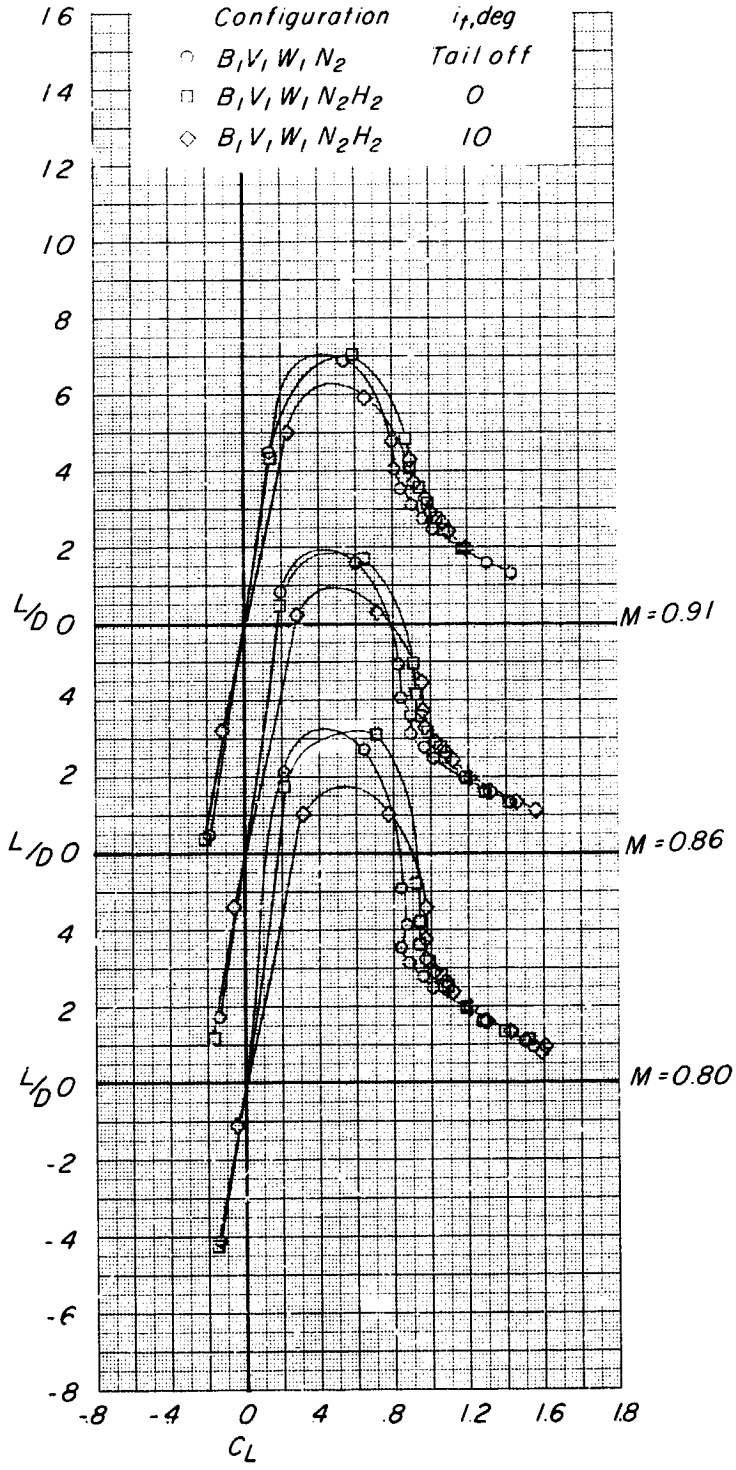

(c) Concluded.

Figure 28.- Concluded.

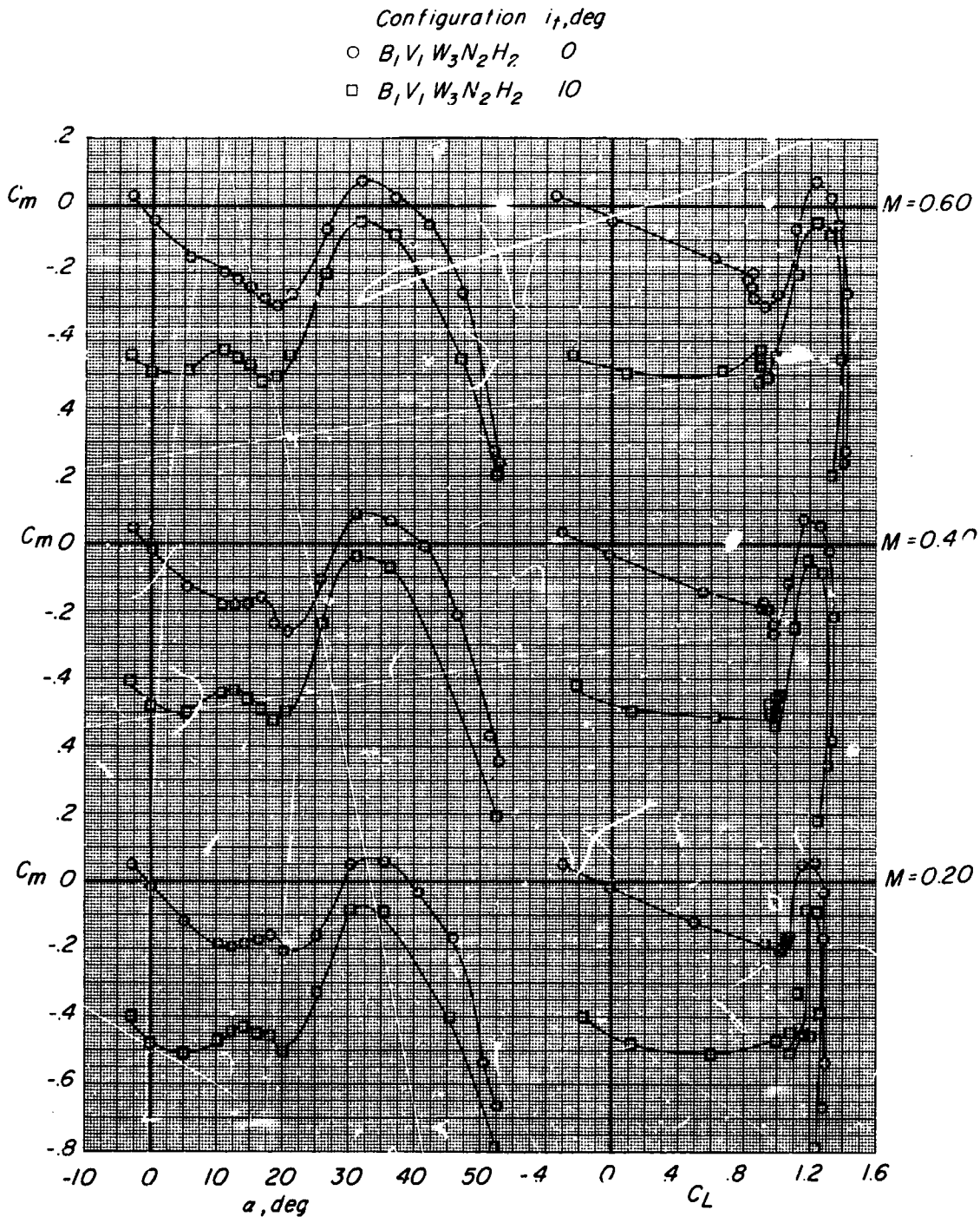

(a) Variation of C_m with α and C_L.

Figure 29.- Effect of Mach number on longitudinal control effectiveness of wing 3 configuration $(B_1V_1W_3N_2H_2)$. R = 0.71 × 10^6 at M = 0.20, 0.40, and 0.60; R = 0.43 × 10^6 at M = 0.86 and 0.91.

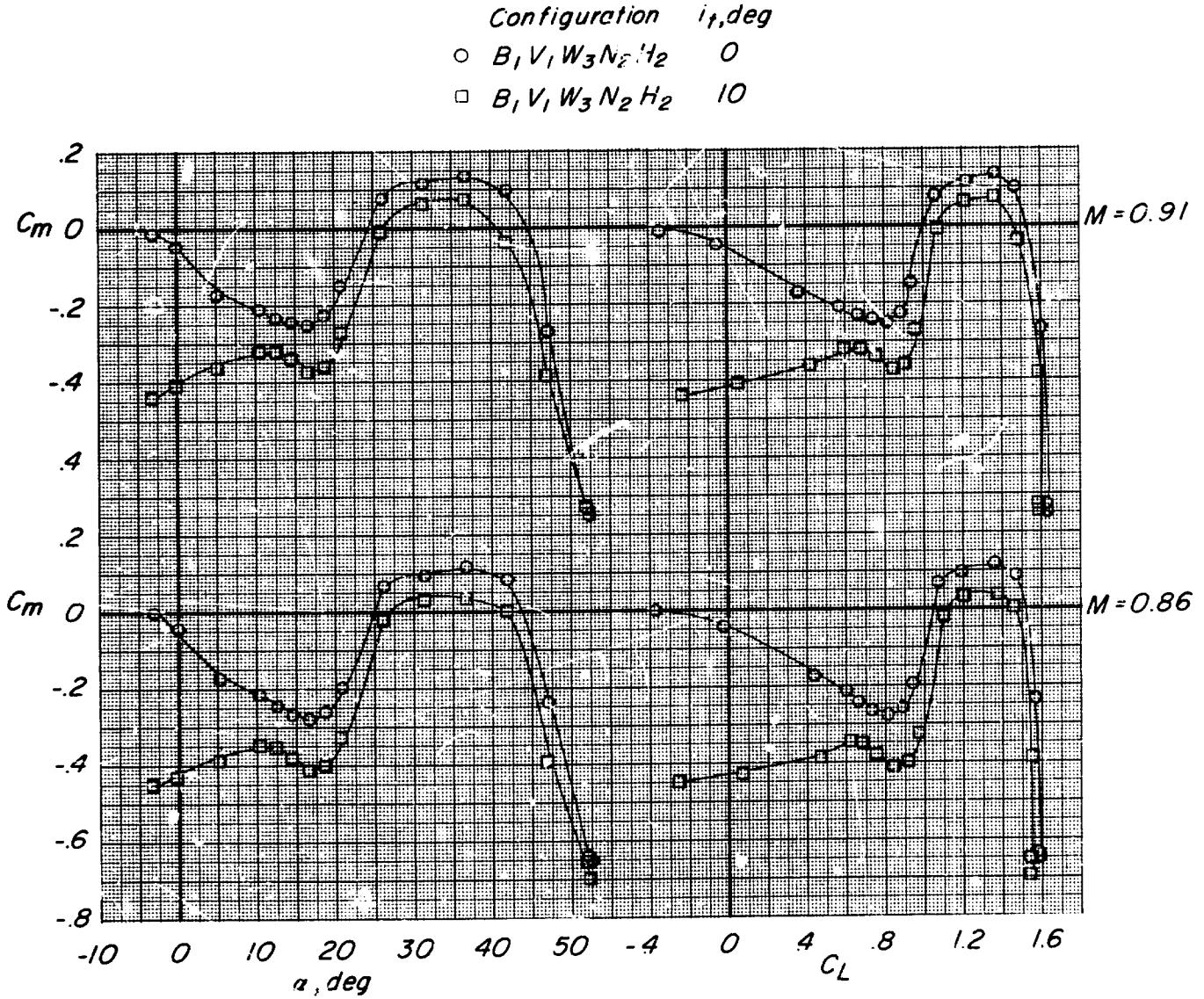

(a) Concluded.

Figure 29.- Continued.

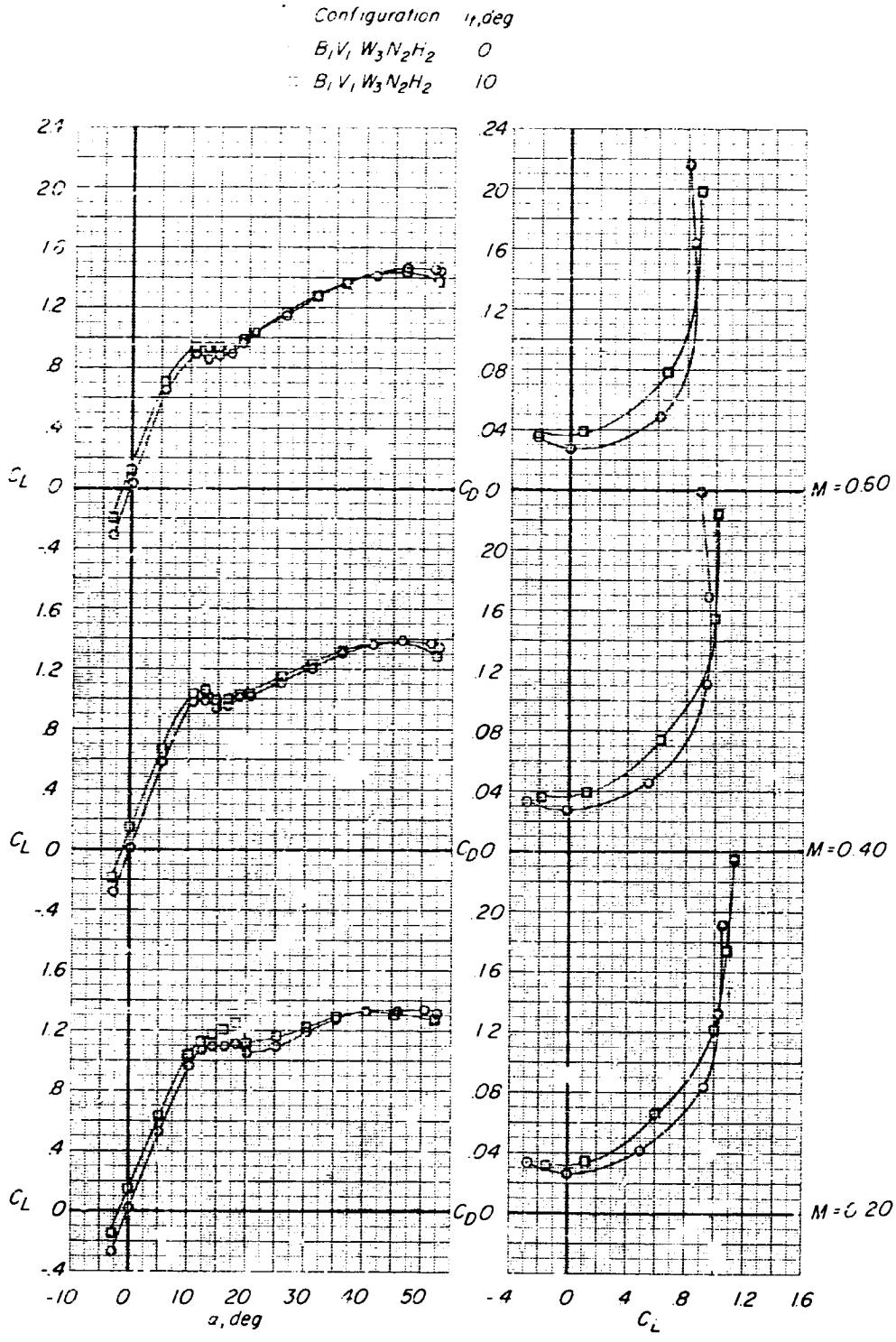

(b) Variation of C_L with α and C_D with C_L

Figure 29.- Continued.

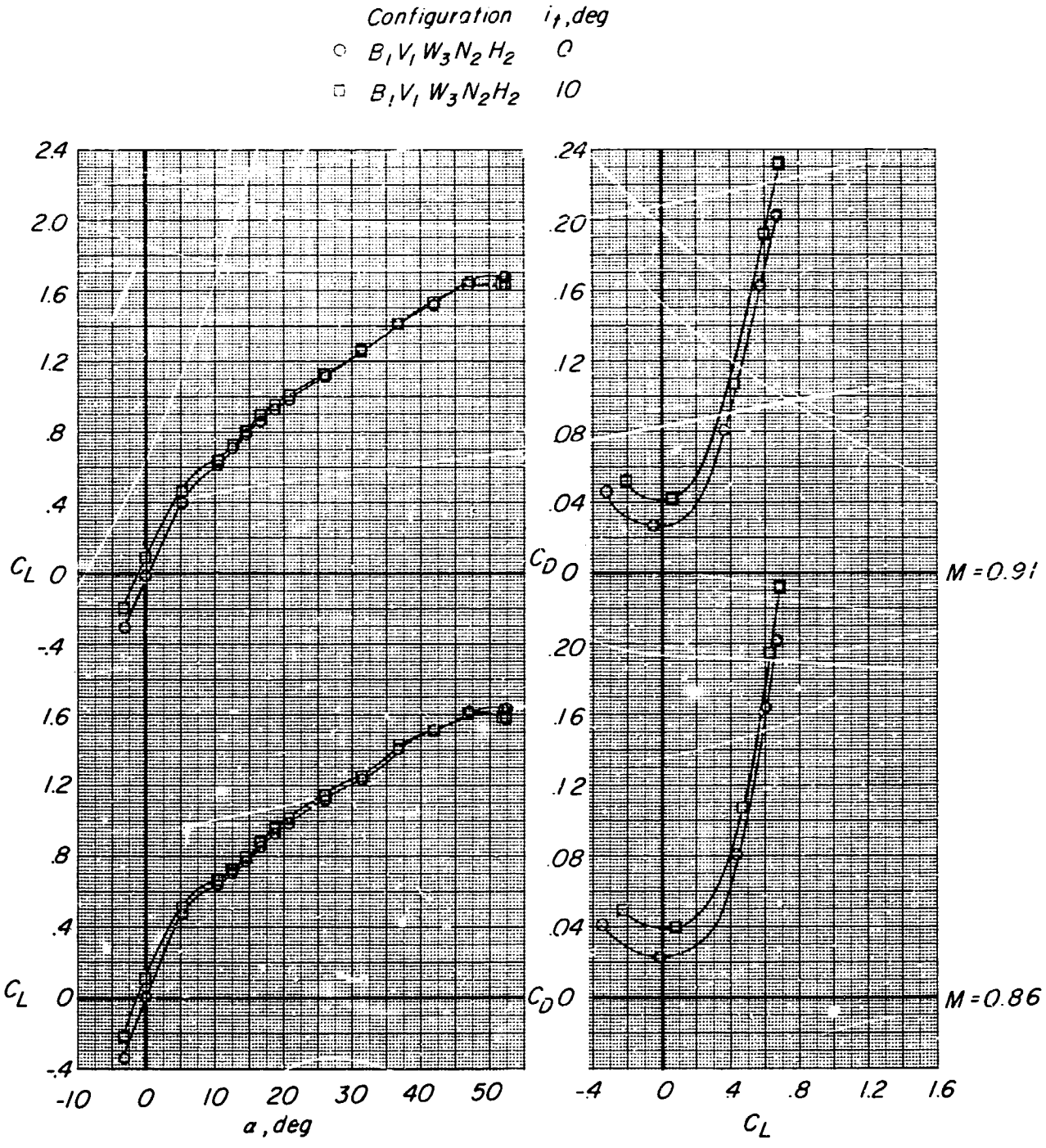

(b) Concluded.

Figure 29.- Continued.

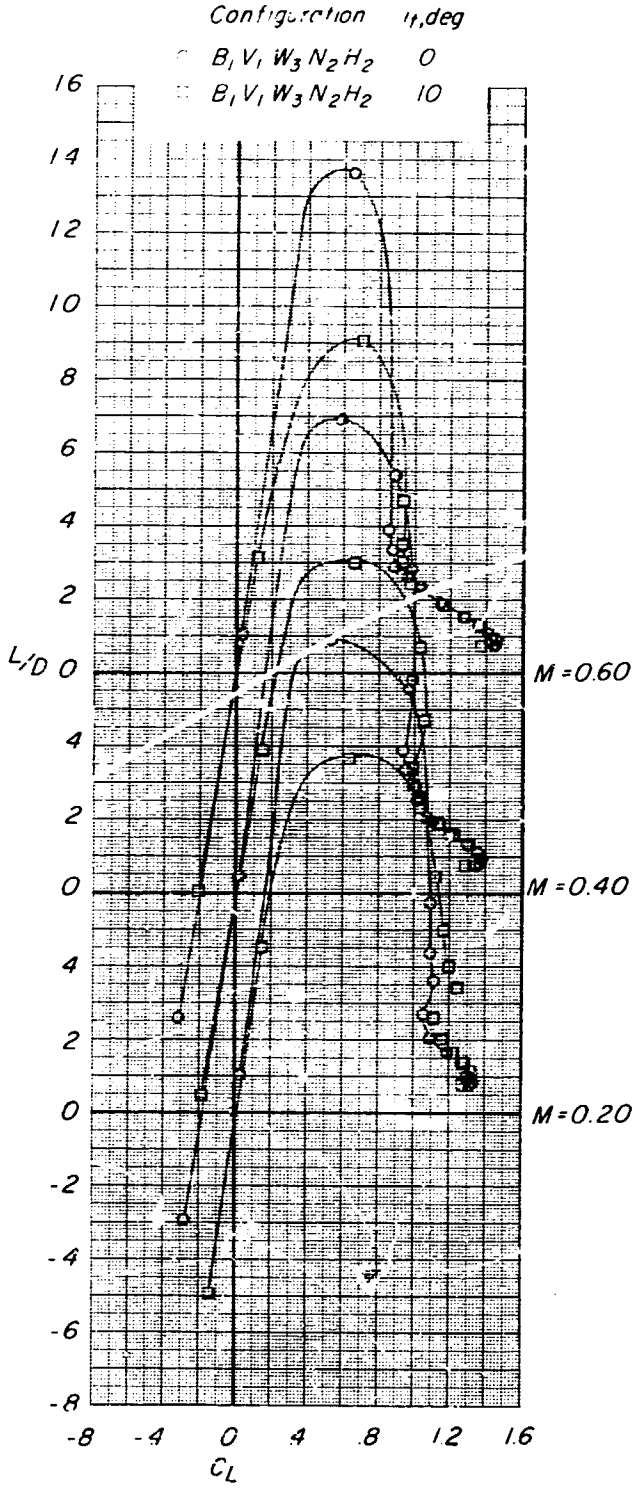

(c) Variation of L/D with C_L.

Figure 29.- Continued.

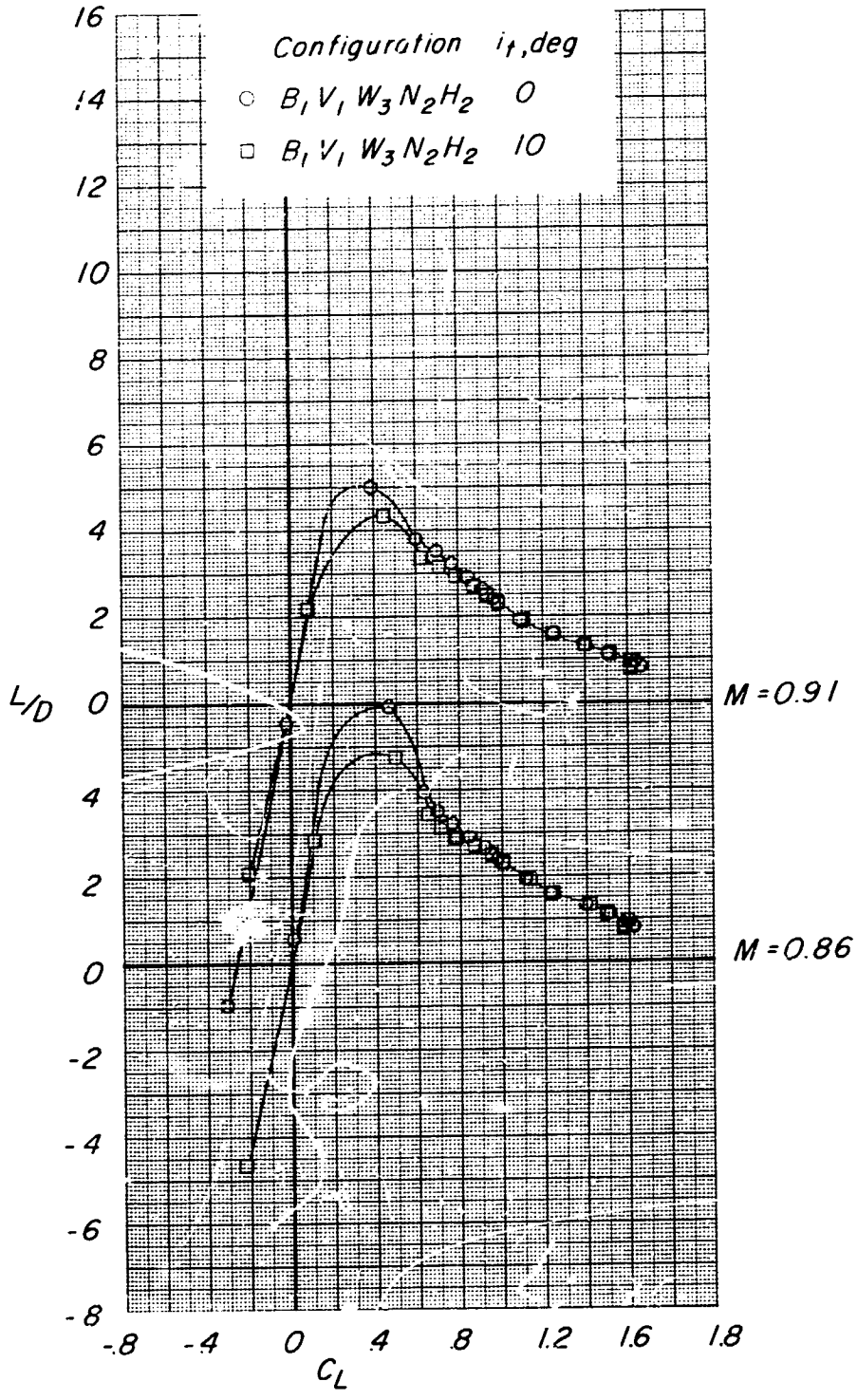

(c) Concluded.

Figure 29.- Concluded.

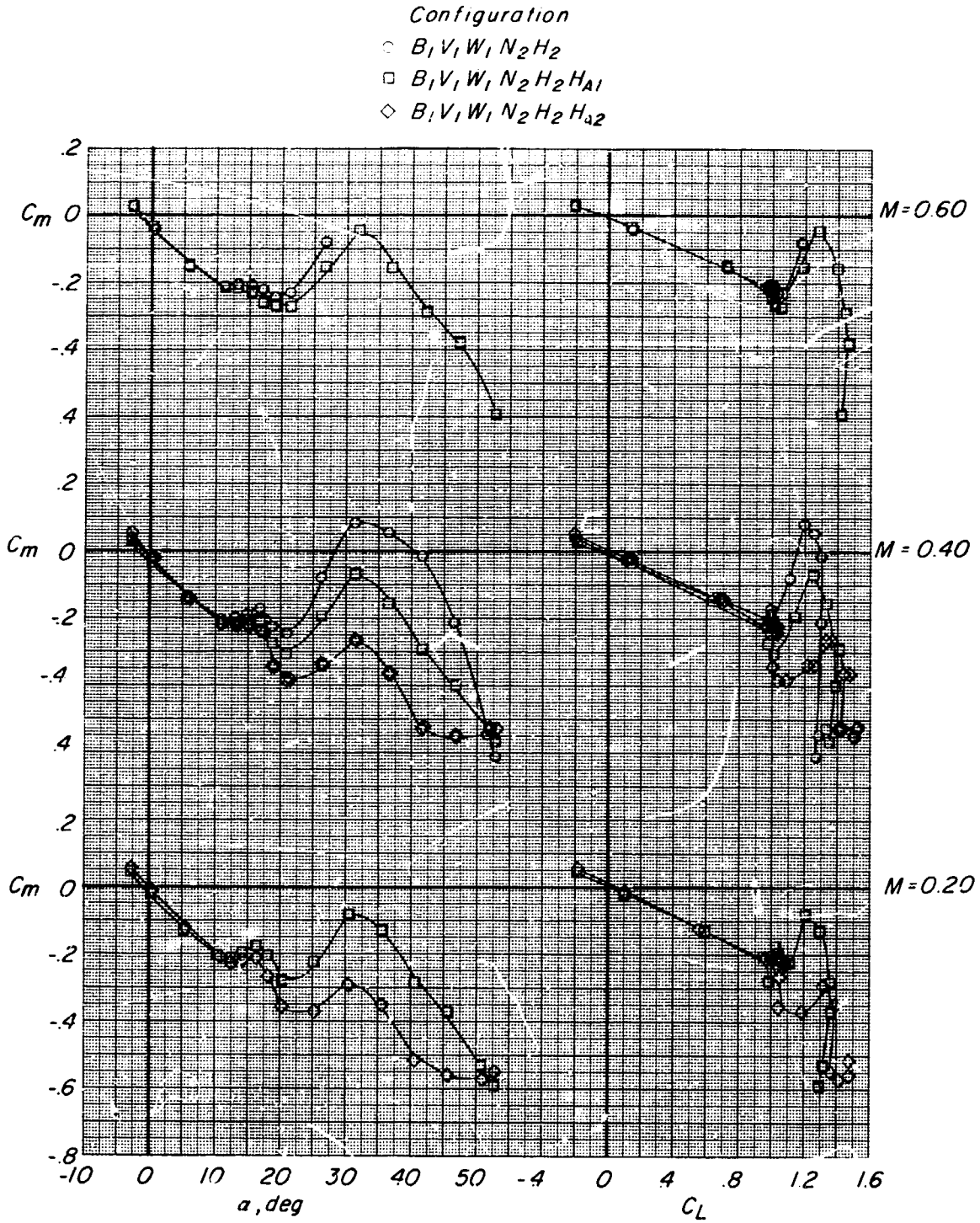

(a) Variation of C_m with α and C_L.

Figure 30.- Effect of auxiliary horizontal tail on longitudinal aerodynamic characteristics of basic configuration $(B_1V_1W_1N_2H_2)$ at Mach numbers from 0.20 to 0.60. $R = 0.71 \times 10^6$.

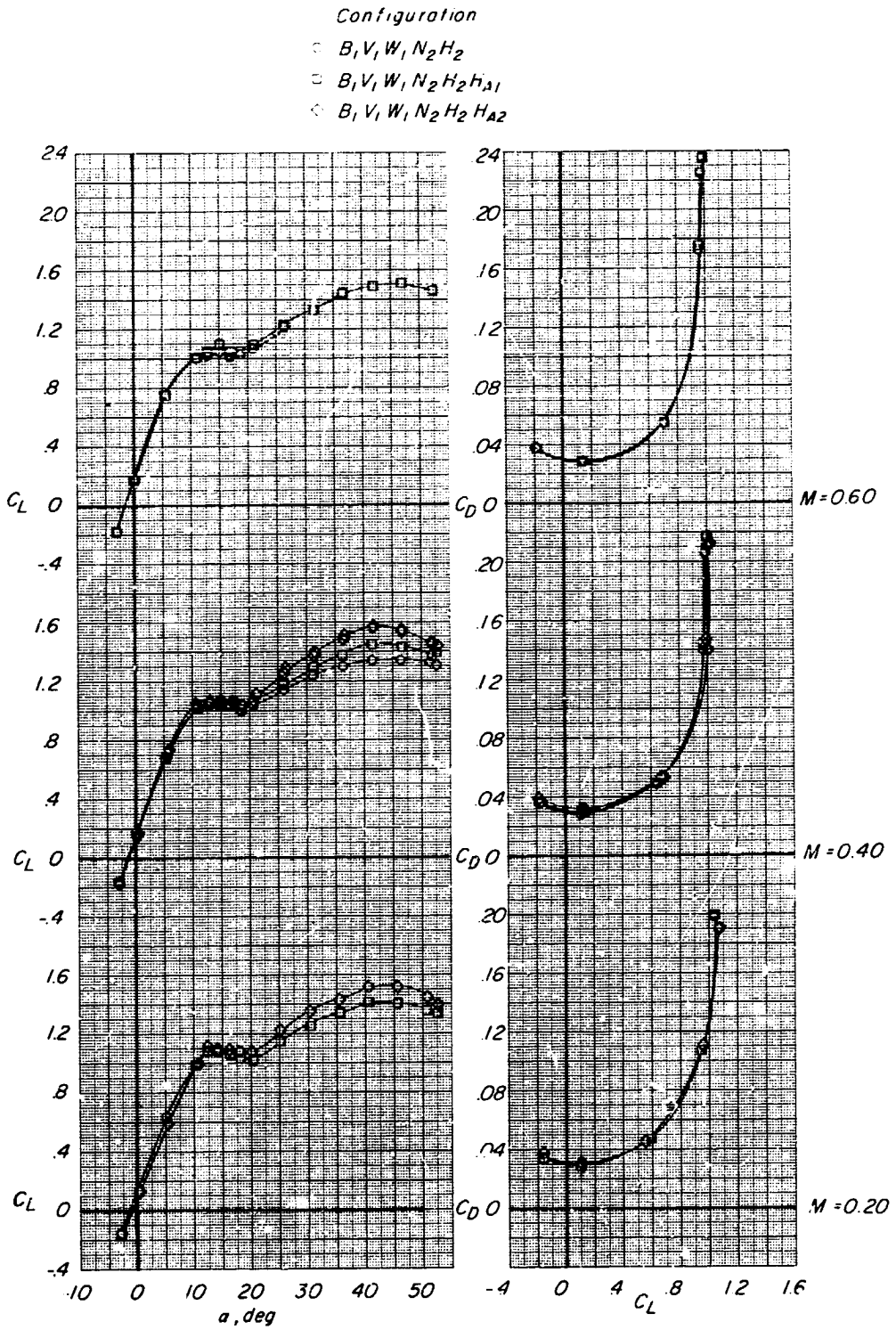

(b) Variation of C_L with α and C_D with C_L.

Figure 30.- Continued.

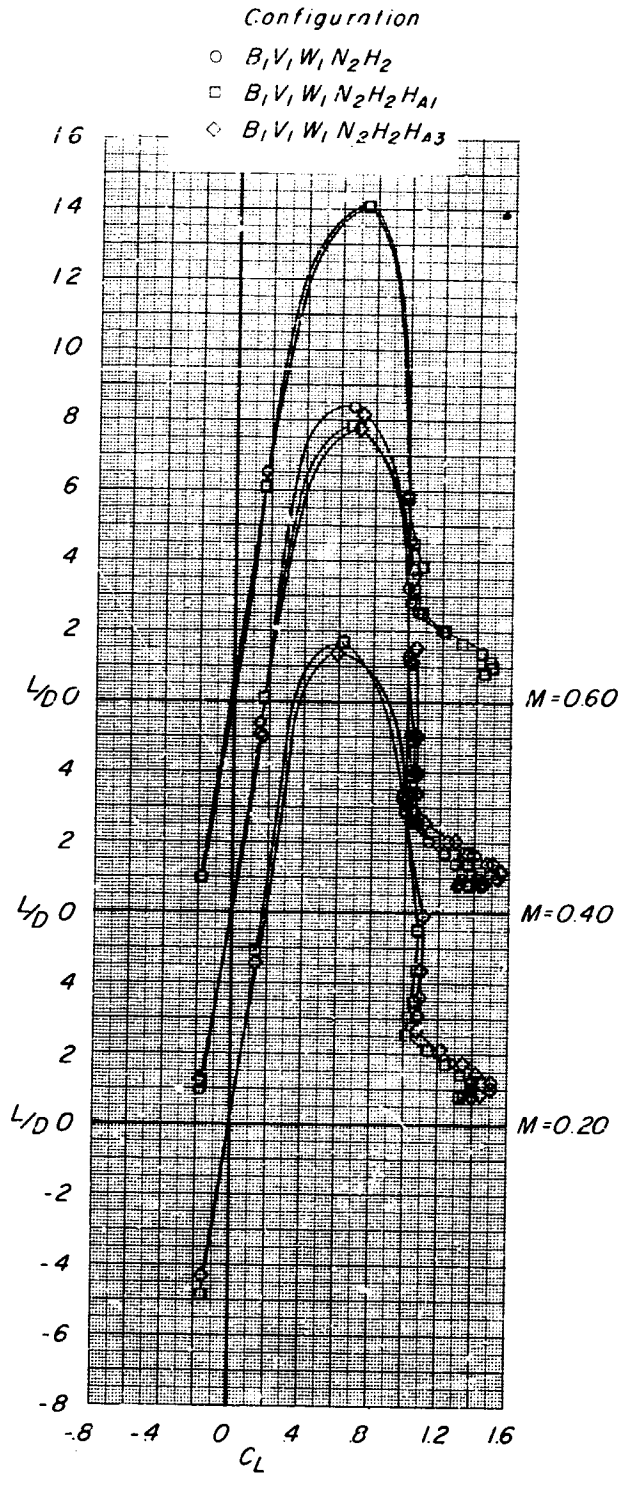

(c) Variation of L/D with C_L.

Figure 30.- Concluded.

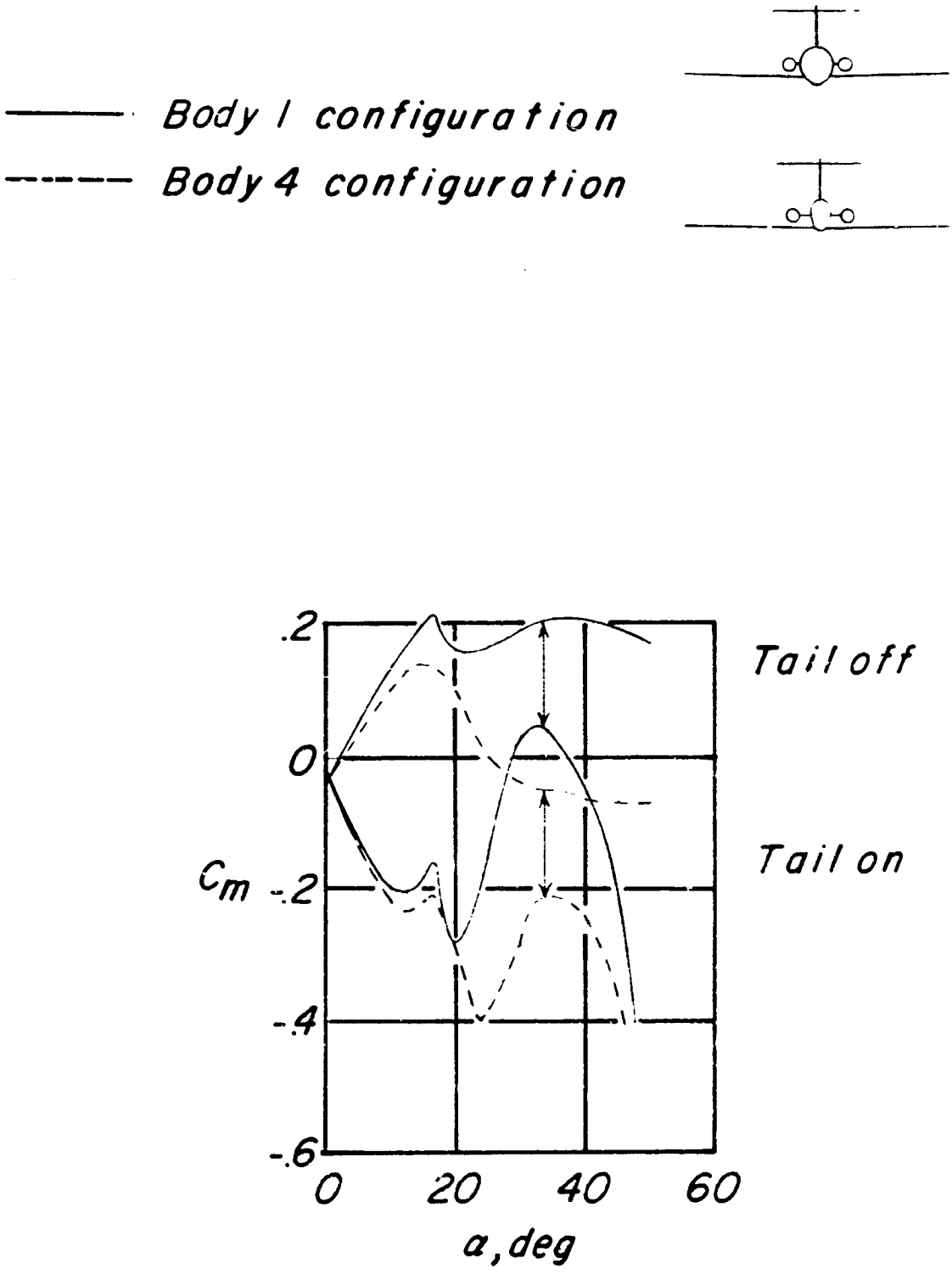

Figure 31.- Effect of body size and shape on longitudinal stability characteristics of basic configuration ($B_1V_1W_1N_2H_2$). M = 0.21; R = 0.78 x 10^6.

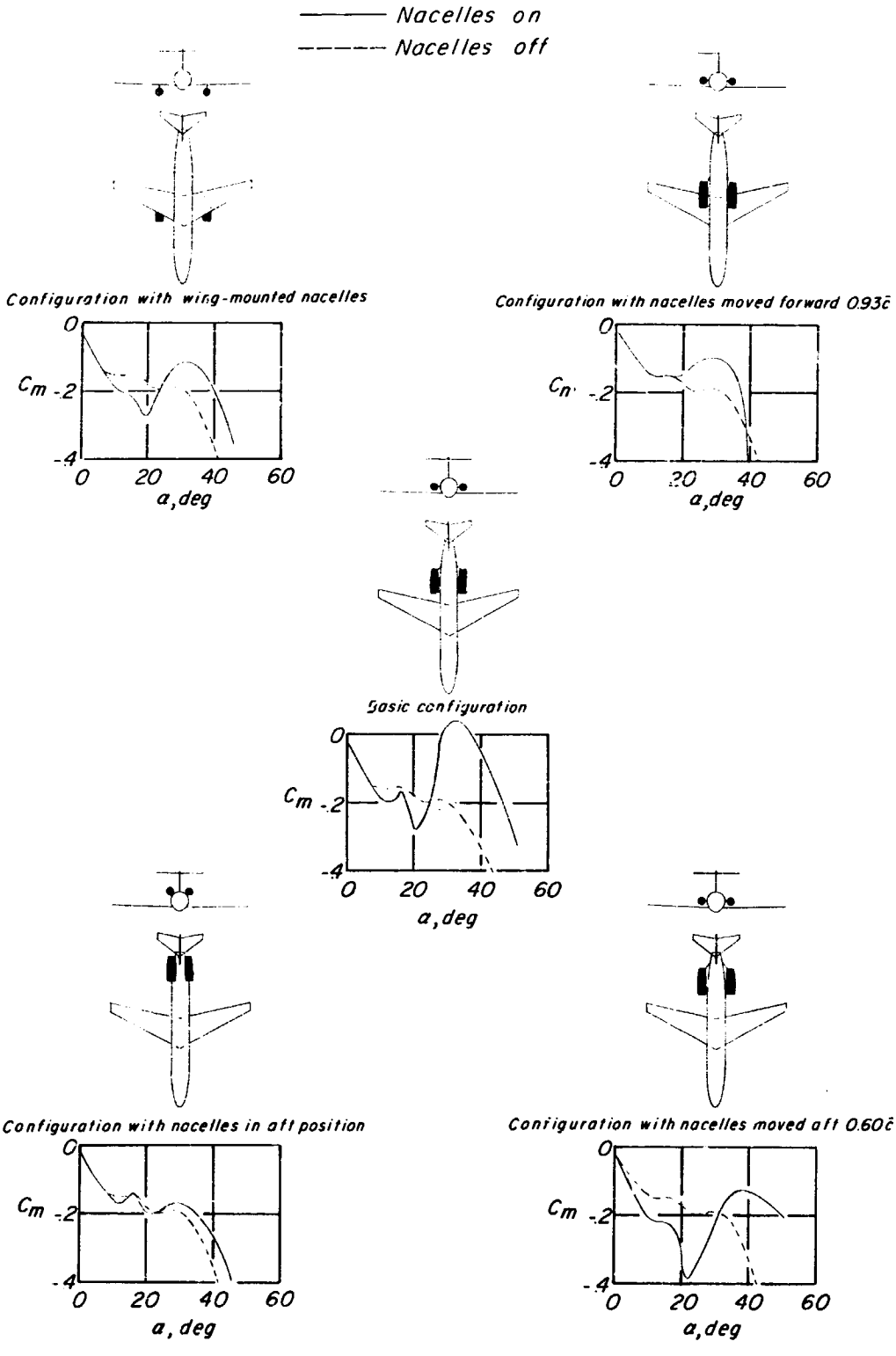

Figure 32.- Effect of nacelle position on longitudinal stability characteristics of basic configuration ($B_1V_1W_1N_2H_2$). M = 0.21; R = 0.78 × 10^6.

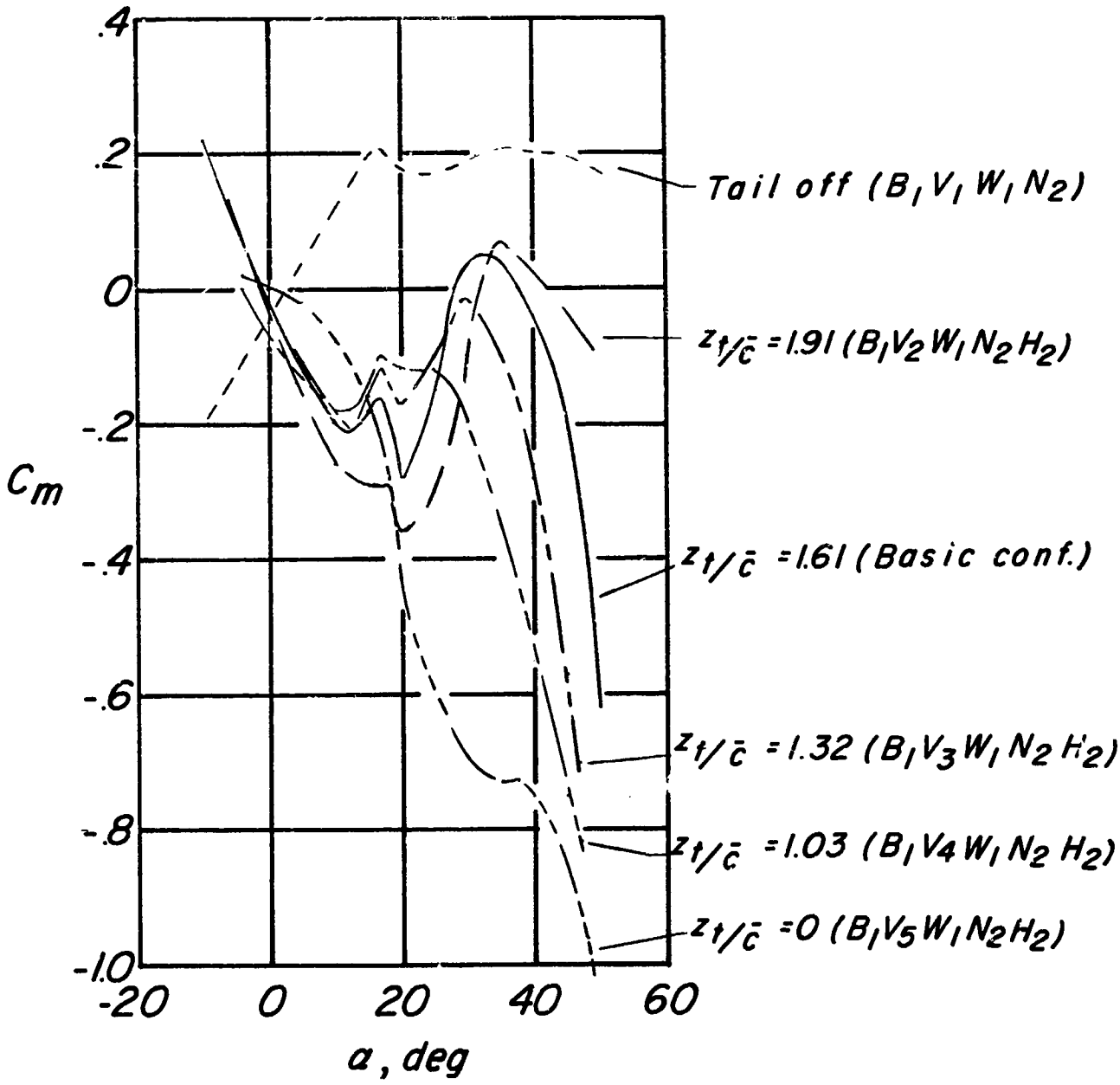

Figure 33.- Effect of horizontal-tail height, at a constant pitching-moment arm, on longitudinal stability characteristics of basic configuration $(B_1V_1W_1N_2H_2)$. M = 0.21; R = 0.78×10^6; $i_t = 0^\circ$.

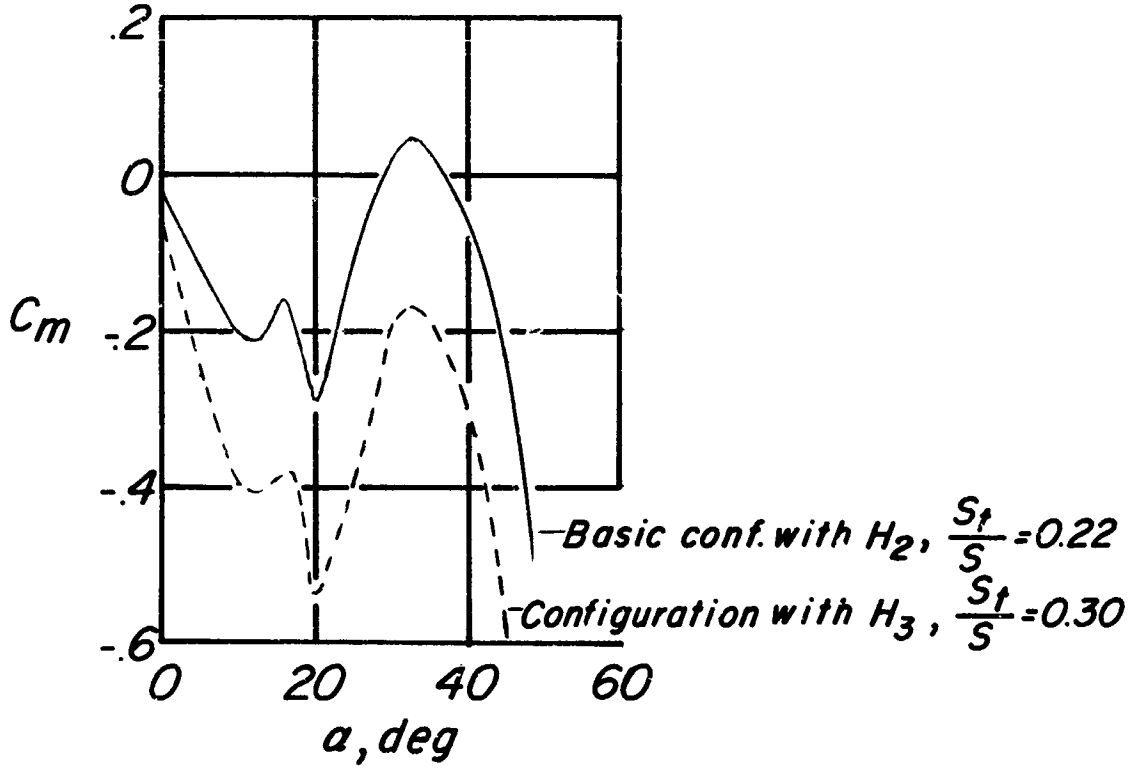

Figure 34.- Effect of horizontal-tail size, at constant horizontal-tail arm, on longitudinal stability characteristics of configuration $B_1V_1W_1N_2$. M = 0.21; R = 0.78 x 10^6.

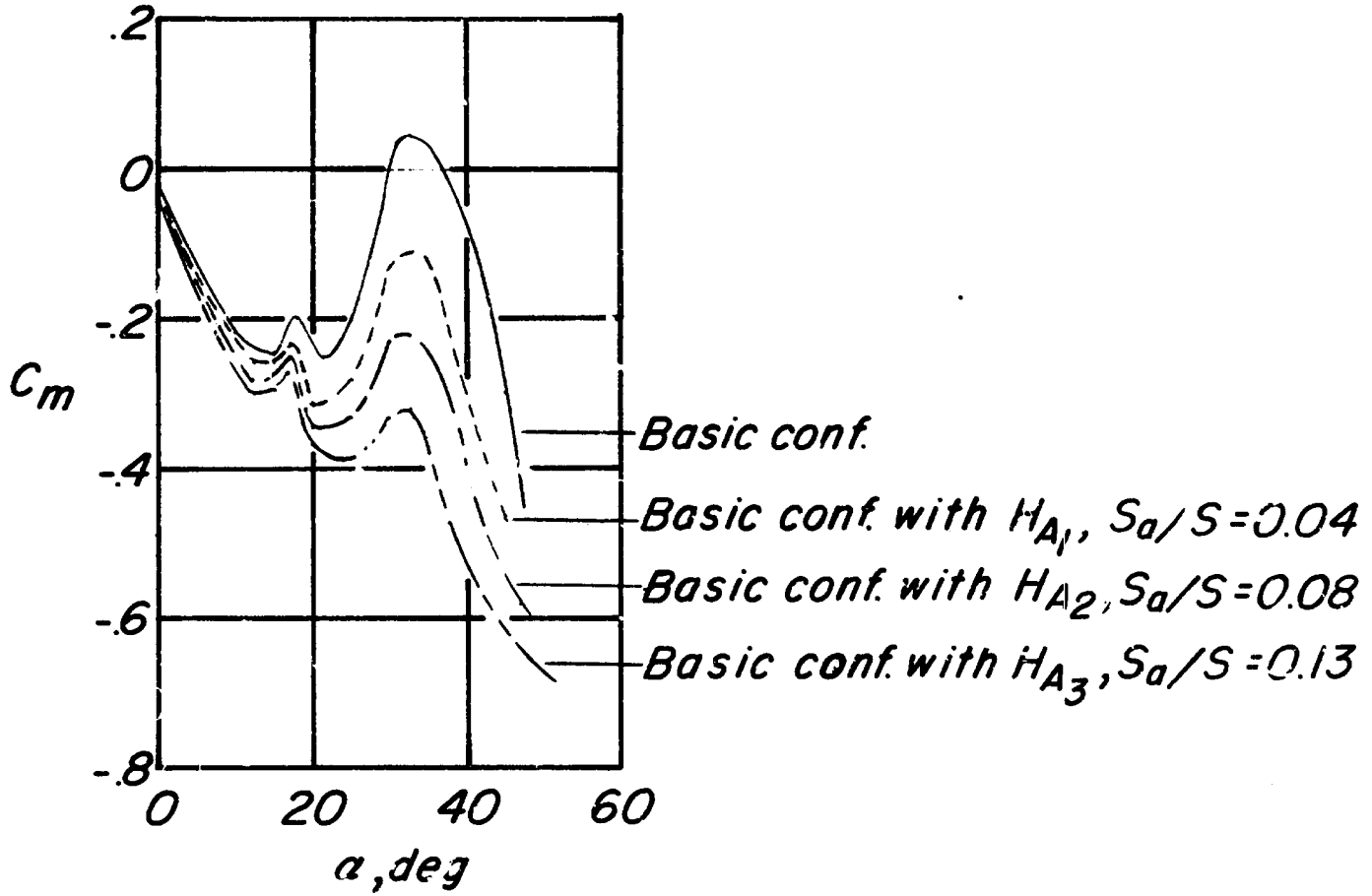

Figure 35.- Effect of auxiliary horizontal tails on longitudinal stability characteristics of basic configuration ($B_1W_1N_2H_2$). M = 0.21; R = 0.78×10^6.